AD-A033 540 PROTOTYPE DEVELOPMENT ASSOCIATES INC SANTA ANA CALIF F/G 11/4
EVALUATION OF CARBON-CARBON COMPOSITE NOSETIP MATERIALS.(U)
OCT 76 J R STETSON, J C SCHUTZLER DAAG46-75-C-0099
UNCLASSIFIED PDA-TR-1042-00-09 AMMRC-CTR-76-34 NL

1 OF 2
ADA033540

2

AMMRC CTR 76-34

EVALUATION OF CARBON-CARBON COMPOSITE NOSETIP MATERIALS

October 1976

J. R. Stetson and J. C. Schutzler
PROTOTYPE DEVELOPMENT ASSOCIATES, INC.
1740 Garry Avenue, Suite 201
Santa Ana, California 92705

FINAL REPORT Contract Number DAAG46-75-C-0099

Prepared for

ARMY MATERIALS AND MECHANICS RESEARCH CENTER
Watertown, Massachusetts 02172

The findings in this report are not to be construed as an official Department of the Army position, unless so designated by other authorized documents.

Mention of any trade names or manufacturers in this report shall not be construed as advertising nor as an official indorsement or approval of such products or companies by the United States Government.

DISPOSITION INSTRUCTIONS

Destroy this report when it is no longer needed.
Do not return it to the originator.

UNCLASSIFIED

SECURITY CLASSIFICATION OF THIS PAGE (When Data Entered)

REPORT DOCUMENTATION PAGE	READ INSTRUCTIONS BEFORE COMPLETING FORM
1. REPORT NUMBER: AMMRC CTR-76-34	2. GOVT ACCESSION NO. / 3. RECIPIENT'S CATALOG NUMBER
4. TITLE (and Subtitle): Evaluation of Carbon-Carbon Composite Nosetip Materials	5. TYPE OF REPORT & PERIOD COVERED: Final Report, 1 July 1975 - 30 April 1976
	6. PERFORMING ORG. REPORT NUMBER: PDA-TR-1042-00-09
7. AUTHOR(s): John F. R. Stetson and J. C. Schutzler	8. CONTRACT OR GRANT NUMBER(s): DAAG46-75-C-0099
9. PERFORMING ORGANIZATION NAME AND ADDRESS: Prototype Development Associates, Inc., 1740 Garry Avenue, Suite 201, Santa Ana, CA 92705	10. PROGRAM ELEMENT, PROJECT, TASK AREA & WORK UNIT NUMBERS: D/A Project: 62306AH72, AMCMS Code: 1W362306AH72, Agency Accession:
11. CONTROLLING OFFICE NAME AND ADDRESS: Army Materials and Mechanics Research Center, Watertown, Massachusetts 02172	12. REPORT DATE: October 1976
	13. NUMBER OF PAGES: 180 (173 p.)
14. MONITORING AGENCY NAME & ADDRESS (if different from Controlling Office)	15. SECURITY CLASS. (of this report): Unclassified
	15a. DECLASSIFICATION/DOWNGRADING SCHEDULE

16. DISTRIBUTION STATEMENT (of this Report)

Approved for public release; distribution unlimited.

17. DISTRIBUTION STATEMENT (of the abstract entered in Block 20, if different from Report)

18. SUPPLEMENTARY NOTES

19. KEY WORDS (Continue on reverse side if necessary and identify by block number)

Carbon/carbon composites
Passive nosetip
Terminal interceptors
Erosion resistant material
ABM materials

20. ABSTRACT (Continue on reverse side if necessary and identify by block number)

Fourteen orthogonally-reinforced carbon-carbon materials were evaluated for application to terminal defense interceptor (ATDI) nosetip concepts. The preforms were woven from four different types of graphite yarns manufactured from PAN, rayon and an experimental pitch-precursor. Weave geometries represented a complete range of preform characteristics in terms of weave fineness and balance. Ablation tests were performed at three stagnation pressure levels up to 168

→ over

DD FORM 1 JAN 73 1473 EDITION OF 1 NOV 65 IS OBSOLETE

UNCLASSIFIED

SECURITY CLASSIFICATION OF THIS PAGE (When Data Entered)

390 714

bpg

atmospheres and post-test analyses of the material ablation performance were conducted. Five of the most promising materials were strength-tested and a complete engineering properties data base was developed for one of the materials (AMMRC/FMI 221). Nosetip designs were developed for a typical ATDI mission and four prototype full-scale models were fabricated and tested in a high pressure rocket exhaust facility. One nosetip model of AMMRC/FMI 221 was fabricated for flight test and analyzed for thermal and structural performance. It was demonstrated in this program that certain fine-weave carbon-carbon materials of the type evaluated will provide stable, symmetric nosetip shapes while undergoing high pressure, turbulent recession in ATDI environments. In addition, it was shown that these materials can be tailored, by weave configuration design, for specific bending strength requirements. Intercept missions through severe weather environments require an erosion-resistant subtip such as tungsten.

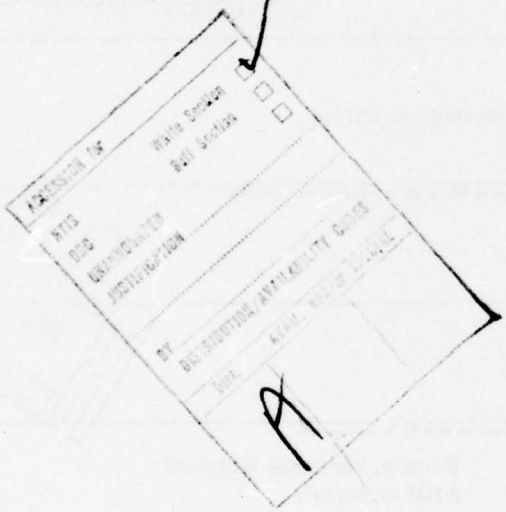

FOREWORD

This report documents the work performed and the results obtained on the Advanced Interceptor Materials (AIM) program during the period 1 July 1975 to 30 April 1976. The program is being conducted by Prototype Development Associates, Inc. (PDA), Santa Ana, California, for the Army Materials and Mechanics Research Center (AMMRC) under contract number DAAG 46-75-C-0099.

Mr. John F. Dignam is the AMMRC Program Manager and Mr. John R. Stetson is the Program Manager at PDA. The Principal Investigator for materials evaluation is Mr. J. C. Schutzler. The project was supported also by Mr. E. C. Alexander (Ablation Testing), and by Mr. Jim Joe (Ablation Data Reduction).

All of the carbon-carbon materials evaluated in this program were woven and densified by Fiber Materials, Inc. (FMI). These materials and the test time at the Air Force Flight Dynamics Laboratory 50 Megawatt arc-jet and at the Air Force Rocket Propulsion Laboratory rocket exhaust facilities were provided to PDA by AMMRC. Engineering properties characterization of the FMI 221 material was conducted at Southern Research Institute under the sponsorship of the Air Force Materials Laboratory (AFML contract F33615-74-C-5029). High velocity particle impact tests of the FMI 221 material were performed at Science Applications, Inc. (SAI) under sponsorship of the Air Force Space and Missile Systems Organization.

This page intentionally left blank

TABLE OF CONTENTS

TABLE OF CONTENTS (Continued)

LIST OF FIGURES

LIST OF FIGURES (Continued)

LIST OF FIGURES (Continued)

LIST OF FIGURES (Continued)

LIST OF TABLES

LIST OF TABLES (Continued)

1.0 INTRODUCTION AND SUMMARY

This report presents the results of tests and analytical evaluations of carbon-carbon materials for application to Advanced Terminal Defense Interceptor (ATDI) nosetips. The tests and evaluations performed during the period of this report were the second phase of the Advanced Interceptor Materials (AIM) Development program sponsored by the Army Materials and Mechanics Research Center (AMMRC) for the Department of Defense. The overall objective of this program is to develop materials concepts and designs for the next generation of Anti-Ballistic Missile (ABM).

The performance levels of the next generation of Anti-Ballistic Missiles (ABM), in particular, the Advanced Terminal Defense Interceptors (ATDI), impose severe design and performance requirements on missile nosetips. The nosetip is subjected to severe aerodynamic heating that may be coupled with high velocity particle impact from rain and nuclear dust clouds. Additionally, blast encounter and aerodynamic maneuvering will impose large dynamic bending loads on the nosetip.

To this end, the Army Materials and Mechanics Research Center (AMMRC), Watertown, Massachusetts, has pursued a program to develop and evaluate improved structural materials and designs for Advanced Terminal Defense Interceptors. The principal structural component considered in this study is the nosetip. The study was further restricted to materials and designs for passive (ablative) nosetips. This report covers the results of Phase II of the AIM program. The relationship of Phase II to the overall development plan for the Advanced Interceptor Material (AIM) program is shown in Figure 1.

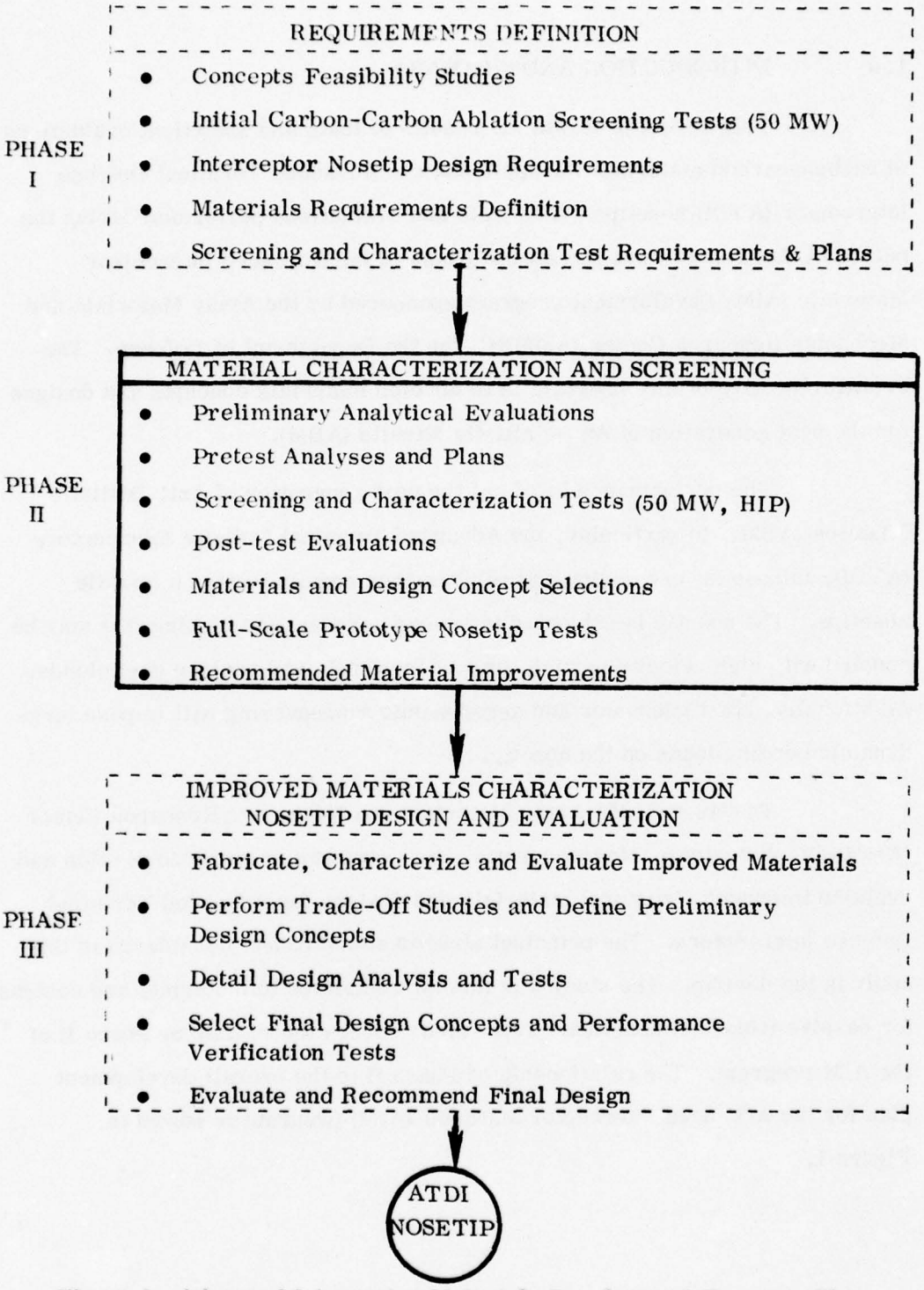

Figure 1: Advanced Interceptor Materials Development Program Plan

The present AMMRC passive nosetip program began in 1969 when early "SPRINT" flight test results showed that rain and dust erosion were major design-limiting factors in nosetip performance. When terminal defense (SAFEGUARD) became the primary defense mode in 1971, the development of a more advanced interceptor nosetip became a goal of AMMRC. This goal ultimately resulted in the inception of the AIM program at PDA in 1973.

A review of the limited amount of carbon-carbon data available at that time indicated that the way to achieve improved ablation performance and shape stability was to make higher density materials with finer weave spacings. In Phase I of the AIM program, performed by PDA under contract DAAG46-73-C-0174, several types of advanced carbon-carbon materials were reviewed and evaluated for ablation performance by arc-jet testing. The ablation performance was evaluated for carbon-carbons densified by resin, furfural, pitch, and chemical vapor deposition (CVD). One material appeared particularly promising, a fine-weave spacing preform densified with liquid pitch subsequently designated AMMRC/FMI 221.

In addition, ATDI nosetip material and design requirements were defined, and plans were prepared for screening and characterization of candidate ABM nosetip materials. The results of the AIM I program were reported in AMMRC TR 74-14 (Reference 1).

The Phase II program, described in this report, tested and evaluated analytically fourteen (14) carbon-carbon material candidates for passive nosetip concepts. The evaluation included analytical comparisons of material construction, high pressure arc-jet ablation tests, strength tests, and thermostructural tests of full-scale nosetips. Recommendations resulting from the test results have been included in an up-dated version of the nosetip development plan given in the final report of the Phase I program (See Section 3.3). Figure 2 shows a flow chart of the Phase II program tasks.

During the ten month period covered by this report, medium and high pressure ablation tests of the fourteen carbon-carbons were completed. Specimens were fabricated, and ablation tests were performed in the Air Force Flight Dynamics Laboratory (AFDL) 50 Megawatt Arc-Jet Facility and at the McDonnell Research Laboratories (MRL) High Impact Pressure (HIP) Facility. An analytical evaluation of the carbon-carbons was performed, and post-test analyses of the material ablation performance were conducted. Additional

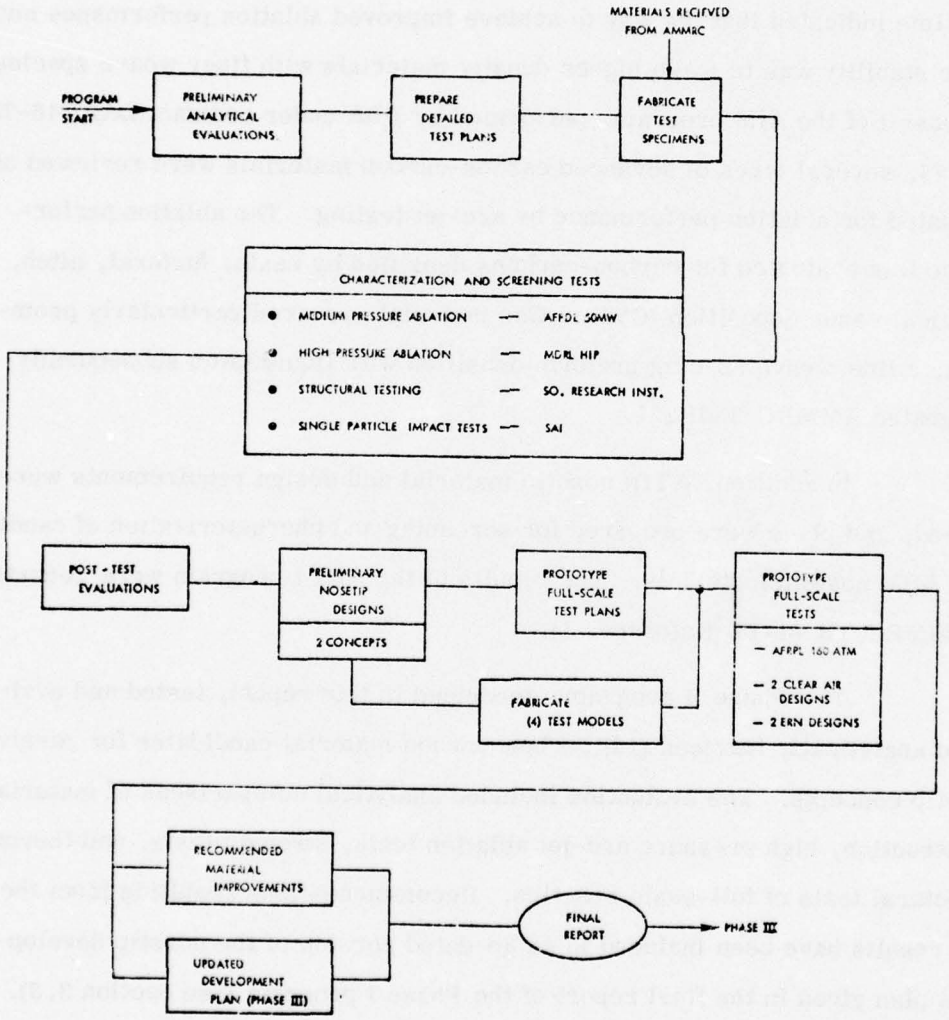

Figure 2: Phase II Program Flow Chart

characterization tests were performed at Southern Research Institute (SoRI) that included strength tests of five of the most promising materials and complete engineering property measurements of one of the materials (FMI 221). Six single-particle impact erosion tests of the FMI 221 were performed at the Science Applications, Inc. (SAI) test facility. Representative ATDI nosetip designs were developed for a typical ATDI mission. Four prototype models (two each of two designs) were fabricated, instrumented, and tested in a high pressure rocket exhaust facility. In addition, one flight test nosetip of FMI 221 was fabricated and analyzed for thermal and structural performance.

The results and conclusions developed during the performance of the work on this program are summarized below:

1. It was demonstrated clearly that advanced fine-weave carbon-carbon nosetip materials produced with Thornel 50 rayon yarns in an orthogonal weave configuration can lead to stable symmetric nosetip shapes while the material undergoes high pressure turbulent ablation processes. The symmetry of the ablating nosetip shapes associated with the AMMRC 221 fine-weave carbon-carbon will result in low trim, low lateral acceleration contributions as a result of the nosetip shape. It was further shown that these advanced fine-weave carbon-carbon materials can be configured to provide the bending load capability required during ATDI trajectories. It was also shown by full-scale tests of selected nosetip materials that these advanced fine-weave carbon-carbon nosetip materials can provide the thermostructural and bending load capabilities needed to meet the requirements of advanced terminal interceptor missions.

2. Design studies performed under this program demonstrated clearly that a carbon-carbon plug nosetip design with a 0.50-inch nose radius and a 2-inch overhang will accommodate the ablation performance requirements for application to an advanced terminal interceptor mission with high burnout velocity in the clear air environment. However, for a severe thunderstorm environment, an erosion-resistant material such as tungsten is required in addition to a carbon-carbon primary nosetip. The design analysis showed that an erosion-resistant concept provides a viable solution for a broad range of ATDI trajectories and weather environments.

3. The data base on the AMMRC/FMI 221 fine-weave carbon-carbon material was expanded substantially during this program. Mechanical and thermal properties were judged to be adequate to design full-scale ground and flight test hardware. One nosetip assembly incorporating the FMI 221 material was fabricated and delivered to Sandia Corporation for a SAMS flight test. Analysis of this design showed adequate thermostructural margins-of-safety.

4. In all, 14 different carbon-carbon materials were evaluated in a variety of arc-jet ablation conditions. The effects of reinforcing yarn types, weave spacings, and weave dimension variables on the ablation performance and strength characteristics of the materials were investigated fully. All the materials were densified with identical pitch processing at pressures of 10,000 psi to give densities of 1.9 grams per cubic centimeter on all materials. During ablation testing, variations in the average recession rate in the order of 10 percent were identified for those materials woven with

Thornel 50 rayon yarns. From the ablation results at the 75 atm test conditions, where ample data were obtained, a dependence of ablation rate on unit cell dimensions was observed. The smaller unit cell dimensions were associated with the lower ablation rates.

5. Tests of materials woven with Thornel 50 filaments demonstrated a tension failure in the yarn when the yarn was loaded to 60 percent of the virgin filament strength. When the pitch precursor filaments were loaded to approximately 100 percent of their virgin filament strength, failure was noted in the composites. This indicated a probable improvement in the matrix-filament bonding of the pitch-yarn system, which may improve both the shear strength and erosion resistance of the material.

6. Prototype full-scale nosetip designs suitable for advanced interceptor mission requirements were demonstrated successfully in high stagnation pressure ablation environments. Full-scale assemblies were evaluated and shown to be compatible with mission requirements. Those components tested included carbon-carbon plug and shell nosetip primary designs, an erosion-resistant tungsten subtip, a carbon phenolic forward skirt assembly, and a tantalum forward substructure for high temperature capability. During the full-scale tests, carbon-carbon-ablation behavior at 160 atm total pressure was shown to provide a symmetric shape with no thermostructural failure. Two thoriated tungsten subtip assemblies demonstrated symmetric ablation without thermostructural failure.

As a result of the work done under this program, recommendations for material improvements were made and those are summarized below:

1. It is recommended that pitch-based yarn materials be processed from yarns having 700 filaments to allow finer weave preforms. Development of these materials is needed to alleviate the dependence on rayon-based yarns now used almost exclusively in advanced carbon-carbon nosetip materials. The use of pitch-based yarn materials should also permit the exploitation of the improvement in filament-to-matrix bonding achieved with the pitch-based materials.
2. It is recommended that a systematic study be performed to optimize performance variations that can be achieved by altering processing variables including such things as carbon vapor deposition densification and billet stabilization, impregnation pressure, graphitization temperature, and the cyclic variations during densification.
3. Additional testing is clearly in order to define the process for optimization of material capability. Both the precursor and processing parameters should be systematically varied, and the test data base should be expanded to include suitable erosion tests and a more extensive tensile strength data base on materials at elevated temperatures.

The Advanced Interceptor Materials Development Plan was updated based on these results. The revised plan is given in Section 3.3.

2.0 PROGRAM RESULTS

Fourteen different three-dimensionally reinforced carbon-carbon materials (3DCC) were evaluated in the AIM Phase II program. The preforms for all the materials were woven by Fiber Materials, Inc. (FMI) from four different Union Carbide Corporation (UCC)-produced graphite yarns. FMI also densified the preforms to nominal densities of 1.9 gm/cc using Ashland A240 pitch at a processing pressure of 10,000 psi. The billets were graphitized at 2700°C. Consequently, a set of materials having identical preform weaving and densification processes were available for evaluation. This provided a unique opportunity to evaluate the effects of yarn types and preform weave geometries on the material properties.

Nineteen billets of the 3DCC materials were provided by AMMRC for evaluation. The materials are listed in Table 1 along with their dimensions, weights and densities. The centerline spacings of X (or Y) and Z-yarn bundles are also given. The material designation code assigned to each material describes the yarn type, the number of X, Y and Z yarns per site, and the number of Z sites per inch in the X or Y directions (reciprocal of the Z-spacing). The yarn types are coded as follows:

T400 - Thornel 400
T50 - Thornel 50
T75 - Thornel 75
P - UCC experimental pitch-precursor yarn.

Ablation tests were conducted in the Air Force Flight Dynamics Laboratory 50 Megawatt arc-jet facility (AFFDL 50 MW) at stagnation pressure conditions of 75 and 100 atmospheres. Additional ablation tests were conducted at the McDonnell Douglas Research Laboratories' High Impact Pressure Arc-jet Facility (MDRL HIP) at 168 atmospheres stagnation pressure. Five of the 3DCC materials were strength-tested at Southern Research Institute

TABLE 1: AMMRC CARBON-CARBON MATERIALS

MATERIAL DESIGNATION	FMI PN	DIMENSIONS X - Y - Z (Inches)	WEIGHT (gms)	DENSITY (gm/cc)	$C_L - C_L$ SPACING - S_x/S_z (Inches)
T400-8832-8	490	2.691 x 2.590 x 6.252	1307	1.83	.027/.125
T400-224-25	491	2.100 x 2.100 x 5.359	737	1.91	.025/.040
T400-222-33	483	2.185 x 2.165 x 5.492	803	1.89	.029/.030
T50-8832-8	228	2.475 x 2.515 x 6.360	1228	1.89	.026/.125
T50-226-25	563	2.112 x 2.168 x 4.090	574	1.87	.027/.040
T50-224-25	482	2.185 x 2.058 x 6.416	896	1.90	.024/.040
T50-223-33	557	4.126 x 3.960 x 3.858	1959	1.90	.034/.030
T50-222-33	893	2.183 x 2.156 x 5.019	740	1.91	.028/.030
	894	2.171 x 2.189 x 5.079	757	1.91	.028/.030
T50-221-44	500	2.211 x 2.229 x 5.251	802	1.90	.040/.023
	551	4.266 x 4.243 x 8.201	4677	1.92	.040/.023
	468	4.163 x 4.164 x 8.174	4418	1.90	.040/.023
	552	Not Received	--	--	.040/.023
T50-111-50	505	2.405 x 2.406 x 5.275	954	1.91	.024/.020
	719	2.425 x 2.430 x 5.212	957	1.90	.024/.020
T50-111-55	507	2.372 x 2.373 x 5.166	907	1.90	.031/.018
	508	2.393 x 2.404 x 5.336	978	1.94	.031/.018
T50-112-40	934	2.008 x 2.012 x 5.013	630	1.90	.021/.025
	935	Not Received	---	---	.021/.025
T75-111-50	718	4.451 x 4.430 x 8.109	5072	1.94	.017/.020
P-111-33	852	2.320 x 2.318 x 5.088	880	1.96	.045/.030

(SoRI) and one 4 x 4 x 8-inch billet was supplied to SoRI for more extensive mechanical and thermophysical properties characterization under joint AMMRC/ Air Force sponsorship. High velocity particle impact tests were conducted by Science Applications, Inc. (SAI) on one material and a nosetip for flight test on the Sandia Corporation SAMS vehicle was fabricated and analyzed for ablation and thermostructural response. Materials for the particle impact tests and the SAMS nosetip were provided by the AIM program in support of SAMSO-ABRES programs. Other material was provided to SAMSO for flight testing on the Advanced Nosetip Experiment A.N.T.-1 and the MINT vehicle. Based on the ablation and erosion test results, preliminary designs of ABM nosetips were sized for both clear air and weather intercept missions. Four prototype full-scale models were then fabricated and tested for performance at 160 atmospheres in the AFRPL/ABRES rocket exhaust facility. Allocation of materials and billet identification for all of these tests is given in Table 2.

The results of the tests performed, the evaluation of the data, and the results of analytical evaluations of the fourteen different 3DCC materials are described in the following sections.

2.1 Evaluation of Carbon-Carbon Materials

The strength, modulus and thermal expansion properties of fourteen 3DCC materials were predicted and compared along with the basic preform characteristics in order to gain a preliminary evaluation of the relative performance of the materials in advanced interceptor environments.

The basic properties of the reinforcement yarns are given in Table 3. The cross-sectional areas of the filaments were calculated from reported yarn deniers and used for subsequent calculations of filament volume fractions. However, for Thornel 50 the more commonly used value of $4.55 \times 10^{-8} in^2$ was used for these calculations. The pitch precursor yarn was not characterized. The strength and modulus values given in Table 3 for the pitch

TABLE 2: AIM II 3DCC BILLET ALLOCATION (FMI PART NUMBERS)*

MATERIAL	50 MW 75 ATM TESTS	50 MW 100 ATM TESTS	50 MW RAMP TESTS (75 ATM)	HIP 100 ATM TESTS	SoRI TENSILE TESTS	SoRI CHARACTER-IZATION	SAI PARTICLE IMPACT TESTS	RPL NOSETIP TEST	SAMS FLIGHT TEST NOSETIP	ANTI FLIGHT TEST NOSETIP	MINT FLIGHT TEST NOSETIP
T50-111-50	505 (2)	505 (4)		505 (3)	505 (3)						
T50-111-55	508 (3)			508 (2)	508 (3)			507 (1)			
T50-112-40	934 (3)	934 (2)		934 (1)	934 (3)			935 (1)			
T50-221-44	551 (4), 551 (2)	551 (4)	551 (3)	551 (3)		468**	551 (6)	551 (1), 500 (1)	551 (1)	552**	551 (1)
T50-222-33	893 (3)	893 (3)		893 (2)							
T50-223-33	537 (2)			537 (8)							
T50-224-25	482 (1)										
T50-226-25	563 (1)										
T50-8832-8	228 (1)										
T75-111-50	718 (3) 718 (1)	718 (1)	718 (1)	718 (2)	718 (3)			718			
P-111-33	852 (3)	852 (3)	852 (1)	852 (3)	852 (3)						
T400-224-25	491 (1)										
T400-222-33	483 (2)										
T400-8832-8	490 (1)										

* The number in parentheses indicates the number of specimens tested.

** The entire billet was consumed.

▭ Material was provided to other programs; data are not included in this report.

—— Material was provided to other programs; data are summarized in this report.

yarns are preliminary quantities from limited testing by FMI (Reference 2). Other data in the table are extracted from UCC literature (References 3, 4, 5).

TABLE 3: GRAPHITE YARN COMPARISON

	THORNEL 400	THORNEL 50	THORNEL 75	UCC PITCH
PRECURSOR	PAN	RAYON	RAYON	PITCH
FILAMENTS PER PLY	1500	720	720	2000
FILAMENTS PER YARN, N_f	1500	1440	1440	2000
DENIER/PLY (gm/9000 M)	698	322	270	2100
DENSITY, ρ (gm/cc)	1.77	1.66	1.80	1.88
FILAMENT CROSS-SECTION AREA, A_f * (10^{-8} in.^{2})	4.52	4.63	3.58	9.61
ELASTIC MODULUS, E (10^6 psi)	34	57	78	50
TENSILE STRENGTH, σ (ksi)	450	315	380	150-200

* $$A_f = \left(\frac{\text{Denier}}{N_f \rho}\right) 1.72 \times 10^{-7} \text{ in.}^2$$

A schematic showing the arrangement of X, Y, and Z-yarn bundles in a unit cell of carbon-carbon is given in Figure 3. The drawing also illustrates the terminology for preform yarn spacings where S_z and S_x are centerline spacings of Z and X (or Y) yarn sites, respectively.

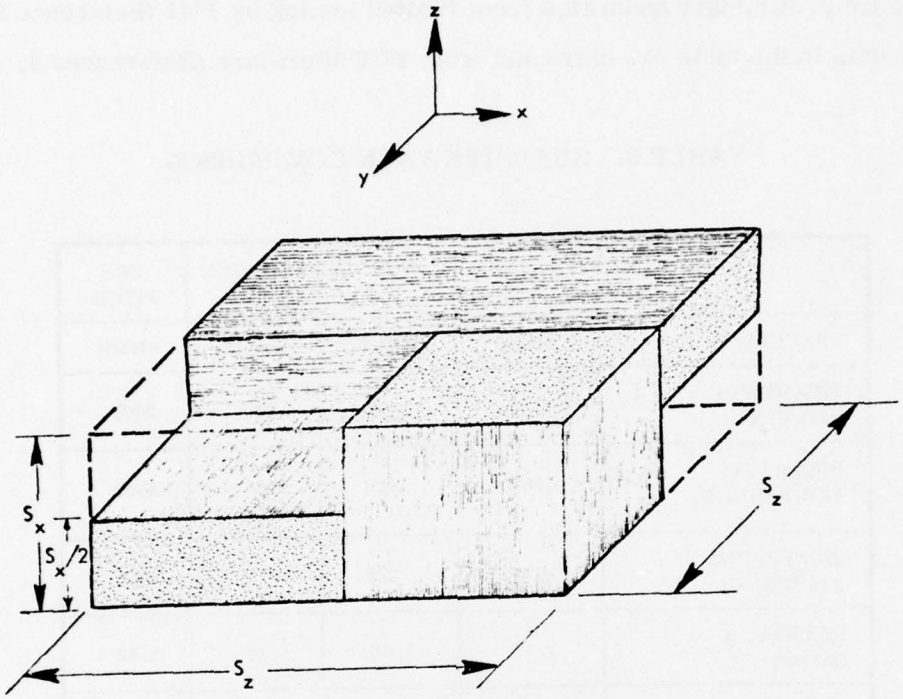

Figure 3: 3D Carbon-Carbon Unit Cell

The preform geometries and the calculated volume fractions of filament reinforcements are given in Table 4. The filament volume fractions were calculated from the following expressions.

$$V_{f_z} = \frac{N_z N_f A_f}{S_z^2}$$

$$V_{f_x} = \frac{N_x N_f A_f}{S_x S_z}$$

$$V_T = V_{f_z} + 2V_{f_x}$$

where N_z and N_x are the numbers of yarns per Z and X site, respectively.

The volume of the unit cell, $V_{uc} = S_x S_z^2$, is a relative measure of preform weave fineness and is also given in Table 4 for the various carbon-carbons.

It is clear from the data in Table 4 that the AIM II materials represent a very broad range of 3DCC preform parameters including filament volume fraction distribution between the X and Z directions and the unit cell volume. This diversity of material constructions provided an ideal base for correlation of the test results. A summary plot of the AIM II materials' unit cell volumes and volume fraction ratios (V_{f_z}/V_{f_x}) is presented in Figure 4. The volume fraction ratio is a measure of the filament distribution in the preform. The AIM materials range from "balanced" configurations, $V_{f_z}/V_{f_x} \simeq 1.0$ to "high-axial" configurations, $V_{f_z}/V_{f_x} \simeq 2.0$, and from "fine weaves", $V_{uc} \simeq 1 \times 10^{-5} in^3$, to "coarse weaves", $V_{uc} \simeq 40 \times 10^{-5} in^3$.

A 3DCC unit cell model previously developed and described in Reference 6 was used to estimate the thermostructural properties of the fourteen AIM II materials. The unit cell model uses constituent properties (filaments and matrix) and boundary conditions of strain compatibility between the constituents to predict the properties of the unit cell. Because the unit cell is a repeatable unit within the composite, it has the same properties as the composite. The properties of ATJS graphite were used to approximate the matrix material. The longitudinal modulus and strengh of the filaments are from Table 3. The transverse moduli and the thermal expansions of the filaments in both directions were computed by a model (described in Reference 6) based on transformation of the principal-direction properties of graphite crystals within the filaments. The resulting properties of the AIM II materials are summarized in Table 5. Tensile strength of a carbon-carbon material depends upon the degree of filament-to-matrix bonding, the in-situ straightness

TABLE 4: AIM 3DCC PREFORM CHARACTERISTICS

MATERIAL DESIGNATION	YARN DISTRIBUTION	YARN TYPE	S_z (Inches)	S_x (Inches)	V_{f_z} (%)	V_{f_x} (%)	V_{f_z}/V_{f_x}	V_T (%)	V_{uc} (10^{-5} in^3)
T50-111-55	1, 1, 1	T50	.018	.031	20.2	11.7	1.72	43.7	1.0
T50-111-50	1, 1, 1	T50	.020	.024	16.4	14.7	1.20	43.7	0.96
T50-112-40	1, 1, 2	T50	.025	.021	21.0	12.5	1.68	45.9	1.3
T50-221-44	2, 2, 1	T50	.023	.040	12.4	14.2	0.87	40.9	2.1
T50-222-33	2, 2, 2	T50	.030	.028	14.6	15.6	0.93	45.8	2.52
T50-223-33	2, 2, 3	T50	.030	.034	21.8	12.9	1.70	47.5	3.1
T50-224-25	2, 2, 4	T50	.040	.024	16.4	13.7	1.20	43.7	3.8
T50-226-25	2, 2, 6	T50	.040	.027	24.6	12.1	2.02	48.8	4.3
T50-8832-8	8, 8, 32	T50	.125	.026	13.4	16.1	0.83	45.7	40.6
T75-111-50	1, 1, 1	T75	.020	.017	12.9	15.2	0.85	43.2	0.68
P-111-33	1, 1, 1	P	.030	.045	21.4	14.2	1.50	49.8	4.1
T400-222-33	2, 2, 2	T400	.030	.029	15.1	15.6	0.97	46.2	2.6
T400-224-25	2, 2, 4	T400	.040	.025	17.0	13.6	1.25	44.1	4.0
T400-8832-8	8, 8, 32	T400	.125	.027	13.9	16.1	0.86	46.0	42.2

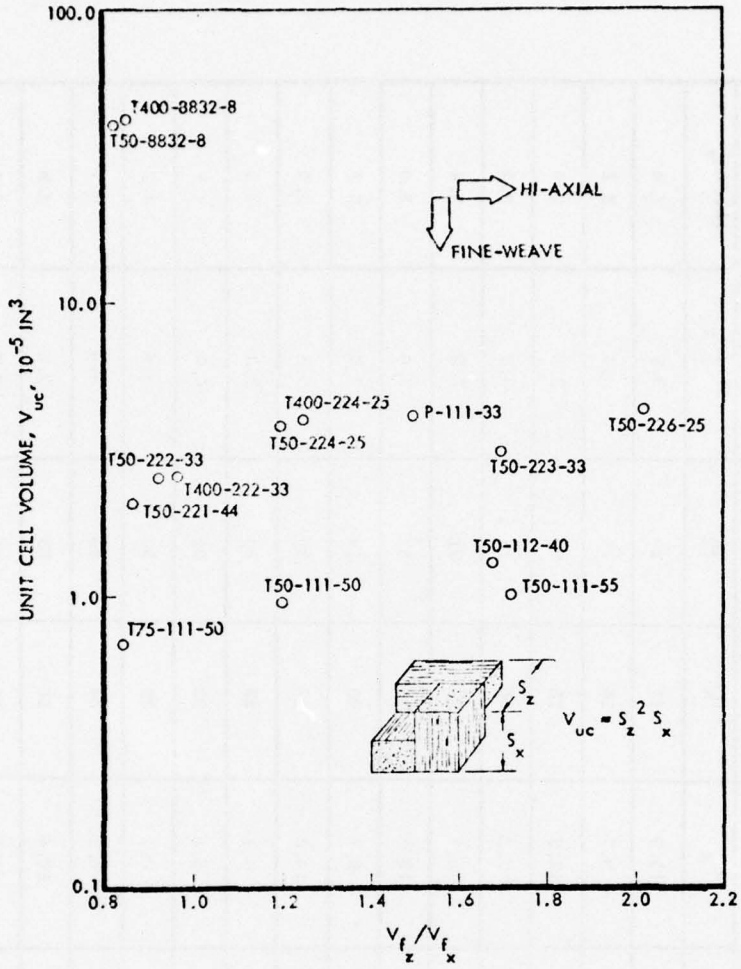

Figure 4: AIM II Materials Preform Geometry Comparison

of the filaments and any filament damage incurred during weaving as well as the filament strength. Tensile data on GE 223 carbon-carbon (Reference 7) were used to determine the effect of the above processing considerations on the effective in-situ strength of Thornel 50 filaments. It was concluded that the in-situ filament strength is about 46 to 53 percent of the average off-the-spool strength (Table 3) for the X and Z

TABLE 5: THERMOSTRUCTURAL PROPERTY PREDICTIONS AIM II 3D CARBON-CARBON

MATERIAL	ELASTIC MODULUS (RT) (MSI)		TENSILE STRENGTH (RT) (KSI)		THERMAL EXPANSION (RT-4000°F) (10^{-3} in/in)	
	E_x	E_z	σ_x	σ_z	$(\Delta L/L)_x$	$(\Delta L/L)_z$
T50-111-55	7.1	11.9	17	29	3.6	3.0
T50-111-50	8.2	9.7	20	24	3.4	3.2
T50-111-40	7.5	12.3	18	30	3.6	3.0
T50-221-44	8.5	7.5	20	18	3.3	3.5
T50-222-33	9.3	8.7	23	21	3.3	3.4
T50-223-33	7.7	12.8	19	32	3.6	3.0
T50-224-25	8.2	9.7	20	24	3.4	3.2
T50-226-25	7.4	14.3	18	35	3.8	2.9
T50-8832-8	9.6	8.1	23	20	3.3	3.5
T400-222-33	5.7	5.5	33	32	4.5	4.5
T400-224-25	5.0	6.1	29	36	4.6	4.2
T400-8832-8	5.8	5.1	34	30	4.4	4.7
T75-111-50	12.4	10.6	26	23	2.8	2.9
P-111-33	7.5	11.0	10	15	3.8	3.3

directions, respectively. An average in-situ filament strength factor of 50 percent was used for all of the AIM II materials, although it was certain that the FMI processing resulted in a different filament strength factor. (This effect was assessed after tensile testing six of the AIM II materials. The results, discussed in Section 2.4, indicated that the FMI-processed AIM materials with Thornel 50 yarns developed in-situ filament strength factors of 54 to 62 percent in the Z direction.)

The estimated axial tensile strengths of the AIM II materials are plotted in Figure 5 versus the fiber volume fraction ratio. The low strength estimated for the pitch yarn material is a result of low filament strengths (Table 3). However, as discussed in Section 2.4, the actual strength of the pitch material is considerably better than the estimate.

2.2 Arc-jet Tests

Medium and high pressure ablation tests of carbon-carbon specimens were performed in the RENT leg of the Air Force Flight Dynamics Laboratory 50 Megawatt arc-jet facility and at the McDonnell-Douglas Research Laboratory HIP arc-jet facility. The objectives of the two test series were as follows:

1. Evaluate fourteen candidate carbon-carbon materials for their possible application to passive nosetip concepts for advanced terminal interceptors.
2. Determine the effects of weave spacing and yarn type on thermochemical ablation rates and shape-change phenomena.
3. Rank the overall ablation performance of each material and compare with the results of earlier (Phase I) AIM program results.

4. Obtain test data needed to modify existing theoretical models used to predict the flight ablation behavior of carbon-carbon nosetip materials. Assess the validity of the models for each material from test results.

5. Establish recommendations for materials improvements.

Fifty specimens of carbon-carbon were tested at the 50 Megawatt facility at stagnation pressures of 75 and 100 atmospheres. Eighteen specimens were tested at the HIP facility at 168 atmospheres stagnation pressure. Table 6 gives the pertinent test conditions and numbers of specimens tested at each facility.

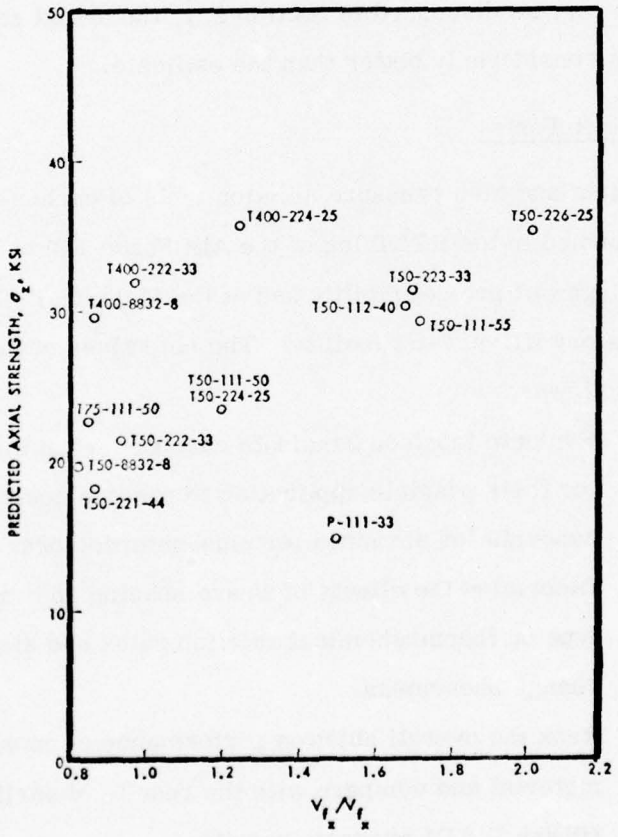

Figure 5: Predicted Strengths of AIM II Materials

TABLE 6: ABLATION TEST CONDITIONS FOR AMMRC CARBON-CARBON MATERIAL

FACILITY	AFFDL 50 MW		MDRL HIP
STAGNATION PRESSURE (ATM)	75	100	168
TOTAL BULK ENTHALPY (Btu/lb)	2300	2300	2500
CENTERLINE ENTHALPY (Btu/lb)	5500	6100	4500
NOZZLE EXIT DIAMETER (IN)	1.38	1.11	0.45
EXIT MACH NO.	1.75	1.8	1.7
SPECIMEN DIAMETER (IN)	0.72	0.50	0.30
AUTOMATIC MODEL POSITIONING	YES	YES	YES
ROTATING STING	YES	NO	NO
NO. OF SPECIMENS TESTED	30	20	18

2.2.1 50 Megawatt Tests

Two 50 Megawatt test series were performed. The first series was conducted in August 1975 and included thirty specimens tested at 75 atmospheres stagnation pressure and ten specimens tested at 100 atmospheres. The 75 atmosphere tests included both rotating and non-rotating specimens; the 100 atmosphere tests had only non-rotating specimens. The rotating sting test method was used for some of the 75 atmosphere tests because the particular flared design of this nozzle was known to result in somewhat asymmetric heating and ablation. This effect was less severe in the 100 atmosphere, parallel flow nozzle. In general, the rotating specimens ablated more symmetrically, although there was no significant difference in comparative ablation rates between spinning and non-spinning results. During the 100 atmosphere tests, a malfunction of the model positioning system occurred, and none of these specimens were maintained at the desired location with respect to the nozzle exit plane. Because of this occurrence, all of the 100 atmosphere data points were questionable. These tests were then repeated in a second entry in November with the same materials. The November entry was completely successful at the 100 atmosphere condition. All of the results have been reported in the following discussion; however, care should be used in the interpretation of the results of runs 74-07 and 74-08.

Ablation Test Specimens

Fourteen carbon-carbon test materials were supplied to PDA in billet form by the Army Materials and Mechanics Research Center. The structures of the different materials have been given in Table 1. The material designation of Table 1 identifies the fiber type, weave configuration (yarns per site), and the Z-sites per inch (reciprocal of C_L to C_L spacing). All of the materials were densified by FMI using Ashland A240 pitch.

Cutting plans for each billet that provided maximum utilization of material were prepared. Two specimen configurations, one for each test condition, were defined. Specimens which were intended for the 75-atmosphere model stagnation pressure test condition were machined into 0.721-inch diameter cone-cylinders as shown in Figure 6. Non-rotating specimens were assembled as shown in Figure 7. Rotating specimens were assembled according to Figure 8.

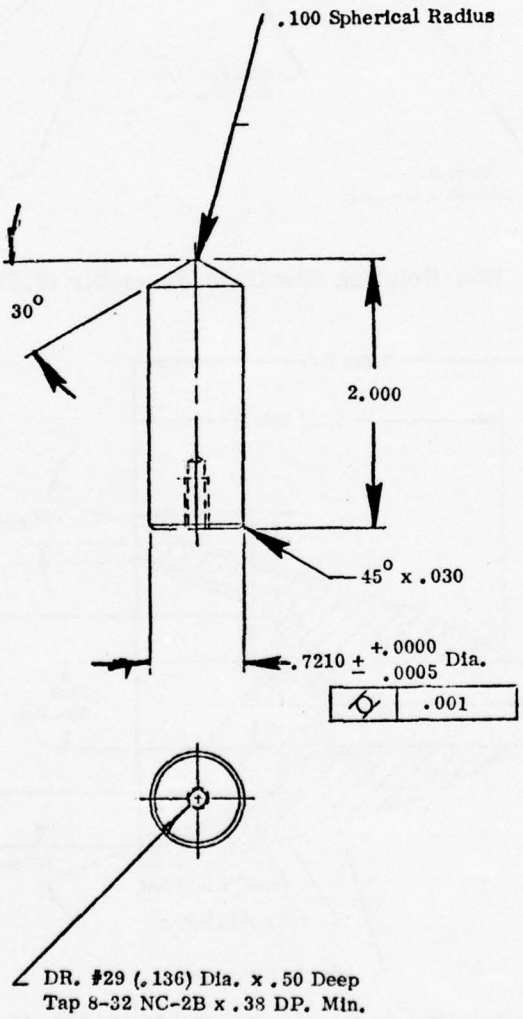

Figure 6: Cone-Cylinder Specimen (0.721-Inch Diameter)

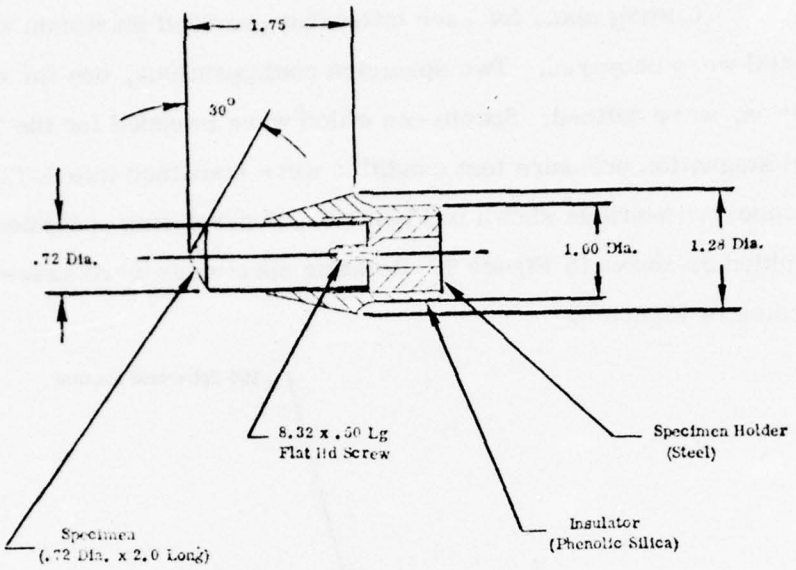

Figure 7: Non-Rotating Specimen Assembly (0.721-Inch Diameter)

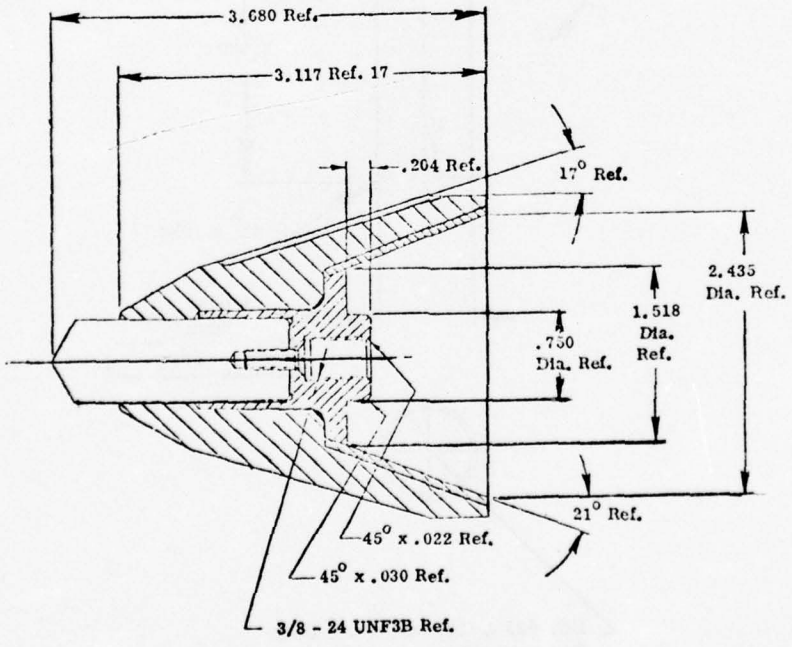

Figure 8: Rotating Specimen Assembly (0.721-Inch Diameter)

Specimens which were intended for the 100-atmosphere model stagnation pressure test condition were machined into 0.500-inch diameter cone-cylinders as shown in Figure 9. These specimens were all non-rotating and were assembled as shown in Figure 10.

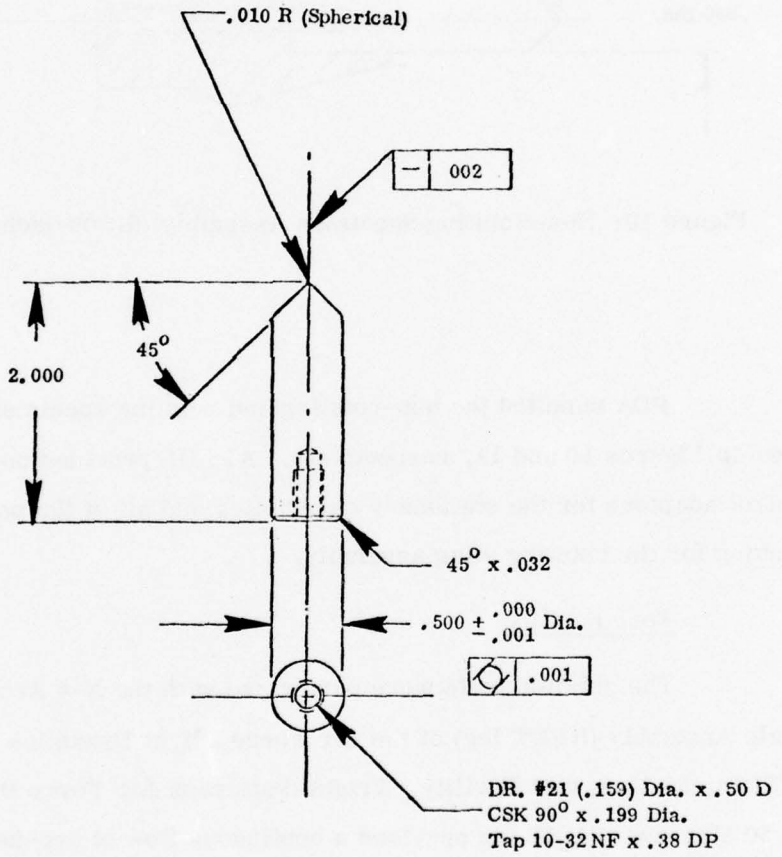

Figure 9: Cone-Cylinder Specimen (0.500-Inch Diameter)

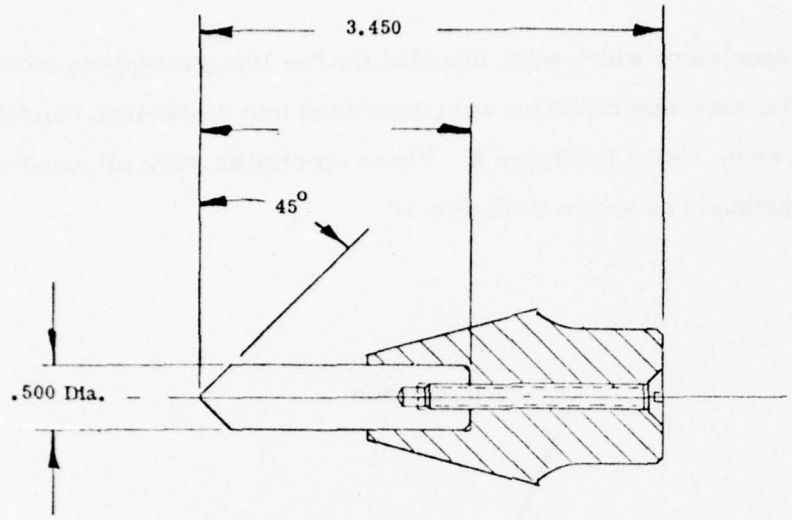

Figure 10: Non-Rotating Specimen Assembly (0.500-Inch Assembly)

PDA supplied the non-rotating and rotating specimen assemblies shown in Figures 10 and 11, respectively. AFFDL provided copper assembly-to-strut adapters for the stationary assemblies and all of the necessary plumbing for the rotating sting assembly.

Test Facility

The ablation tests were performed with the N-4 Arc Heater and Nozzle Assembly (RENT leg) of the Air Force Flight Dynamics Laboratory (AFFDL), 50 Megawatt Facility, Wright-Patterson Air Force Base, Ohio. The 50 Megawatt RENT leg provided a continuous flow of arc-heated air from a high pressure plenum. The high pressure air was exhausted through a water-cooled nozzle into a test section at ambient pressure. The 1.38-inch flared nozzle (10138F) and a plenum pressure of 1500 psia were used to

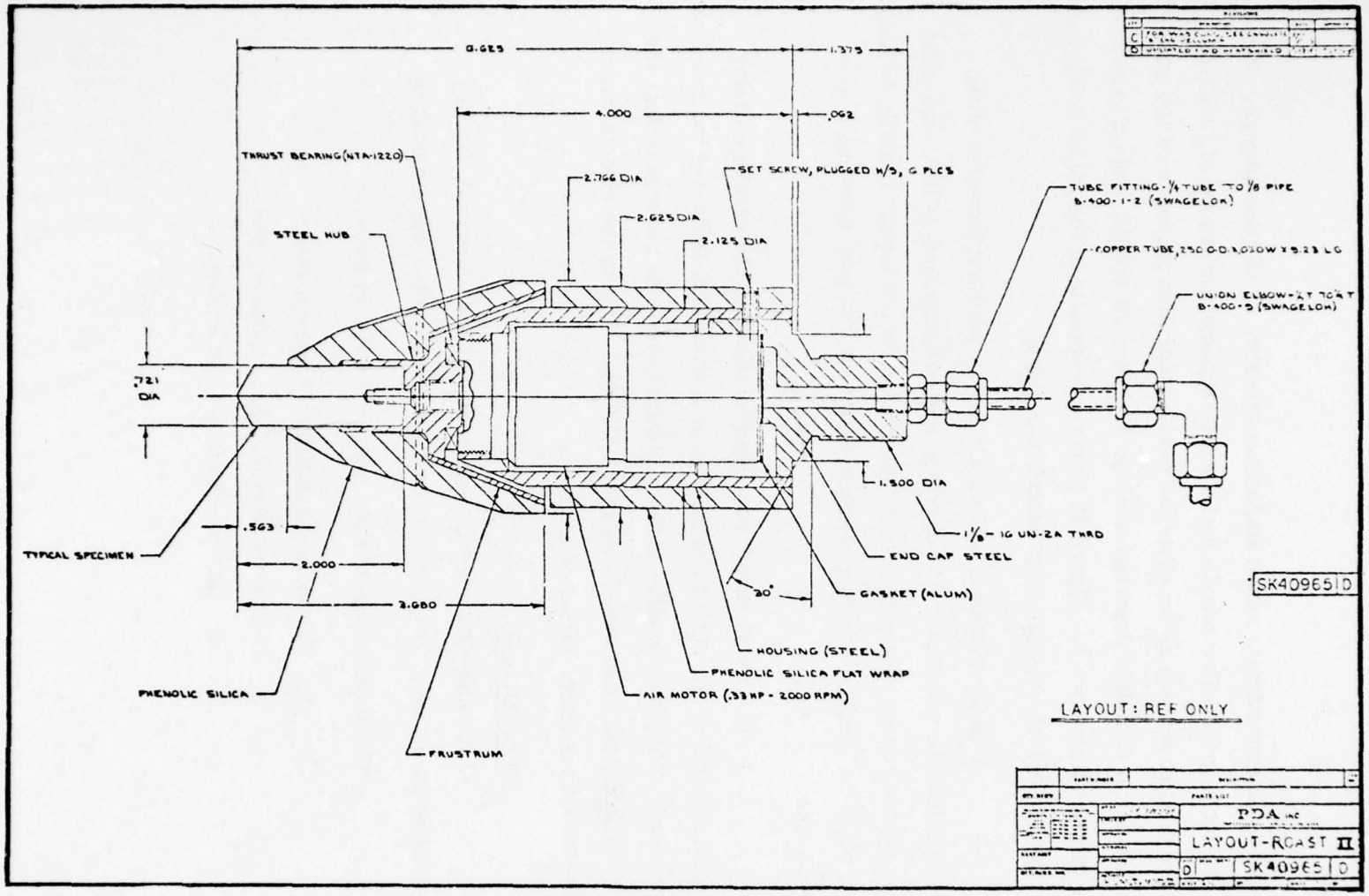

Figure 11: Rotating Sting Assembly

achieve an approximate model stagnation pressure of 75 atmospheres. The 1.11-inch parallel flow nozzle (09111P) and a plenum pressure of 1800 psia were used to achieve an approximate model stagnation pressure of 100 atmospheres. A complete description of the 50 Megawatt facility and its capabilities is given in Reference 8. Figure 12 shows a schematic of the major components of the RENT test leg with a test model in position.

A linear motion model carriage was used for insertion of the models into the test flow. The carriage was programmed so that each strut was pinned on centerline for 2 to 3 seconds and driven forward axially to keep the tip of the ablating model a constant 0.100 ± 0.010 inch from the nozzle exit plane.

A strut abort switch was incorporated into the carriage timing program to allow any strut to be aborted if a structural failure of the specimen occurred. This feature allowed the exposure time to be reduced to less than the present time when model conditions dictate. None of the models were aborted during either series of tests.

Test Method

Ten heater runs were performed by the 50 Megawatt facility operating personnel. Each heater run tested five carbon-carbon models.

The three different test conditions were as follows:

1. 75 atm/non-rotating/2.5 sec exposure
2. 75 atm/rotating/2.5 sec exposure, and
3. 100 atm/non-rotating/2 sec exposure.

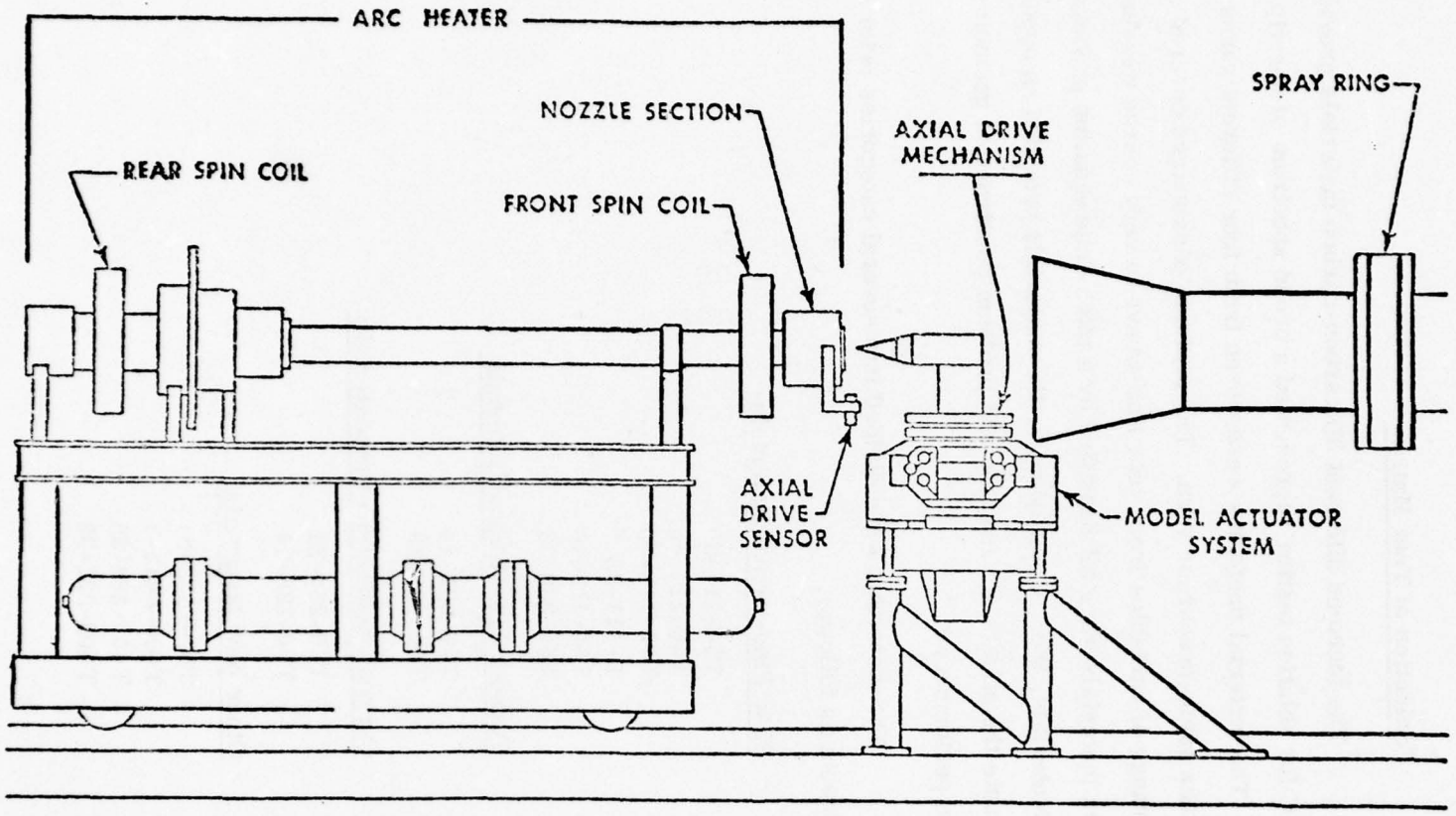

Figure 12: RENT Test Leg Schematic

Selection of Test Matrix

The fourteen different 3D carbon-carbon materials provided by AMMRC for ablation testing represented a broad spectrum of nosetip candidates. The material preforms were woven from four different yarns including a new pitch-precursor yarn. The preform parameters covered a very broad range of variables from very fine-weave to very coarse weaves. The fourteen materials were all densified by a pitch-impregnation process at Fiber Materials, Inc. Consequently, the materials provided an opportunity to evaluate the effects of yarn type and preform construction geometry on ablation performance.

The materials were divided into several categories prior to test assignments as follows:

New Fine-Weave Materials

T50-111-50
T50-111-55
T75-111-50
P-111-33
T50-112-40
T50-222-33

Current Fine-Weave Materials

T50-221-44
T50-223-33

Current Medium-Weave Materials

T50-224-25
T50-226-25

Other New Materials

T50-8832-8
T400-8832-8
T400-224-25
T400-222-33

Emphasis was placed on obtaining ablation test data on the new fine-weave materials. Three 75-atmosphere tests were planned for each of the six materials in this category. At least one of the three specimens was to be rotated during test in the arc. One-hundred atmosphere tests were conducted on the new fine-weave materials and on the T50-221-44 material for reference. At least one test was performed at 75 atmospheres on each of the remaining materials. Where only one sample of a material was tested at 75 atmospheres, it was a rotating specimen.

Table 7 summarizes the assignment of materials and test conditions for the first entry according to the material categories. The assignment of models to each heater run was based on material similarity and expected material delivery date. Table 8 shows the assignment of models for each 75 atmosphere heater run, and Table 9 shows the model assignments for the 100 atmosphere tests.

The exposure duration was initially 3 seconds for the first rack tested. This was reduced to 2.75 seconds for the second rack and to 2.5 seconds for the subsequent runs by mutual agreement between AFFDL and the responsible PDA engineer because of excessive ablation of the heatshield.

The data obtained from each specimen test included recession history, recession profiles from film data, and surface temperature. These data were used to rank the performance of each material. Material performance and recession data were obtained from two sources. Primary data were taken from readings of the high-speed film cameras. Secondary data were available from the strut axial position induction as recorded on a high-speed oscillograph. High-speed photographic coverage included three cameras looking at the tip from overhead and from 45 degrees to either side. Additional instrumentation included recording pyrometers for surface temperature measurement as close to the stagnation point as possible.

TABLE 7: MATERIAL/TEST ASSIGNMENT
(First 50 Megawatt Entry)

CATEGORY	DESIGNATION	NUMBER OF SPECIMENS AT EACH CONDITION			TOTAL SPECIMENS
		75 ATM/NR* (3-SECOND EXPOSURE)	75 ATM/R* (3-SECOND EXPOSURE)	100 ATM/NR ** (2-SECOND EXPOSURE)	
New Fine-Weave Materials	T50-111-50	2	1	4	7
	T75-111-50	2	1	4	7
	P-111-33	1	2	3	6
	T50-111-55	2	1	---	3
	T50-112-40	1	2	2	5
	T50-222-33	2	1	3	6
Current Fine-Weave Materials	T50-221-44	2	1	4	5
	T50-223-33	1	1	---	2
Current Medium-Weave Materials	T50-224-25	---	1	---	1
	T50-226-25	---	1	---	1
Other New Materials	T400-222-33	1	1	---	2
	T400-8832-9	---	1	---	1
	T400-224-25	---	1	---	1
	T50-8832-8	---	1	---	1
TOTAL		14	16	10	40

*NR = Non-Rotating, R = Rotating

**These tests were repeated in the second entry, thereby doubling the number of specimens at this condition.

TABLE 8: 50 MEGAWATT TEST SUMMARY
75 ATM FLARED NOZZLE

Revised
9-17-75

RUN NO. 74-	STRUT	MODEL NO.	MODEL DESCRIPTION	BILLET NO.	ROTATION CODE (a)	DWELL		RECESSION, ΔX (IN)	$\Delta X/\Delta\tau$ (IN/SEC)	$\dot{S}_{ss}$ (IN/SEC) (b)	REMARKS
						PRESSURE (ATM)	TIME, $\Delta\tau$ (SEC)				
01	1	3-1	T50-111-55	508	NR	75	2.95	0.455	0.154	0.166	
	2	3-2	T50-111-55	508	R		2.94	0.424	0.144	0.170	
	3	3-3	T50-111-55	508	NR		2.97	0.459	0.154	0.183	Model Lost After Exit
	4	3-4	T400-222-33	483	R		3.05	0.593	0.194	0.211	
	5	3-5	T400-222-33	483	NR		3.07	0.639	0.208	0.223	
02	1	4-1	T50-221-44	551	NR	75	2.72	0.404	0.148	0.161	
	2	4-2	T50-221-44	551	R		2.76	0.401	0.145	0.160	
	3	4-3	T50-221-44	551	NR		2.80	0.452	0.161	0.186	
	4	4-4	T50-223-33	557	R		2.80	---	---	0.144	Axial Drive Did Not Control
	5	4-5	T50-223-33	557	NR		2.82	0.503	0.178	0.196	
03	1	1-1	T50-111-50	505	NR	75	2.56	0.386	0.150	0.169	
	2	1-2	T50-111-50	505	R		2.55	0.356	0.140	0.159	
	3	11-1	T50-221-44	551	NR		2.56	0.423	0.165	0.181	
	4	1-4	T50-224-25	482	R		2.42	0.422	0.174	0.203	
	5	1-5	T50-226-25	563	R		2.59	0.416	0.160	0.206	
04	1	2-1	T75-111-50	718	NR	75	2.57	0.398	0.154	0.177	
	2	2-2	T75-111-50	718	R		2.56	0.381	0.149	0.169	
	3	2-3	T75-111-50	718	NR		2.60	0.431	0.166	0.171	
	4	2-4	T400-8832-8	490	R		2.44	0.475	0.194	0.215	
	5	2-5	T400-224-25	491	R		2.60	0.435	0.167	0.206	
05	1	5-1	P-111-33	852	NR	75	2.56	0.440	0.172	0.184	
	2	5-2	P-111-33	852	R		2.56	0.410	0.160	0.166	
	3	5-3	T50-112-40	934	NR		2.60	0.375	0.144	0.161	
	4	5-4	T50-112-40	934	R		2.53	0.367	0.145	0.184	Model Broke On Exit
	5	5-5	P-111-33	852	R		2.52	---	---	0.131	Axial Drive Did Not Control
06	1	6-1	T50-222-33	893	NR	75	2.57	0.409	0.159	0.166	
	2	6-2	T50-222-33	893	R		2.55	0.393	0.154	0.172	
	3	6-3	T50-222-33	893	NR		2.61	0.418	0.160	0.177	
	4	6-4	T50-8832-8	228B	R		2.42	**0.435**	0.180	**0.210**	
	5	6-5	T50-112-40	934	R		2.60	0.364	0.140	0.173	

NOTES:
(a) Rotation Code: NR ≡ Stationary
R ≡ Rotating at 1200 rpm
(b) Steady-state recession rate measured from film data

TABLE 9: AIM 50 MEGAWATT TEST SUMMARY - 100 ATM PARALLEL NOZZLE

RUN NO. 74-	STRUT	MODEL NO.	MODEL DESCRIPTION	BILLET NO.	ROTATION CODE (a)	DWELL PRESSURE (ATM)	DWELL TIME (SEC)	RECESSION (IN)	$\Delta X/\Delta\tau$ (IN/SEC)	$\dot{S}_{ss}$ (IN/SEC) (b)	REMARKS
07	1	7-1	T50-221-44	551	NR	100	1.95	0.520	0.267	0.285	All Models Driven Into Nozzle
	2	7-2	T50-111-50	505			1.95	0.415	0.213	0.266	
	3	8-3	T50-222-33	893			1.96	0.559	0.285	0.324	
	4	7-4	T75-111-50	718			1.69	0.417	0.247	0.286	
	5	8-5	T50-112-40	934			1.90	0.554	0.292	0.326	
08	1	8-1	T50-221-44	551	NR	100	1.95	0.550	0.282	0.305	All Models Driven Into Nozzle
	2	8-2	T50-222-33	893			1.95	0.502	0.257	0.273	
	3	7-3	T50-111-50	505			1.97	0.555	0.282	0.310	
	4	8-4	P-111-33	852			1.71	0.549	0.321	0.343	
	5	7-5	T75-111-50	718			1.88	0.572	0.304	0.350	
09	1	9-1	T50-221-44	551	NR	100	2.21	0.538	0.243	0.300	
	2	9-2	T50-111-50	505			2.24	0.537	0.240	0.300	
	3	9-3	T50-222-33	893			2.28	0.560	0.246	0.283	
	4	9-4	P-111-33	852			2.08	0.528	0.254	0.296	
	5	9-5	T75-111-50	718			2.20	0.505	0.230	0.261	
10	1	10-1	T50-221-44	551	NR	100	2.21	0.572	0.259	0.297	
	2	10-2	T50-111-50	505			2.27	0.590	0.260	0.314	
	3	10-3	T50-112-40	934			2.22	0.597	0.269	0.333	
	4	10-4	P-111-33	852			2.15	0.579	0.269	0.312	
	5	10-5	T75-111-50	718			2.17	0.514	0.237	0.278	

NOTES:

(a) Rotation Code: NR ≡ Stationary
R ≡ Rotating at 1200 rpm

(b) Steady-state recession rate measured from film data

Results

The first eight heater runs were performed in August 1975. Table 8 gives a summary of the results of the first six steady-state runs performed at 75 atmospheres in the 1.38-inch diameter flared nozzle. The seventh and eighth runs were performed at 100 atmospheres in the 1.11-inch diameter parallel flow nozzle and are summarized in Table 9.

Examination of the film data showed the results of the seventh and eighth runs to be questionable because the model axial positioner drove each specimen forward into the nozzle during exposure. This problem was caused by a broken sensor cable in the positioner control circuit. As a result, the sidewall heating was increased on these models and the steady-state turbulent biconic shape was not maintained during ablation. It was decided to machine additional test specimens and retest at these same conditions. The retests were completed successfully in November as run numbers nine and ten. These data are reported also in Table 9. It should be noted that in some cases there was little change in ablation rate due to the effect of the model positioner. This was due to the parallel flow design of the nozzle.

The data obtained from each specimen tested included recession history and recession profiles from film data, model positioner data, and surface temperature histories. The detailed test results including stagnation point recession histories and shape profiles observed from the films and post-test photographs of each specimen tested were given in the Program Interim Report (Reference 9); the overall results are discussed in the next few paragraphs.

Discussion of Results

The first heater run (74-01) exposed each specimen for 3.0 seconds. This exposure time exceeded the protective capability of the non-rotating model

holder and heatshield for this diameter specimen, and consequently, one of the specimens (3-3) was lost on exit from the arc-jet. Therefore, the second run (74-02) was set to expose each specimen for only 2.75 seconds. This time also appeared to be marginal in terms of heatshield survival for the non-rotating holder, although all test specimens were recovered. The exposure time was then reduced to 2.5 seconds for the remainder of the 75 atmosphere tests. Only one other specimen (5-4) was lost during exit from the arc-jet, and this was due to striking the side of the nozzle. Valid recession data were obtained for both of these models from the films. The axial drive model positioner did not control properly for two other specimens (4-4 and 5-5). Because model position was more critical in the flared nozzle flowfield than in the parallel flow nozzle, the results of these two tests were of doubtful validity and were not included in the analysis of the results. In addition, model 1-3 (T50-111-50) was broken during pretest operations and was replaced with a spare T50-221-44 specimen (11-1).

Table 10 summarizes the average steady-state recession results for each of the materials tested, listed in order of increasing average recession rate. From this table it is seen that the steady-state recession rate of all replicate specimens was within $\pm$ 8 percent of the average for each material. In general, the measured rates from rotating specimens were nearly always slightly lower than the average rate. This may have been due to the effects of model asymmetry on local heating and ablation.

The mean recession rates of the first seven materials listed in Table 10 varied less than the maximum variation indicated for replicate specimens. However, the remainder of the materials (indicated below the dashed line of Table 6) had significantly higher recession rates. The principal interest lies therefore with the seven materials above the dashed line, which include all of the new materials of interest in addition to T50-221-44.

TABLE 10: AVERAGE RECESSION RATE AT 75 ATMOSPHERES

- 10138F Nozzle
- Steady-state Data from Films
- Ranked According to Average Recession Rate

MATERIAL	STEADY-STATE TURBULENT RECESSION RATE (IN/SEC)				
	ROTATING SPECIMENS	NON-ROTATING SPECIMENS	AVERAGE	VARIATION	
				Maximum	Percent
T50-111-50	.159	.169	.164	.005	3.9
T75-111-50	.169	.171, .177	.172	.005	2.9
T50-221-44	.160	.161, .181, .186	.172	.014	8.1
T50-222-33	.172	.166, .177	.172	.006	3.5
T50-111-55	.170	.166, .183	.173	.010	5.8
T50-112-40	.173, .184	.161	.173	.012	6.9
P-111-33	.166	.184	.175	.009	5.1
T50-223-33	---	.196	.196	---	---
T50-224-25	.203	---	.203	---	---
T400-224-25	.206	---	.206	---	---
T50-226-25	.206	---	.206	---	---
T50-8832-8	.210	---	.210	---	---
T400-8832-8	.215	---	.215	---	---
T400-222-33	.211	.223	.217	0.06	2.8

Three specimens of this latter material had been tested in the 50 Megawatt during the AIM Phase I program, and an average recession rate of 0.235 inch per second was measured at 80 atmospheres stagnation pressure. This difference in recession rate should be attributed to differences in specimen size and nozzle configuration. The measured ablation rate in the 75 atmosphere, flared nozzle may be corrected to the 80 atmosphere parallel flow nozzle by the relation:

$$\dot{S}_{80} = \dot{S}_{75} \left(\frac{P_{80}}{P_{75}} \right)^{0.8} \left(\frac{D_{80}}{D_{75}} \right)^{-0.2}$$

where $\dot{S}$ is the steady-state recession rate
P is the local surface pressure
D is the specimen diameter, and
the subscripts 80 and 75 refer to the respective nozzle and test conditions.

Applying this correction to the data for T50-221-44 gives

$$\dot{S}_{80} = 0.172 \left(\frac{80}{75}\right)^{0.8} \left(\frac{0.50}{0.72}\right)^{-0.2} = 0.195 \text{ inches/second}$$

which is still less than the average rate measured for the Phase I tests. This difference is attributed to the different flow and enthalpy expansion characteristics of the flared nozzle used in the Phase II tests.*

As indicated above, all of the 100 atmosphere specimens from runs 7 and 8 were driven into the nozzle. Initially therefore, these data were not considered valid and the tests were repeated. The latter two racks performed satisfactorily. Table 11 compares the average steady-state ablation rate of each 100 atmosphere specimen. These materials tested at 100 atmospheres were ranked in order of increasing recession rate based on the average of runs 9 and 10, which were repeatable to within $\pm$ 3 percent of the mean. If the materials were ranked on the basis of the average rates from all four 100 atmosphere tests, the relative performance would be almost the same except for the T50-111-50 material. The mean ablation rate from all four runs was within 10 percent of the mean rate from runs 9 and 10. On this basis, the test data of four specimens from runs 7 and 8 that varied by greater than 10 percent from the mean of runs 9 and 10 were considered questionable because of the inaccurate sting positioning.

---

* Indeed subsequent tests of two T50-221-44 specimens taken from the same billet as the above specimens gave an average steady-state turbulent ablation rate of 0.241 inches/second (Reference 10), which was nearly identical to the average recession rate measured in the Phase I tests. See Section 2.5 for a compilation of all T50-221-44 ablation data.

TABLE 11: AVERAGE RECESSION RATE AT 100 ATMOSPHERES

- 09111P Nozzle
- Steady-state Data from Films

MATERIAL	STEADY-STATE TURBULENT RECESSION RATE (IN/SEC)					
	74-07	74-08	74-09	74-10	Average of 9 & 10	Average of 7, 8, 9 & 10
T75-111-50	.286	.350*	.261	.278	.270 ± .009	.294
T50-222-33	.324*	.273	.283	---	.283	.293
T50-221-44	.285	.305	.300	.297	.298 ± .002	.298
P-111-33	---	.343*	.296	.312	.304 ± .008	.317
T50-111-50	.266*	.310	.300	.314	.307 ± .007	.298
T50-112-40	.326	---	---	.333	.333	.330

*Variation greater than ± 10 percent from average of tests 9 and 10; Questionable data point.

Table 12 summarizes all of the 50 Megawatt recession data points that were obtained. Of fifty specimens tested, valid recession data were obtained on thirty-eight specimens and probably on six more. Forty-eight of the fity specimens were recovered for post-test analysis and evaluation. Post-test analysis of individual specimen performance will be discussed in Section 2.3.

Conclusions

Based on the ten 50 Megawatt runs at 75 and 100 atmospheres, the following conclusions were made:

1. Measured 75 atmosphere, steady-state recession rates were consistent and repeatable to within or less than ± 8 percent for all replicate specimens.
2. Rotating models gave more symmetrical results and usually a slightly lower than average steady-state recession rate.

TABLE 12: SUMMARY OF 50 MEGAWATT DATA OBTAINED

NOZZLE	10138F	09111P	TOTAL
STAGNATION PRESSURE (ATM)	75	100	
NO. OF HEATER RUNS	6	4	10
NO. OF MODELS TESTED	30	20	50
SPECIMENS RECOVERED	28	20	48
AXIAL DRIVE DID NOT CONTROL	2	0	2
STRUT DROVE INTO NOZZLE	0	10*	10
VALID RECESSION DATA OBTAINED	28	10	38

*Some results from these runs may still be valid because the parallel flow nozzle was used. Data analysis indicates that six of these data points from runs 7 and 8 may be valid.

3. Measured 100 atmosphere, steady-state recession rates were repeatable to within ± 3 percent for the two runs which had correct operation of the model positioner. The data from the first two 100 atmosphere runs exhibited excessive scatter due to a malfunction of the sting positioner.

4. Steady-state ablation rates measured in the flared nozzle were lower than in the parallel flow nozzle used for the Phase I tests (after correcting for pressure and model size differences). This effect was caused by flowfield differences between the two nozzles.

5. All specimens maintained approximately their initial shape during ablation (except when the model positioner failed to operate correctly). This is indicative of steady-state, turbulent flow. High-quality, turbulent recession data were obtained on relatively small diameter specimens of carbon-carbon.

6. The seven best-performing carbon-carbons were as follows (listed in order of increasing average recession rate):

P_{T_2} = 75 ATM	P_{T_2} = 100 ATM
T50-111-50	T75-111-50
T75-111-50	T50-222-33
T50-221-44	T50-221-44
T50-222-33	P-111-33
T50-111-55	T50-111-50
T50-112-40	T50-112-40
P-111-33	---

These are the seven materials that were recommended for further evaluation at the HIP high pressure ablation test facility and for strength characterization tests.

2.2.2 HIP Tests

High pressure ablation tests of seven different carbon-carbons were performed in the McDonnell-Douglas Research Laboratories (MDRL) High Impact Pressure (HIP) Arc-Jet Facility in St. Louis, Missouri. Seven of the fourteen materials tested in the 50 Megawatt series were selected for high pressure tests at 168 atmospheres.

Ablation Test Specimens

The selection of materials tested in the HIP facility is shown in Table 13. Cutting plans were prepared for each billet that provided maximum utilization of material. The indicated number of specimens were machined by PDA to the configuration shown in Figure 13.

Test Facility

The ablation tests were performed at the MDRL HIP arc-jet facility in St. Louis, Missouri, at a nominal model stagnation pressure of 168 atmospheres. The Mach 1.7, 0.45-inch exit diameter nozzle was used.

TABLE 13: AMMRC CARBON-CARBON MATERIALS
TESTED IN HIP FACILITY

MATERIAL DESIGNATION (1)	FIBER TYPE	WEAVE CONFIGURATION (YARNS/SITE)	℄ TO ℄ SPACING (IN)	BILLET NUMBER	BILLET DENSITY (GM/CC)	NUMBER OF SPECIMENS
T50-111-50	T50	1, 1, 1	.020	505	1.91	3
T75-111-50	T75	1, 1, 1	.020	718	1.94	2 + 1 Spare
P-111-33	PITCH	1, 1, 1	.030	852	1.96	3
T50-111-55	T50	1, 1, 1	.018	508	1.94	2
T50-112-40	T50	1, 1, 2	.025	934	1.90	3
T50-222-33	T50	2, 2, 2	.030	893	1.91	2
T50-221-44	T50	2, 2, 1	.023	551	1.92	3

(1) Yarn Type - Weave Configuration (Yarns/Site in X, Y, Z Directions - Z-Yarn Sites Per Inch)

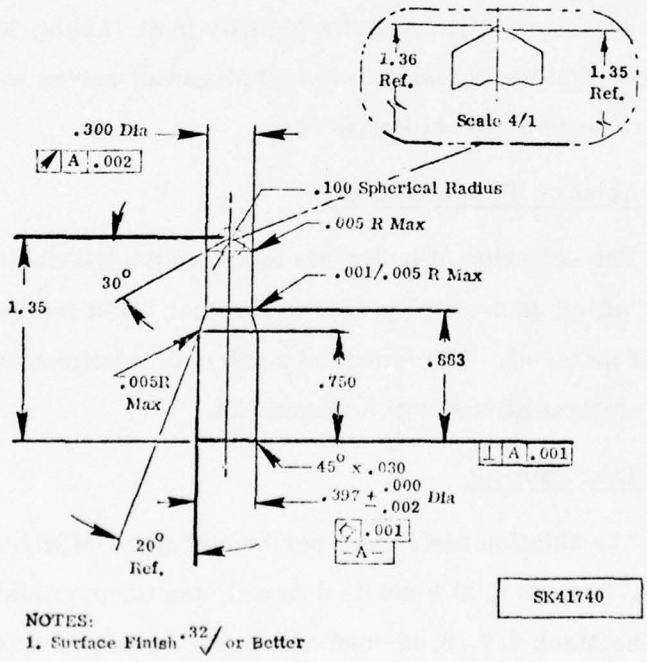

Figure 13: HIP Ablation Specimen Configuration

Test Method

The seven sting positions for each of three arc-jet runs were occupied by six ablation models andone HIP-supplied calorimeter. The models were inserted into the jet stream at a fixed position from the nozzle exit plane. As recession occurred, the models were driven forward by a laser-controlled servo compensator to maintain the model stagnation point in the constant pressure test region. The models were removed from the test position after two-tenths inch of total compensator travel (or approximately 0.2 inch of model recession).

Three heater runs were performed by MDRL operating personnel. Each run included six carbon-carbon models and one facility-supplied calorimeter. Table 14 shows the assignment of models for each run. The data obtained from each specimen test included recession history and recession profiles from film data, model compensator data, and surface temperature.

The results of all three heater runs are summarized also in Table 14. This table gives the total measured recession, the average recession and the steady-state turbulent recession rate obtained by analysis of the high-speed film data. The detailed stagnation point recession histories and shape profiles observed from the films of each specimen tested were given in Reference 9.

Discussion of Results

In Table 15 the materials are listed in the order of increasing average steady-state turbulent recession rate. The average steady-state ablation rate varied from 0.374 inch per second for T50-222-33 to 0.423 inch

TABLE 14: AIM HIP TEST RESULTS

RUN NO.	STRUT	MODEL NO.	MODEL DESCRIPTION	BILLET NO.	DWELL		RECESSION, ΔX (IN)	$\Delta X/\Delta\tau$ (1) (IN/SEC)	$\dot{S}_{ss}$ (2) (IN/SEC)
					PRESSURE (ATM)	TIME, $\Delta\tau$ (SEC)			
001	2	1-2	T50-112-40	934	168	.51	.182	.357	.375
(MDRL	3	1-3	T50-221-44	551	↓	.62	.227	.366	.407
1019)	4	1-4	P-111-33	852		.63	.222	.352	.383
	5	1-5	T50-111-55	508		.80	.204	.255	.281
	6	1-6	T50-222-33	893		.65	.227	.349	.376
	7	1-7	T50-111-50	505		.52	.199	.383	.398
002	2	2-2	T50-112-40	934	168	.67	.277	.413	.454
(MDRL	3	2-3	T50-221-44	551	↓	.61	.200	.328	.360
1020)	4	2-4	P-111-33	852		.45	.182	.404	.435
	5	2-5	T50-111-55	508		.64	.234	.366	.400
	6	2-6	T75-111-50	718		.63	.239	.379	.392
	7	2-7	T50-111-50	505		.69	.259	.375	.466
003	2	3-2	T50-112-40	934	168	.63	.259	.411	.440
(MDRL	3	3-3	T50-221-44	551	↓	.69	.252	.365	.383
1021)	4	3-4	P-111-33	852		.66	.260	.394	.414
	5	3-5	T50-222-33	893		.68	.238	.350	.374
	6	3-6	T75-111-50	718		.60	.214	.357	.386
	7	3-7	T50-111-50	505		.56	.208	.371	.400

NOTES: (1) Average recession rate based on post-test measurement
(2) Steady-state, turbulent recession rate from film data

per second for T50-112-40. The repeatability of sample results varied from less than .001 inch per second to 0.05 inch per second for the T50-112-40 A conservative estimate of repeatability from 0.03 to 0.05 inch per second was was made for those materials that were tested on all three runs. This would indicate a "confidence" or repeatability factor of about $\pm$ 10 percent for each data point. Nevertheless, the data of Table 15 do indicate a definite trend of increasing ablation.

TABLE 15: AVERAGE RECESSION RATES OF AIM-HIP MATERIALS
(Ranked in Order of Increasing Recession)

MATERIAL	STEADY-STATE, TURBULENT RECESSION RATE (IN/SEC)				
	R-1019	R-1020	R-1021	Average	Maximum Variation
T50-222-33	.374	---	.374	.374	<.001
T50-221-44	.407	.360	.383	.383	.024
T75-111-50	---	.392	.386	.389	.003
T50-111-55	.281*	.400	---	.400	---
T50-111-50	.398	.406	---	.402	.004
P-111-33	.383	.435	.414	.411	.028
T50-112-40	.375	.454	.440	.423	.048

*Not Used in Average Due to Excessive Asymmetry

The film data were then analyzed to determine if mechanical loss of material occurred. Evidence of surface material loss at the shoulder was found for all specimens. Although mechanical loss may have been caused by dusting, in only one case (112 carbon-carbon) may such losses have biased the results. From a visual analysis of the films, approximately eighty percent of the mass loss occurred at the shoulder (a region of high aerodynamic shear

stress). In the region near the stagnation point, mass loss was almost entirely due to thermochemical ablation. The materials which developed rougher surfaces experienced more mechanical removals, and the coarser matrices developed rougher surfaces. From visual analysis of the film data, the relative mass loss due to mechanical means was estimated as follows:

Material	Fraction of Mass Loss Due to Mechanical Removal
T75-111-50 T50-111-55 T50-111-50	~10%
T50-221-44 T50-112-40	~ 15%
T50-222-33 P-111-33	~ 20%

This type of mechanical mass loss may also have been present in the 50 Megawatt tests, but may not have been observed due to lower resolution of surface detail on the 50 Megawatt films.

The following conclusions were made from the results of the HIP tests:

1. The 222 and 221 materials experienced the lowest average ablation rates. A discussion of the correlation with unit cell volume and additional post-test analyses are given in the following section (2.3).
2. All of the materials tested had comparable ablation rates to within $\pm$ 6.5 percent of the mean. Although some mechanical losses occurred near the shoulders of all materials, no massive structural failure occurred.
3. Steady-state turbulent recession rate could be measured at 168 atmospheres stagnation pressure with a repeatability of 10 percent or less.

2.3 Post-Test Analysis of Arc-Jet Results

The characteristics of the AIM II carbon-carbon materials were described in Section 2.1 and the arc-jet ablation data were presented in Section 2.2. In this section, an attempt is made to correlate the data and present it in a manner useful for evaluation of the materials, and to provide a basis for selection of materials for further testing.

2.3.1 Mechanical Erosion Effects

Analysis of the high resolution films of the HIP tests suggested that mechanical removal was contributing to the mass loss mechanisms at higher pressures. A short investigation was performed to ascertain if there were measurable differences in relative mechanical mass loss rates between materials. To determine this, the average steady-state ablation rate in each facility was normalized to the ablation rate of the reference material, FMI 221, at each condition. It was necessary to use a reference material for the comparison because of the differences in facility enthalpy and model configuration that were present in the three series. The relative ablation rates of the seven materials tested at all conditions are shown as a function of model stagnation pressure in both tabular and graphical form in Figure 14. This figure shows that the T50-222-33 ablated slightly less relative to T50-221-44 at the higher pressures, but the remaining materials ablated about the same or slightly more than T50-221-44. Since the variation of ablation rate between materials was of the same magnitude as the specimen-to-specimen variation in both facilities, no firm conclusion on relative mechanical erosion effects could be made without evaluating a statistically larger group of tests. It was therefore concluded that relative mechanical erosion effects at high pressure were less than the variability of individual specimen ablation rates.

MATERIAL	SYM	RELATIVE ABLATION RATE ($S_{221} = 1.0$)		
		75 ATM	100 ATM	168 ATM
T50-222-33	□	1.0	.95	.98
T75-111-50	△	1.0	.91	1.02
T50-221-44	●	1.0	1.0	1.0
P-111-33	◇	1.0	1.0	1.05
T50-111-55	▲	1.0	--	1.02
T50-111-50	○	.95	1.08	1.10
T50-112-40	◆	1.0	1.11	1.10

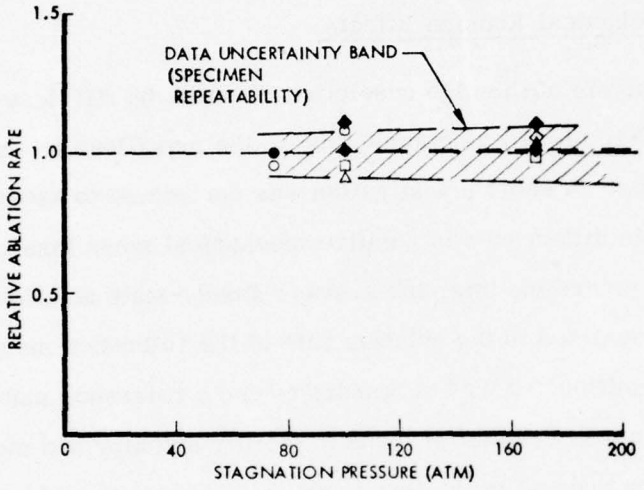

Figure 14: Relative Ablation Rate Versus Pressure

2.3.2 Unit Cell Volume and Roughness Effects

The materials examined in this program provided an opportunity to evaluate the effect of weave spacing on ablation performance with the remaining processing parameters held constant. The test matrix for the initial series in the AFFDL 50 Megawatt facility at the 75 atmosphere test condition was established to provide comparative turbulent recession data on the entire range of weave spacings and yarn types. In anticipation that the the finer weave materials would provide improved ablation performance, more tests were scheduled for them than for the coarser-weave materials.

The unit cell volume, $V_{uc} = S_z^2 S_x$, provides a convenient means of quantitatively defining the coarseness of the weave spacing and was chosen as a parameter for comparison of the materials recession performances. Projections of the unit cells of the fourteen materials in the X-Z planes are shown schematically in Figure 15 for reference. As shown in the figure, the materials cover a very broad range of unit cell sizes.

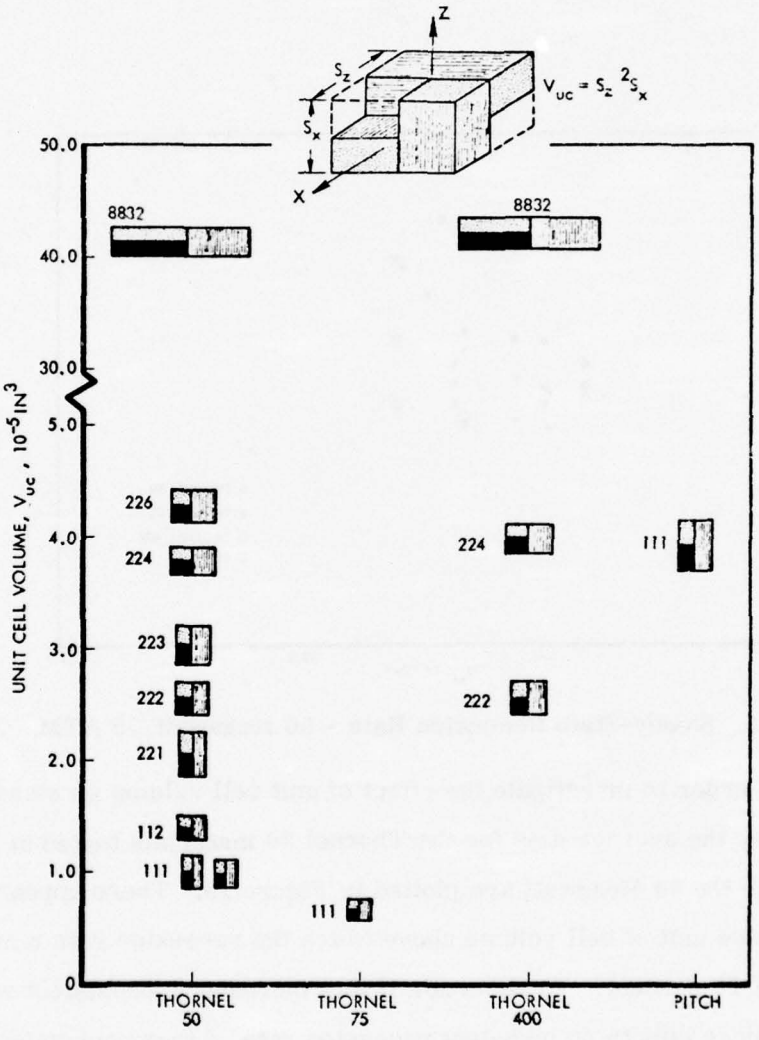

Figure 15: Unit Cell Comparison of AIM II Materials

Steady-state, turbulent recession rate data from the three ablation test series are plotted in Figures 16, 17, and 18 versus the unit cell volumes of the materials. The 75 atmosphere, 50 Megawatt data suggest a possible trend of increasing recession rate with unit cell volume. The materials selected for test at the other two conditions did not span a large enough band of unit cell volumes to establish the effect on recession rate.

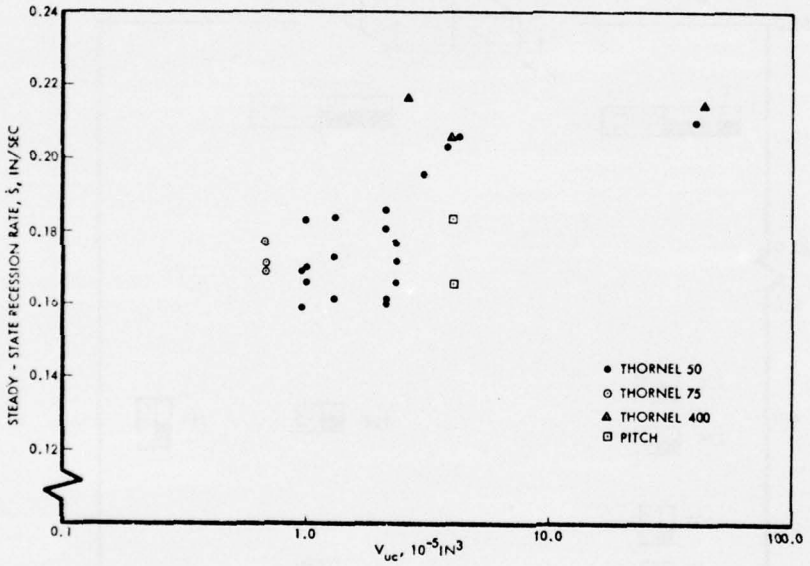

Figure 16: Steady-State Recession Rate - 50 Megawatt/75 ATM

In order to investigate the effect of unit cell volume on steady-state recession rate, the average data for the Thornel 50 materials tested at 75 atmospheres in the 50 Megawatt are plotted in Figure 19. There appears to be a threshold value unit of cell volume above which the recession rate may increase about 20 percent. To ascertain if this increase in consistent with surface roughness effects on turbulent recession rate, a thermochemical

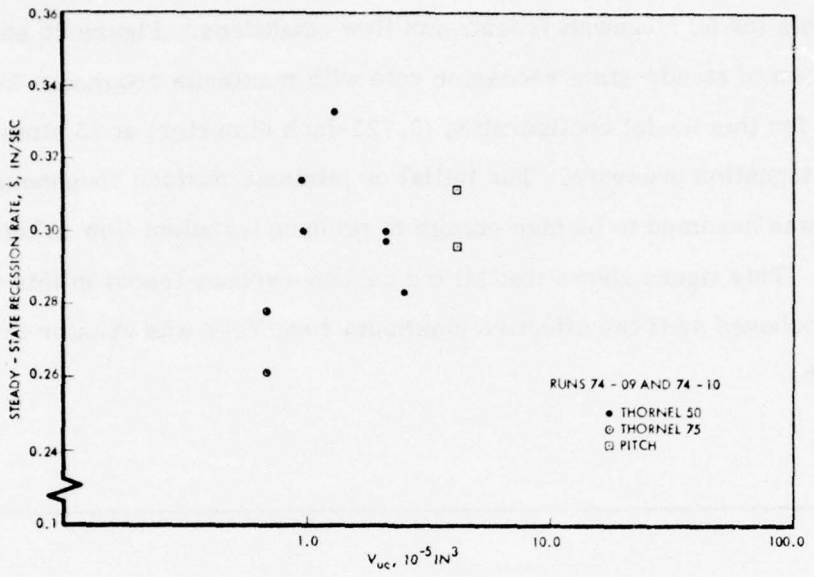

Figure 17: Steady-State Recession Rate Data - 50 Megawatt/100 ATM

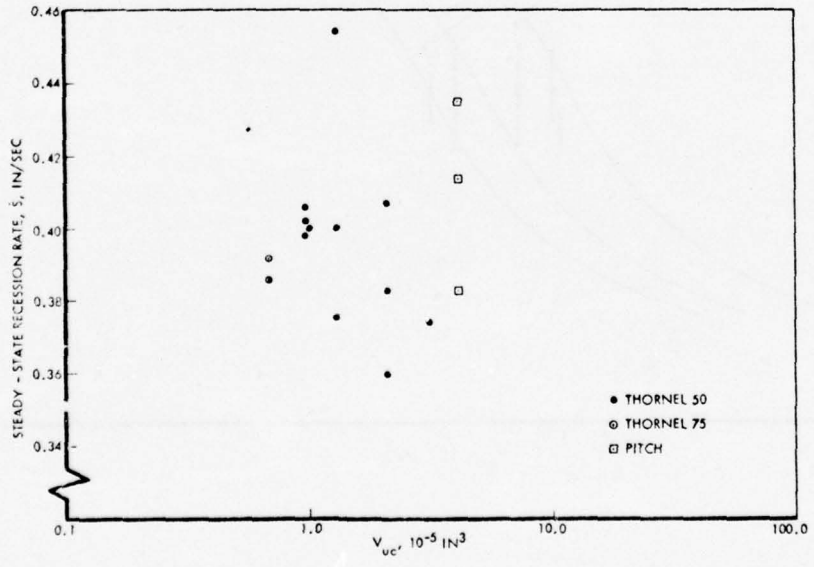

Figure 18: Steady-State Recession Rate Data - HIP/168 ATM

ablation analysis of carbon-carbon was made with variable maximum roughness heights for 50 Megawatt freestream flow conditions. Figure 20 shows the variation of steady-state recession rate with maximum roughness height predicted for this model configuration (0.721-inch diameter) at 75 atmospheres stagnation pressure. The initial or intrinsic surface roughness of the material was assumed to be high enough to produce turbulent flow at this pressure. This figure shows that all the carbon-carbons tested in this program program behaved as if the effective maximum roughness was greater than 0.009 inch.

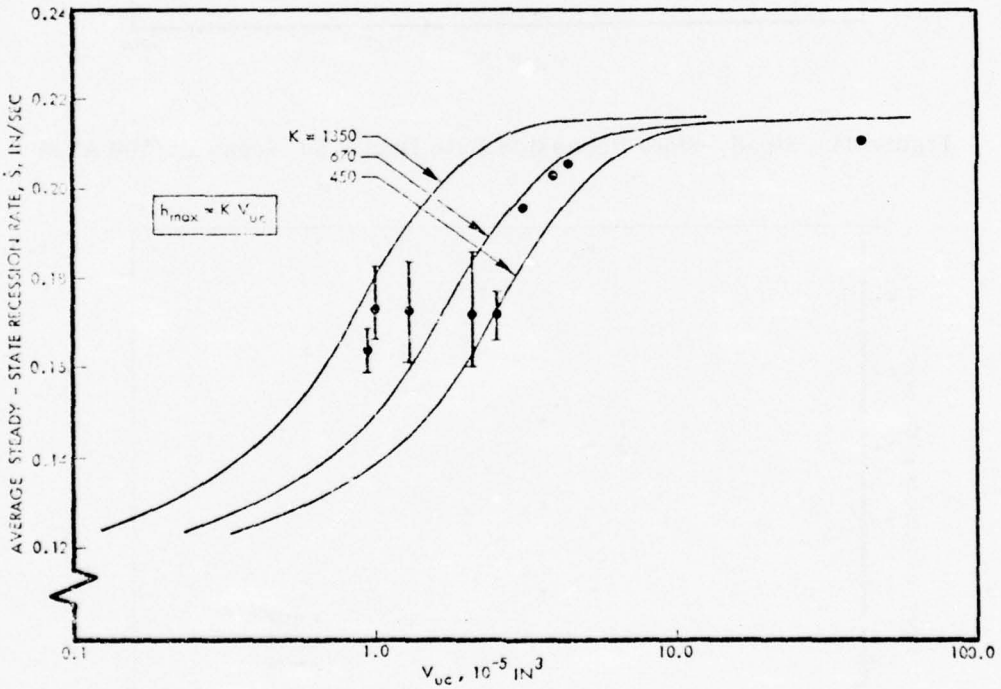

Figure 19: Recession Rate Summary of Thornel 50 Materials - 50 Megawatt/75 ATM

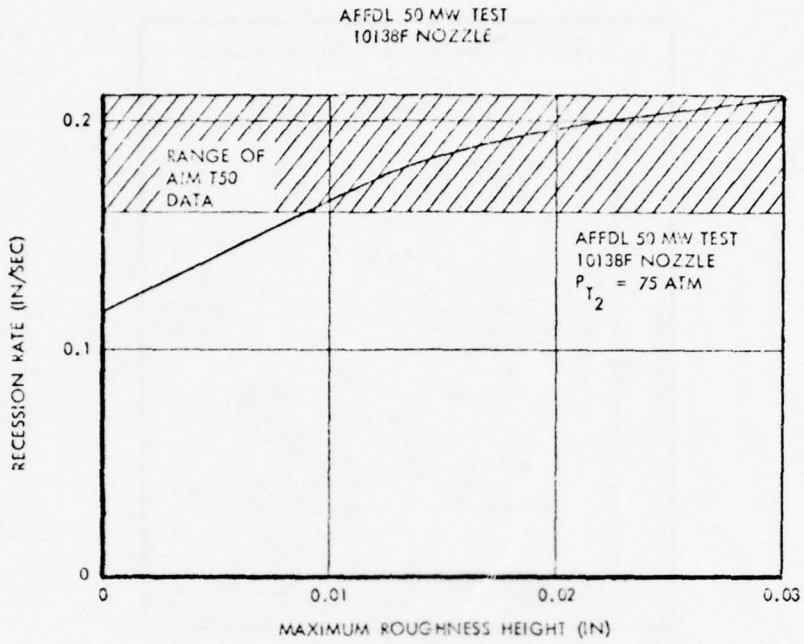

Figure 20: Recession Rate Versus Roughness Height for Carbon-Carbon

Based on this evidence, analytical predictions were made of the recession and shape change profiles for carbon-carbon 50 Megawatt specimens with maximum roughness heights of 0.010 and 0.015 inch, respectively. The freestream conditions of the arc-jet used for this analysis were as follows:

Pressure:	243 psi
Temperature:	9,900°R
Velocity:	9,065 fps (Mach 1.8)

The recession histories and shape profiles predicted for these flow conditions are compared with the results of two of the actual tests in Figures 21 and 22 for T50-111-55 and T50-112-30, respectively. Very good agreement was observed between the predicted and measured recession using maximum roughness heights of 0.010 inch for the T50-111-55 and 0.015 inch

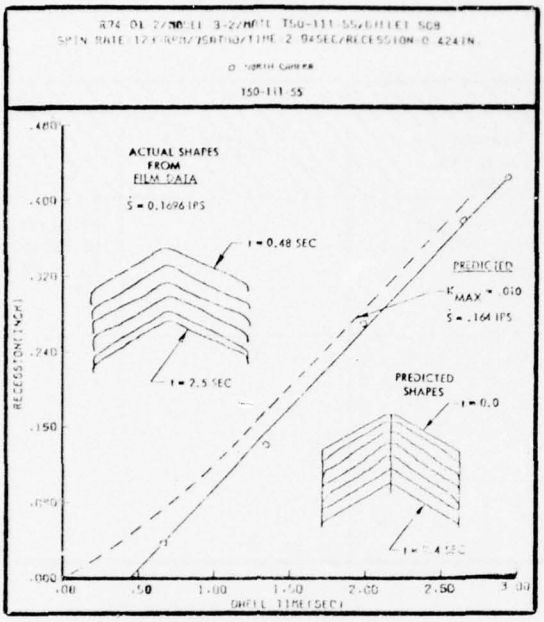

Figure 21: Ablation Summary for T50-111-55

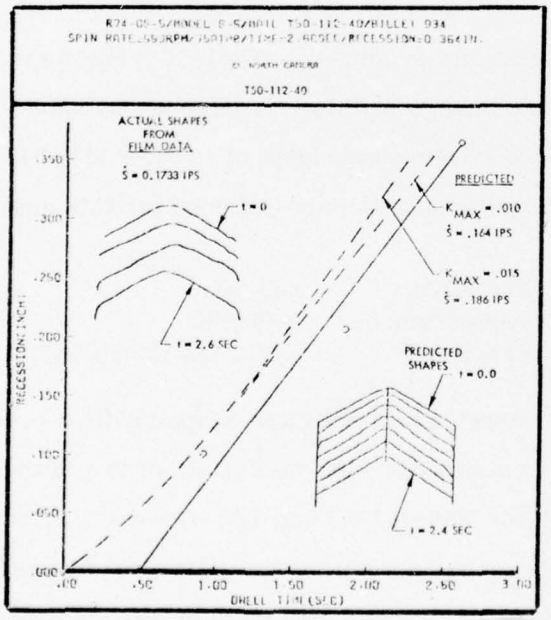

Figure 22: Ablation Summary for T50-111-40

for the T50-112-40. This suggested that there should exist a meaningful correlation between roughness height and turbulent ablation rate. It was then assumed that the maximum roughness height, h_{max}, developed during turbulent ablation is proportional to the unit cell volume, V_{uc}. The proportionality factor, K, was selected such that the analytical prediction of recession rate yielded a best fit to the 50 Megawatt data. The result, shown in Figure 19 for maximum roughness heights given by $h_{max} = K V_{uc}$, correlated well with the data. The sensitivity of the result to the proportionality factor between maximum roughness height and unit cell volume is also shown in the figure.

Two of the specimens tested at the 50 Megawatt 75 atmosphere condition were further tested for surface roughness characteristics. The surface contours were measured with a profilometer having a 0.0001-inch stylus. Each model was characterized along four rays of the ablated surface. Typical contour plots are shown in Figures 23 and 24 for the T50-111-55 and the T50-112-40 materials, respectively. The plots are distorted in the direction normal to the surface by a factor of ten. The weave configurations of the two materials are sketched in the figures to show the surface roughness in perspective with the weave. Although the character of the roughness on the T50-111-50 surface is more pronounced than the T50-112-40 material, the standard deviation of the surface contours relative to the mean surface is only about 30 percent greater. Other means of quantifying the surface roughness, such as RMS peak-to-valley measurements, may provide a better distinction between materials.

2.4 Strength Tests

Nineteen specimens of six of the AIM II materials were strength-tested by Southern Research Institute. The six materials selected for tensile testing were those exhibiting the best recession rate behavior in the AFFDL

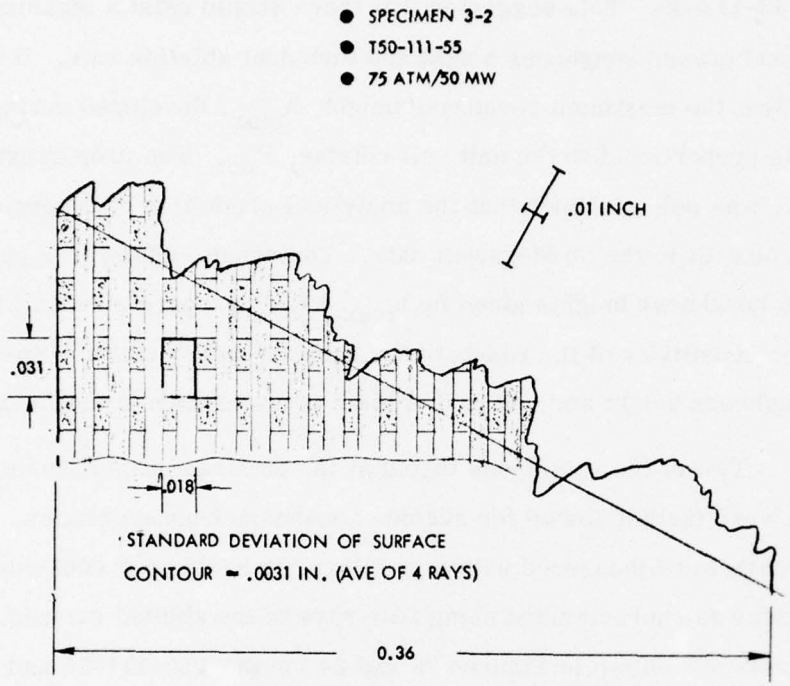

Figure 23: Post-test Surface Contour Plot, T50-111-55

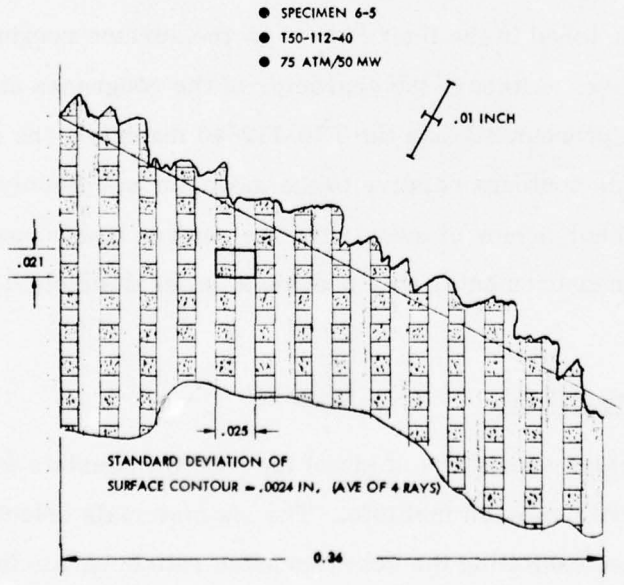

Figure 24: Post-test Surface Contour Plot, T50-112-40

50 Megawatt ablation tests. The materials and a summary of results are given in Table 16. All test specimens were oriented in the Z-direction and the tests were conducted at room temperature. The measured tensile strengths, σ_t, initial elastic moduli, E_t, and the strains at failure, STF, are given in Table 16. The measured tensile strength of the materials are plotted versus the previously-predicted values (Section 2.1) in Figure 25. The strengths of the Thornel 50 and Thornel 75 composites are about 25 percent greater than predicted. The pitch-yarn composite developed much better strength than expected.

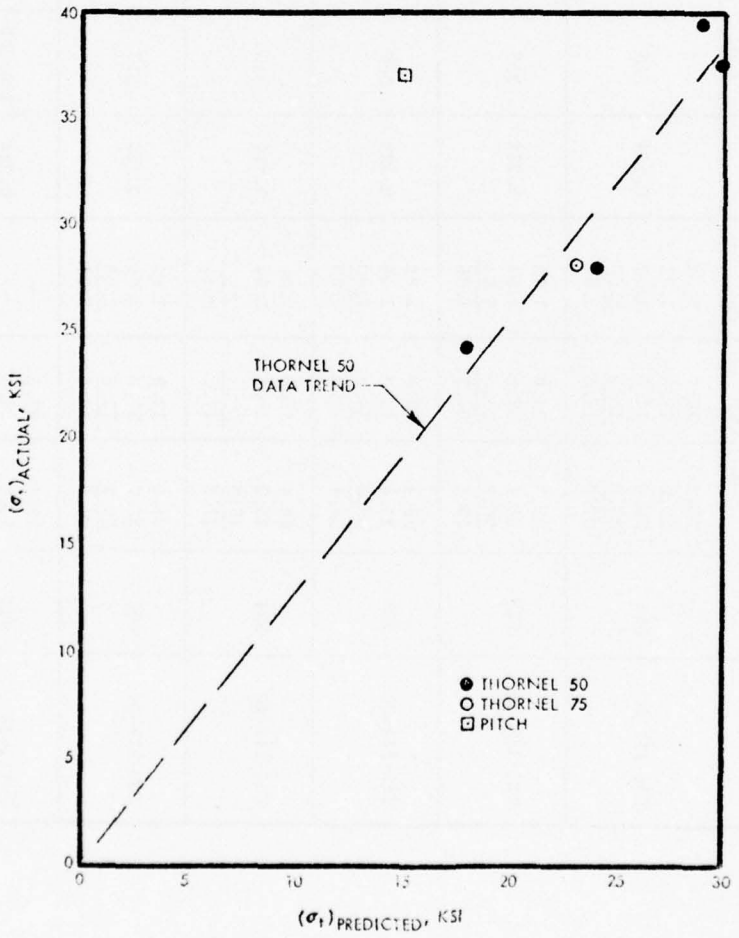

Figure 25: Measured Versus Predicted Strength Comparison

TABLE 16: SUMMARY OF AIM II CARBON-CARBON AXIAL DIRECTION STRENGTH TESTS

MATERIAL	BILLET NO.	σ_t (ksi)	E_t (10^6 psi)	STF (mils/in)	V_{f_z}	σ_f (ksi)	E_f (10^6 psi)	$\frac{\sigma_{t\,AVE}}{\sigma_f V_{f_z}}$	$\frac{E_{t\,AVE}}{E_f V_{f_z}}$
T50-111-50	505	25.2 29.6 29.8 26.8 27.9	16.7 17.1 17.5 18.3 17.4	1.52 1.75 1.67 1.50 1.61	0.164	315	57	0.54	1.86
T50-111-55	508	43.8 38.4 36.4 39.5	23.0 22.1 23.0 22.7	1.73 1.60 1.64 1.66	0.202	315	57	0.62	1.97
T75-111-50	718	29.4 25.6 29.3 28.1	15.9 18.0 16.9 16.9	1.82 1.45 1.80 1.69	0.129	380	78	0.57	1.68
T50-112-40	934	39.6 36.2 36.8 37.5	15.8 18.4 -- 17.1	2.30 1.92 -- 2.11	0.210	315	57	0.57	1.43
T50-221-44	468	24.0 23.7 25.1 24.3	12.3 12.3 12.5 12.4	1.95 2.00 2.06 2.00	0.124	315	57	0.62	1.75
P-111-33	852	39.4 35.2 36.4 37.0	23.1 24.4 23.3 23.6	-- -- -- --	0.214	150-200	50	1.15-0.86	2.21

A measure of the in-situ effective strength of the graphite filaments can be gained by comparing the strength of the unprocessed (off-the-spool) filaments, σ_f, to the effective strength of the filaments in-situ, σ_t/V_{f_z}. This ratio is tabulated in Table 16 for the six AIM II materials tested and ranges from 54 percent to 62 percent for the Thornel 50 and Thornel 75 materials. This is slightly higher than the ratio determined for GE 223 carbon-carbon (discussed in Section 2.1), and is indicative of good filament-matrix bonding. The pitch-yarn composite presents a large departure from typical filament strength ratios with a value between 86 percent and 115 percent depending upon the value used for the unprocessed filament strength. This represents a large apparent improvement in carbon-carbon structure that is probably derived from improved matrix-filament bonding, and possibly better in-situ filament alighment with less filament damage during weaving. It is also possible that the matrix develops a unique crystalline structure at the filament interface in such a way as to contribute significantly to the composite strength.

The initial elastic moduli, E_f, of the unprocessed filaments were compared to the effective moduli of the filaments in-situ, E_t/V_{f_z}, which ignores the contribution of the matrix and transverse filaments to composite stiffness. This ratio, given in Table 16, shows that the composite moduli are in all cases larger than the contribution from the filaments alone. This indicates that the matrix has a large contribution to the composite stiffnesses or that, possibly the modulus of the filaments increases during processing. The latter phenomenon may be related to additional graphitization of the filaments during processing or to matrix filling of filament porosity.

The axial (Z-direction) tensile strengths and moduli of the six materials are plotted in Figures 26 and 27 versus the theoretical filament contributions to strength and modulus ($\sigma_f V_{f_z}$ and $E_f V_{f_z}$, respectively). The slopes of lines through the data give the filament utilization factors discussed above.

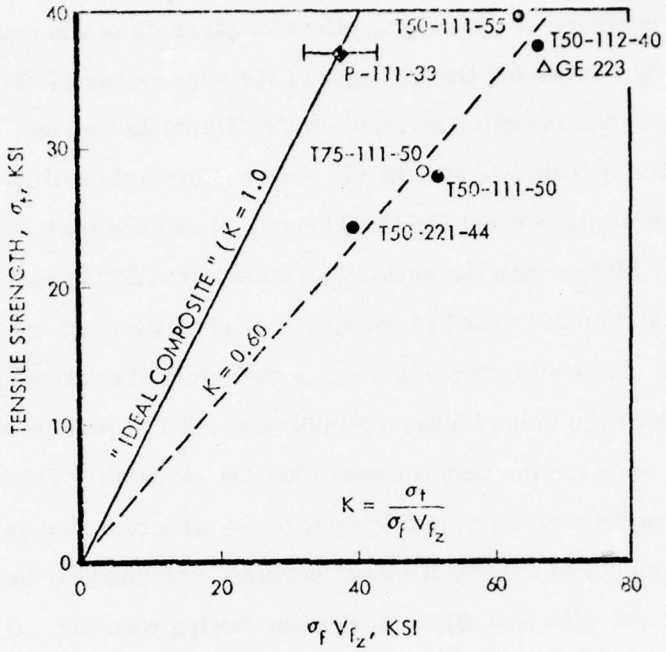

Figure 26: Tensile Strength Summary

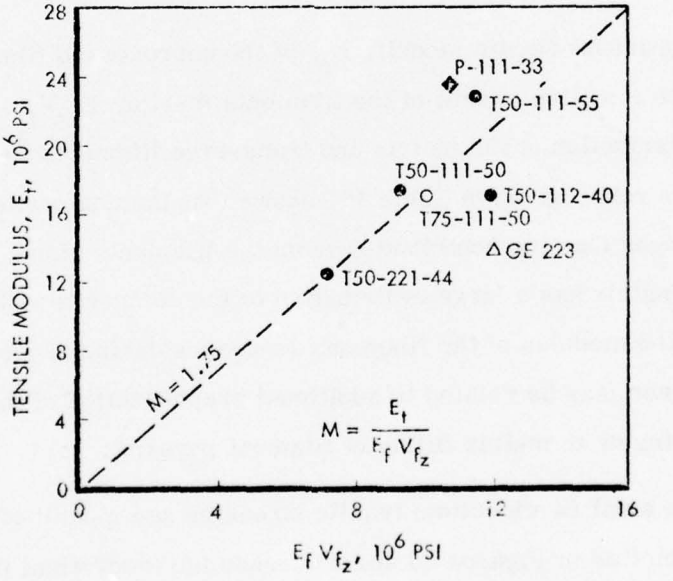

Figure 27: Elastic Modulus Summary

2.5 Additional Tests

2.5.1 Single Particle Impact Tests

Six samples of the T50-221-44 material were subjected to high velocity particle impact tests at Science Applications, Inc. (SAI). The specimens were cut from the AMMRC/AIM materials. Testing was provided by the United States Air Force Space and Missile Systems Organization (SAMSO). Three tests were conducted at room temperature and three at 4050°F. One-millimeter glass particles were impacted at nominal velocities of 12,000 feet per second in five tests and at 20,000 feet per second in one test. The mass loss and volume loss ratios, G_W and G_V, were determined by SAI using weight measurements and mercury-fill method. The data are summarized in Table 17. The mass and volume loss ratios were normalized to the nominal velocities assuming a velocity-squared relationship. These data are also tabulated in Table 17 and show good consistency in the test results. Comparison of the room temperature mass and volume loss ratios at a nominal velocity of 12,000 feet per second to the data point at 20,000 feet per second indicates the velocity dependency is better represented by a power of about 1.5. That is, mass or volume loss ratios scale with velocity according to

$$G_2 \simeq G_1 \left(V_2/V_1\right)^{1.5}$$

This is lower than normally assumed for normal-impact on fine-weave carbon-carbon, but is probably a consequence of the minimal data available.

2.5.2 FMI 221 Characterization of Engineering Properties

One 4 x 4 x 8-inch billet (FMI 468B) of the AIM II T50-221-44 material (FMI 221 carbon-carbon) was characterized by Southern Research Institute (SoRI) under sponsorship of the Air Force Materials Laboratory

TABLE 17: SUMMARY OF 221 CARBON-CARBON SINGLE-PARTICLE IMPACT TESTS

SPECIMEN ID	VELOCITY ft/sec	TEMPERATURE (^{o}F)	PARTICLE DIAMETER (mm)	PARTICLE WEIGHT (mg)	G_V	G_W	NORMAL VELOCITY (ft/sec)	NORMAL G_V	NORMAL G_W
221-1	12,400	70	1.0	1.39	20.27	18.09	12,000	19.0	16.9
221-2	12,500	70	1.0	1.40	20.65	18.20	12,000	19.0	16.8
221-3	12,300	4050	1.0	1.45	28.95	37.93	12,000	27.6	36.1
221-4	11,500	4050	1.0	1.44	23.05	33.80	12,000	25.1	36.8
221-5	11,900	4050	1.0	1.39	25.08	36.17	12,000	25.50	36.8
221-6	20,700	70	1.0	1.42	43.22	37.85	20,000	40.3	35.3

NOTE: Tests conducted by SAI, Santa Ana, California

(AFML). The test matrix is given in Table 18, indicating the number of samples tested at the various test conditions.

TABLE 18: AIM II 221 CHARACTERIZATION MATRIX

TEST	ORIENTATION	RT	2000	3000	3500	4500	5000
TENSION	X	3	3				
	Z	3	3				
	45° XY	2					
COMPRESSION	X	3			3		3
	Z	3			3		3
	45° XY						2
FLEX	Z	3	3				
TORSION	XZ-YZ	3	3	3		3	
FRACTURE TOUGHNESS	XY	3					
	XZ	3					
TEMP. STRESS	XY	3 →					
	XZ	3 →					
HARDNESS	ON-Z	3	(NO MATERIAL REQUIRED)				
	OFF-Z	3					
THERMAL EXPANSION	X	2 →					
	Z	2 →					
THERMAL CONDUCTIVITY	X	2 →					
	Z	2 →					

The characterization tests of FMI 221 were completed by SoRI in December 1975 (Reference 11). The mechanical properties, thermal conductivity and thermal expansion data are summarized in Tables 19 through 22 and in Figures 28 and 29. The mechanical properties in tension are unusually consistent with little scatter among replicate specimens. Exceptionally high tensile strengths were measured in the 45° X-Y directions compared to data previously measured on GE 223 (~10 ksi compared to ~4 ksi). This result is an indication of good filament-to-matrix bonding within the composite.

TABLE 19: FMI 221 TENSILE TEST SUMMARY

TEMPERATURE (°F)	SPECIMEN ORIENTATION	STRENGTH (ksi)	MODULUS (10^6 psi)	TOTAL STRAIN (%)
70	X	---	13.30	---
		24.2	12.25	0.203
		25.2	15.47	0.161
	Z	24.0	12.30	0.195
		23.7	12.34	0.200
		25.1	12.47	0.206
	45° X-Y	9.6	1.29	---
		10.1	1.30	---
2000	X	34.5	17.78	0.230
		24.2	14.17	0.175
	Z	30.0	13.9	0.225
		31.7	14.9	0.215
		25.5	14.4	0.185

TABLE 20: FMI 221 COMPRESSION TEST SUMMARY

TEMPERATURE (°F)	SPECIMEN ORIENTATION	INITIAL MODULUS (10^6psi)
70	X	14.12
		10.24
		12.50
	Z	15.05
		11.29
		8.75
3500	X	14.12
		19.18
		12.10
	Z	11.02
		10.21
		8.59
5000	X	4.14
		4.45
		4.69
		4.14
	Z	4.62
		4.45
		4.80
		4.62
	45° X-Y	1.11
		1.39

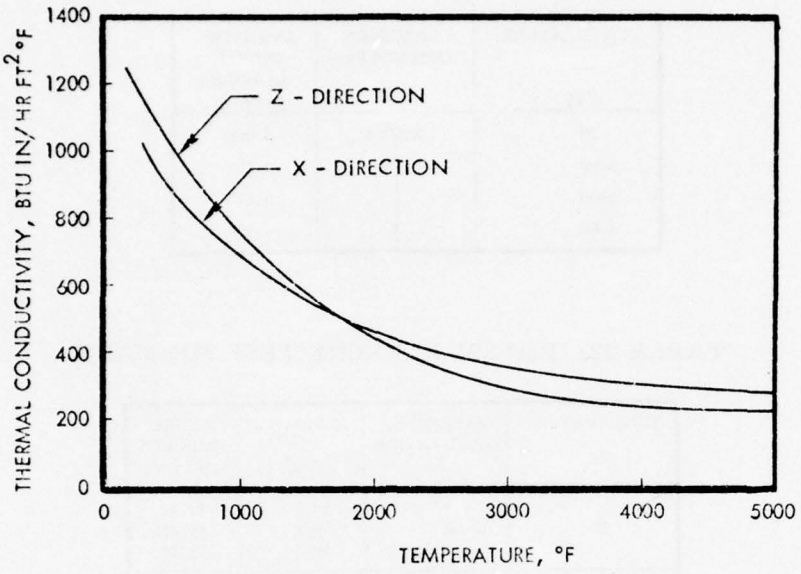

Figure 28: FMI 221 Thermal Conductivity Summary

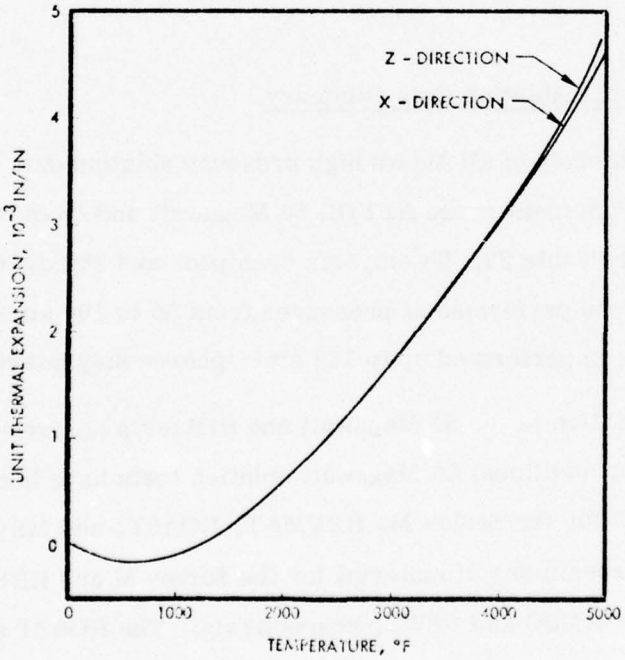

Figure 29: FMI 221 Thermal Expansion Summary

TABLE 21: FMI 221 TORSION TEST SUMMARY

TEMPERATURE (°F)	SPECIMEN ORIENTATION	AVERAGE INITIAL MODULUS (10^6 psi)
70	XZ/YZ	0.368
2000	↓	0.362
3000		0.473
4500		0.453

TABLE 22: FMI 221 FLEXURE TEST SUMMARY

TEMPERATURE (°F)	SPECIMEN ORIENTATION	STRENGTH (ksi)	INITIAL MODULUS (10^6 psi)
70	Z	21.0 19.2 20.6	11.42 10.83 11.58
3000	Z	25.4 29.2 26.6	9.33 10.58 10.25

2.5.3 FMI 221 Ablation Data Summary

A summary of all known high pressure ablation data for FMI 221 carbon-carbon from tests at the AFFDL 50 Megawatt and from the MDRL HIP facility is given in Table 23. Twenty-six "ramped" and steady-state 50 Megawatt tests have been performed at pressures from 56 to 100 atmospheres. Five HIP tests have been performed up to 168 atmospheres stagnation pressure.

In addition to the 50 Megawatt and HIP tests performed as a part of the AIM program, additional 50 Megawatt ablation tests have been sponsored by SAMSO and NSWC for the Series M, REVMAT, ROAST, and MSV screening programs. The specimens of material for the Series M and REVMAT tests were supplied by SAMSO and NSWC, respectively. The ROAST and MSV materials were supplied by AMMRC and the specimens were prepared by PDA.

TABLE 23: SUMMARY OF 221 ABLATION TEST DATA

50 MW TESTS

RUN NO.	BILLET NO.	SPECIMEN DIAMETER (in)	SPECIMEN CONFIGURATION	NOZZLE AND MODEL ROTATION CODE *	DWELL PRESSURE (atm)	DWELL TIME (sec)	RECESSION (in)	$\dot{S}_{turb}$ (Steady State Turbulent Recession Rate) (in/sec)	REMARKS
48-19	Not	1.0	Sphere-Cone	10138F/NR	Ramp→75	2.2/4.4/0.6	0.366	---	Series "M" Tests
48-20	Available	1.0	Sphere-Cone	10138F/NR	Ramp→75	2.0/4.6/0.4	0.330	---	Trans. @ 30 atm
48-32		1.0	Sphere-Cone	10138F/NR	75	7.56	0.375	0.154	
50-1	256B	0.50	45° Cone-Cylinder	09111P/NR	80	2.10	0.503	0.24	AIM 1 Program Tests
50-1	257B	0.50	45° Cone-Cylinder	09111P/NR	80	2.10	0.498	0.23	
50-1	258B	0.50	45° Cone-Cylinder	09111P/NR	80	2.10	0.508	0.235	
68-5	365B	0.721	60° Cone-Cylinder	10138F/NR	75	2.0	0.272	0.167	REVMAT
68-6	365B	0.721	60° Cone-Cylinder	10138F/NR	75	2.0	0.272	0.173	Program Tests
70-6	258B	0.721	60° Cone-Cylinder	10138F/R	75	2.8	0.42	0.15	ROAST I rogram:
70-6	258B	0.721	Sphere-Cylinder	10138F/NR	Ramp→75	1.8/3.3/0.3	0.254	---	Trans. @ 60 atm
70-6	258B	0.721	Sphere-Cylinder	10138F/R	Ramp→75	1.8/3.4/0.4	0.316	---	Trans. @ 57 atm
70-10	258B	0.721	Sphere-Cylinder	10138F/R	56 (ave.)	3.00	0.278	0.111	
70-11	258B	0.721	Sphere-Cylinder	10138F/R	Ramp→75	2.0/4.0/1.2	0.601	---	Trans. @ 51 atm
72-21	551B	1.0	Sphere-Cone	10138F/NR	Ramp→75	2.2/4.4/0.6	0.428	---	MSV Screening Tests:
72-23	551B	1.0	Sphere-Cone	10138F/NR	Ramp→75	2.1/4.3/0.9	0.277	---	Flat Enthalpy - Dusted
72-25	551B	1.0	Sphere-Cone	10138F/NR	Ramp→75	2.0/4.1/0.9	0.236	---	Flat Enthalpy - Dusted
72-27	551B	0.5	Sphere-Cylinder	09111P/NR	80	1.87	0.375	0.238	
72-28	551B	0.5	Sphere-Cylinder	09111P/NR	80	1.87	0.390	0.244	
74-2	551B	0.721	60° Cone-Cylinder	10138F/NR	75	2.72	0.404	0.161	AIM Phase II
74-2	551B	0.721	60° Cone Cylinder	10138F/R	75	2.76	0.401	0.160	
74-2	551B	0.721	60° Cone-Cylinder	10138F/NR	75	2.80	0.452	0.186	
74-3	551B	0.721	60° Cone-Cylinder	10138F/NR	75	2.56	0.423	0.181	
74-7	551B	0.500	45° Cone-Cylinder	09111P/NR	100	1.95	0.520	0.285	AIM Phase II
74-8	551B	0.500	45° Cone-Cylinder	09111P/NR	100	1.95	0.550	0.305	
74-9	551B	0.500	45° Cone-Cylinder	09111P/NR	100	2.21	0.538	0.300	
74-10	551B	0.500	45° Cone-Cylinder	09111P/NR	100	2.21	0.572	0.297	

HIP TESTS

RUN NO.	BILLET NO.	SPECIMEN DIAMETER (in)	SPECIMEN CONFIGURATION	NOZZLE AND MODEL ROTATION CODE	DWELL PRESSURE (atm)	DWELL TIME (sec)	RECESSION (in)	$\dot{S}_{turb}$ (Steady State Turbulent Recession Rate) (in/sec)	REMARKS
1019	551B	0.30	60° Cone-Cylinder	04045P/NR	168	0.62	0.227	0.407	AIM Phase II:
1020	551B	0.30	60° Cone-Cylinder	04045P/NR	168	0.61	0.200	0.361	Asymmetric
1021	551B	0.30	60° Cone-Cylinder	04045P/NR	168	0.69	0.252	0.383	
1053	(GE/ANT)	0.30	60° Cone-Cylinder	04045 P/NR	124	1.18	0.272	0.26	STM Program
1056	(GE/ANT)	0.30	60° Cone-Cylinder	04045 P/NR	168	0.9	0.191	0.32	

* NOZZLE CODES	THROAT DIAMETER	EXIT DIAMETER	DIVERGENCE
10138F	1.00"	1.38"	FLARED
09111P	0.90"	1.11"	PARALLEL FLOW
04045P	0.375"	0.45"	PARALLEL FLOW

* MODEL ROTATION CODE

NR = NON-ROTATING MODEL
R = ROTATING MODEL (~1000 RPM)

Caution should be exercised when attempting to correlate these data with independent variables such as model stagnation pressure. It should be noted that several other independent variables may influence the ablation rate, such as specimen diameter, fore-cone configuration, and the flowfield emanating from the test nozzle (parallel or flared). In spite of these variables, however, it is clear that all data are reasonably consistent.

2.6 Full-Scale ABM Nosetip Design

Carbon-carbon nosetip designs were configured for an advanced terminal defense interceptor to provide a basis for the full-scale ground tests described in the following section. A trajectory, representative of those evaluated in advanced terminal interceptor systems studies, was used for sizing the nosetip overhang to provide sufficient material for recession in clear air and weather flights. The trajectory was previously identified as 67-D in References 1 and 12. The weather environment is given in Figure 30. The spacial distribution of liquid water content (LWC) is representative of a severe thunderstorm and was used for the SPRINT II system specification (References 13 and 14). The maximum LWC is typical of a North Dakota continuous rainstorm that should be exceeded less than 0.3 percent of the time.

The cloud base location relative to the missile launch site which yielded the maximum nosetip erosion for the 25-degree launch-angle trajectory was determined in Reference 1. As may be expected, this trajectory penetrated the cloud such that the maximum velocity (at burn-out) occurred in the densest region of the cloud. This trajectory superimposed on the liquid water content distribution is shown in Figure 30. The resulting distribution of liquid water content with altitude is given in Figure 31.

Nosetip design requirements were determined for both clear air and weather missions. The trajectory and weather environment described above represented severe design conditions for the nosetip. As discussed in

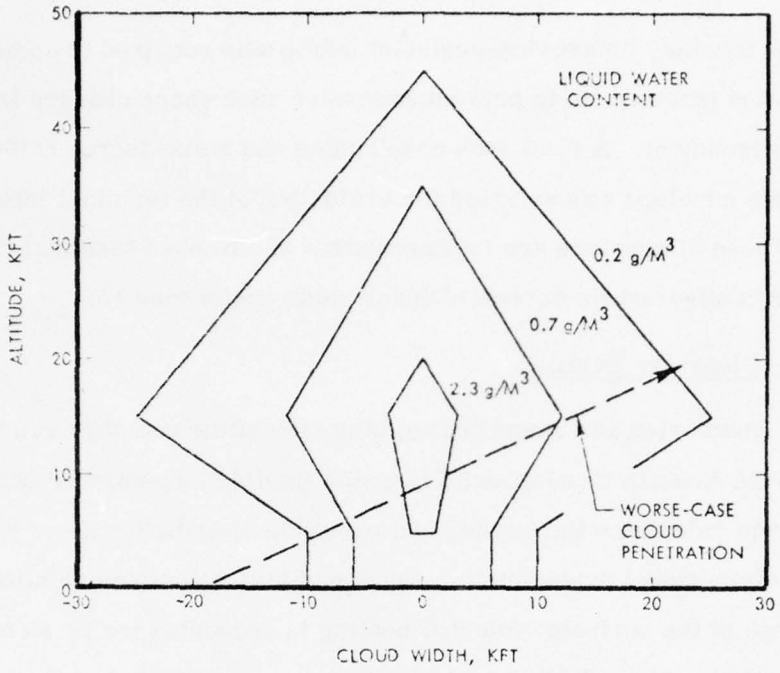

Figure 30: Weather Specification - Thunderstorm Profile

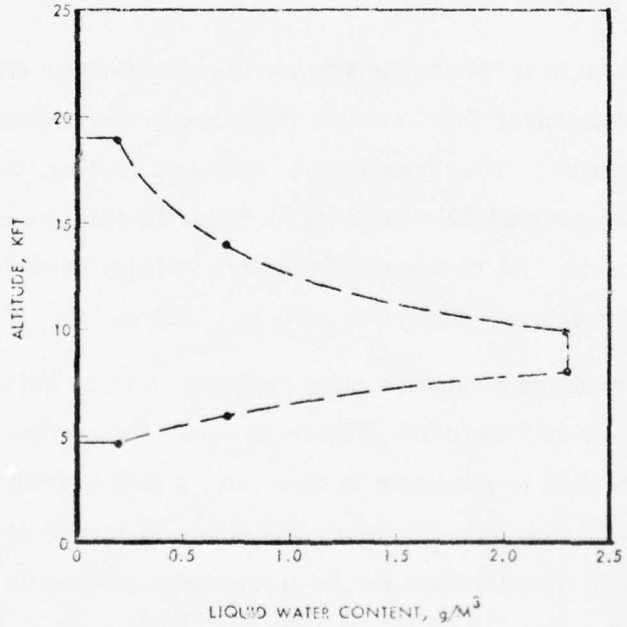

Figure 31: Vertical Liquid Water Distribution for Worse-Case Cloud Penetration

Section 2.6.2 below, an erosion-resistant subtip was required in addition to the carbon-carbon primary tip to prevent excessive nose shape changes in the weather environment. A 0.50-inch nose radius and a six-degree half-cone angle vehicle envelope was selected for evaluation of the terminal interceptor vehicle. These dimensions are representative of advanced terminal defense interceptor configurations currently under study (Reference 15).

2.6.1 Clear Air Design

Recession and shape change histories of the nosetip were predicted using the PDA Nosetip Heating and Recession (NOHARE) computer program. This program calculates the heating and pressure distribution about any arbitrary two-dimensional axisymmetric shape and also calculates ablation and shape change of the surface. Internal heating is accounted for by an energy integral method. The calculations of local pressure and heating are coupled to the instantaneous shape of the body.

The local heat rate to the surface is calculated for either laminar or turbulent boundary layer flow based on transition criteria developed by the SAMSO/PANT program. After transition to turbulent heating, the local turbulent heat rate assumed fully-scalloped flow on the fore-cone and aft-cone where applicable. Aft of this region, rough-wall turbulent heating was used with surface roughness allowed to grow to 0.020 inch.

The predicted stagnation point recession history based on these calculations is shown in Figure 32. Figure 33 shows the predicted shape profiles. For this ablation requirement in clear air, a plug nosetip having a 1.5-inch overhang is required. However, as shown in Figure 34, the moment of inertia of the plug nosetip shank can be increased significantly by increasing the overhang length. This effect is a result of the larger shank diameters that can be designed in the available envelope. The figure shows that for the

range of sidewall heatshield thicknesses considered, the moment of inertia of the plug shank (proportional to the fourth power of the shank diameter) can be nearly doubled by increasing the overhang length to 2.0 inches. This greatly improves the bending strength of the nosetip with little penalty on material billet size requirements. Consequently, for a clear air mission, a carbon-carbon plug nosetip configuration with a 2.0-inch overhang, a 0.5-inch nose radius and a six-degree half-cone angle is representative of design requirements for advanced terminal interceptor missiles. This configuration formed the basis for the design of single-material nosetip models for full-scale ground testing as discussed in Section 2.7.

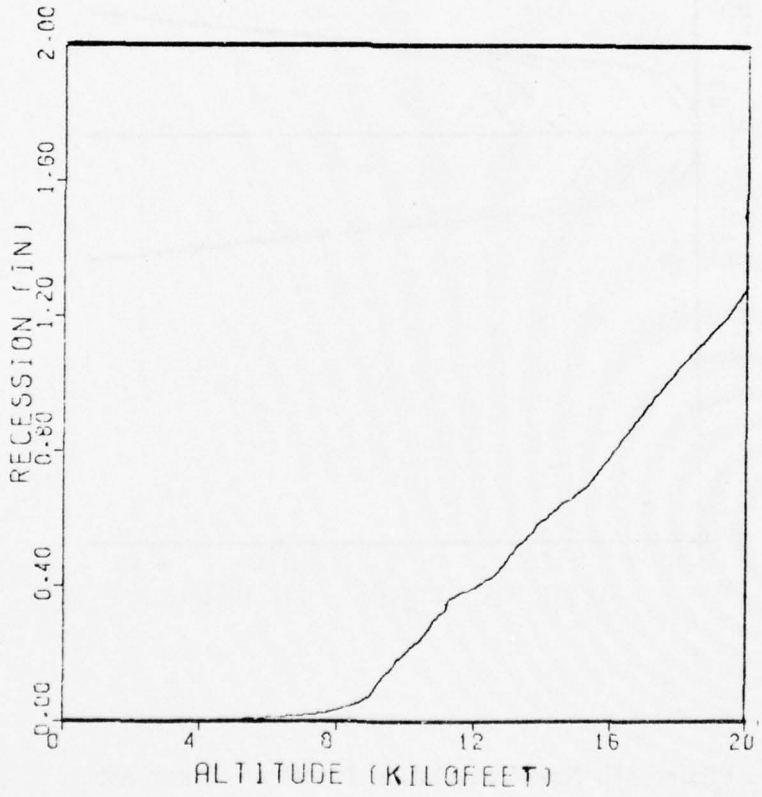

Figure 32: Nosetip Stagnation Point Recession History - Clear Air

TIME (SEC)	ALTITUDE (KFT)
0.000	0.60
1.800	7.50
2.400	11.43
3.000	15.20
3.600	17.72
4.200	20.00

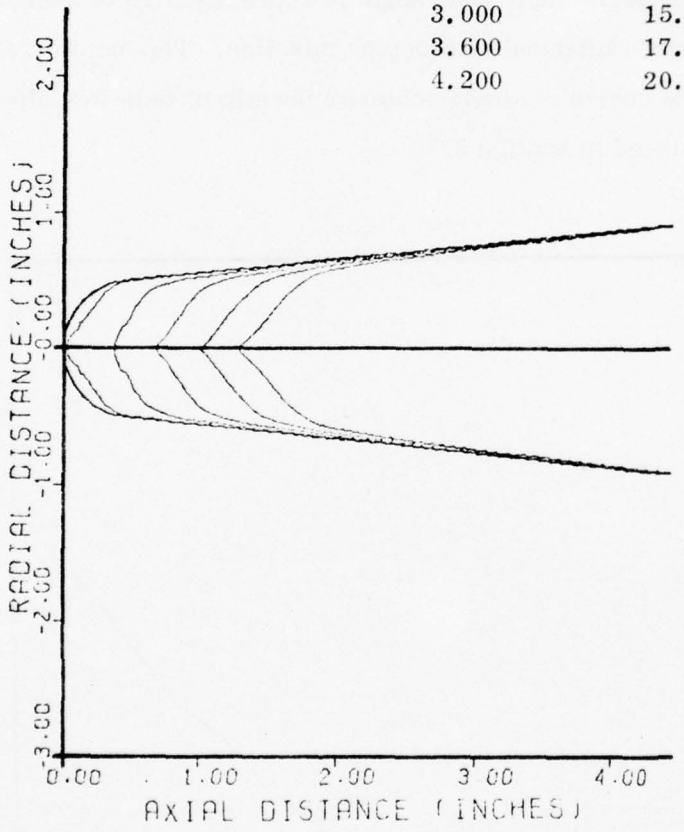

Figure 33: Nosetip Ablation Profiles - Clear Air

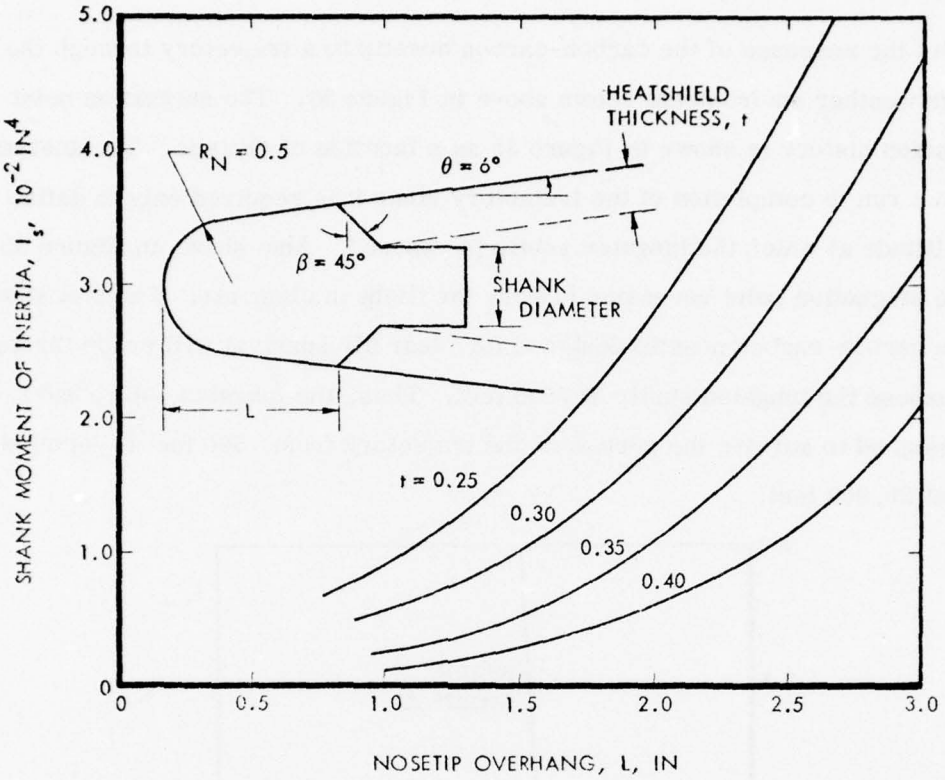

Figure 34: Effect of Nosetip Overhang on Shank Moment of Inertia

2.6.2 Erosion-Resistant Design

In high velocity flights through clouds having relatively high liquid water content, the total recession of an all carbon-carbon nosetip can be excessive. To minimize the total nosetip recession in weather, an erosion-resistant subtip material such as tungsten is required in addition to the carbon-carbon primary nosetip. With this concept, a carbon-carbon shell is designed for survival in clear air, but is backed up by a tungsten plug subtip which provides erosion resistance for flights through weather (Reference 1).

The clear-air ablation history of a carbon-carbon nosetip was calculated in the previous section. The PDA NOHARE code was used also to

predict the response of the carbon-carbon nosetip to a trajectory through the design weather environment shown above in Figure 30. The stagnation point recession history is shown in Figure 35 as a function of altitude. The analysis was not run to completion of the trajectory since it is required only to define the altitude at which the tungsten subtip is exposed. Also shown in Figure 35 is the stagnation point recession history for flight in clear air. The plot shows that a carbon-carbon nosetip designed for clear air survival will erode through and expose the tungsten subtip at 7500 feet. Thus, the tungsten subtip had to be designed to survive the portion of the trajectory from 7500 feet to termination at 20,000 feet.

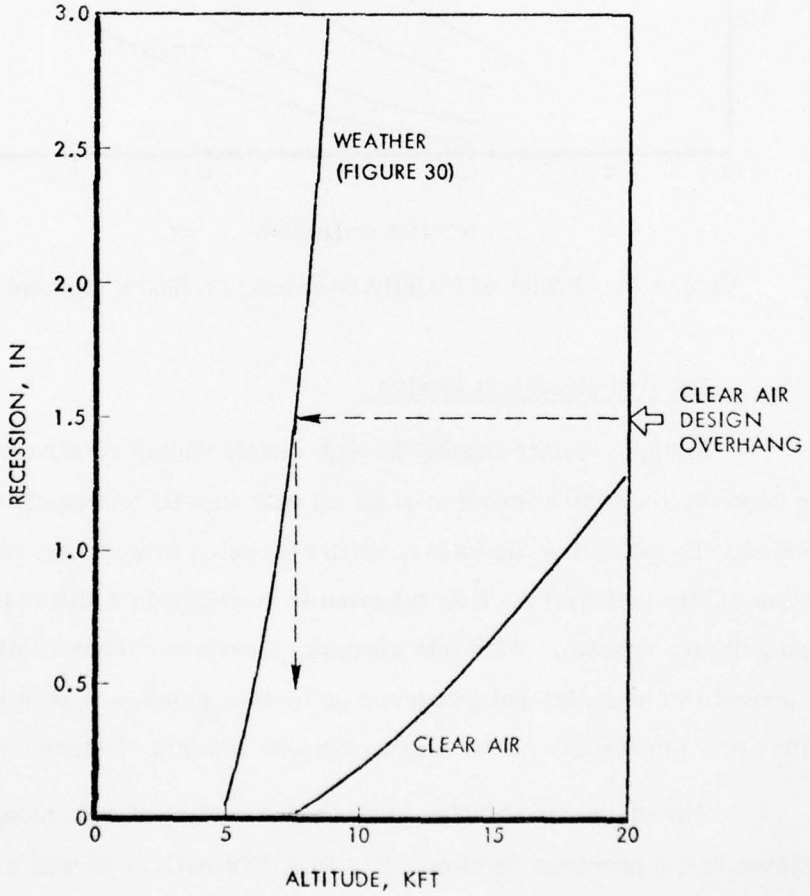

Figure 35: Stagnation Point Recession - Carbon-Carbon Primary Nosetip

The predicted tungsten subtip recession history is plotted in Figure 36 for a subtip configured to be compatible geometrically with a carbon-carbon primary shell nosetip. As the plot shows, a tungsten subtip overhang length of approximately 3.5 inches is required to survive the design environment. This recession would result in vehicle stability changes during flight that may exceed the capabilities of vehicle control systems (Reference 15). Consequently, this specific mission may require an actively-cooled, erosion-resistant nosetip. For less severe burn-out velocity trajectories or more realistic weather environments, the erosion-resistant design concept provides a simple minimum-shape change nosetip solution. The weather environment assumed (Figure 30) represents a liquid water content that should be exceeded less than 0.3 percent of the time. A shorter tungsten subtip having a 1.75-inch overhang was selected for full-scale ground testing and represents a design for the trajectory and weather environment considered here, but terminated at approximately 13,000 feet. The erosion-resistant configuration is shown in Figure 37 with the erosion profiles at shell removal and at trajectory termination superimposed.

2.7 Full-Scale Prototype Nosetip Tests

2.7.1 Objectives

This section describes the method, model configurations and results of the ablation and thermostructural tests of full-scale prototype nosetips for advanced interceptor missile concepts. This test program was the final task of Phase II. The overall objectives of these full-scale development tests were as follows:

1. Assess the thermochemical and thermomechanical ablation performance of full-size carbon-carbon nosetip configurations at high stagnation pressures.
2. Evaluate the thermostructural response of the candidate carbon-carbon materials and configurations.

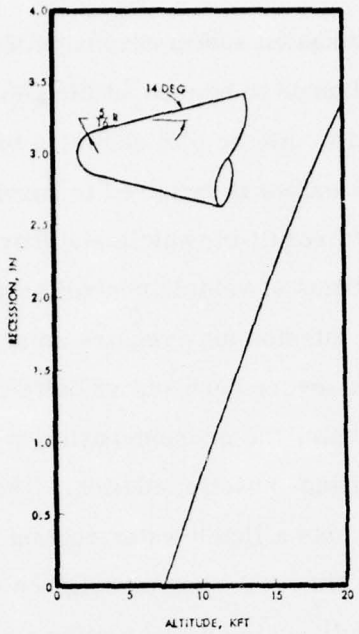

Figure 36: Stagnation Point Recession - Tungsten Subtip

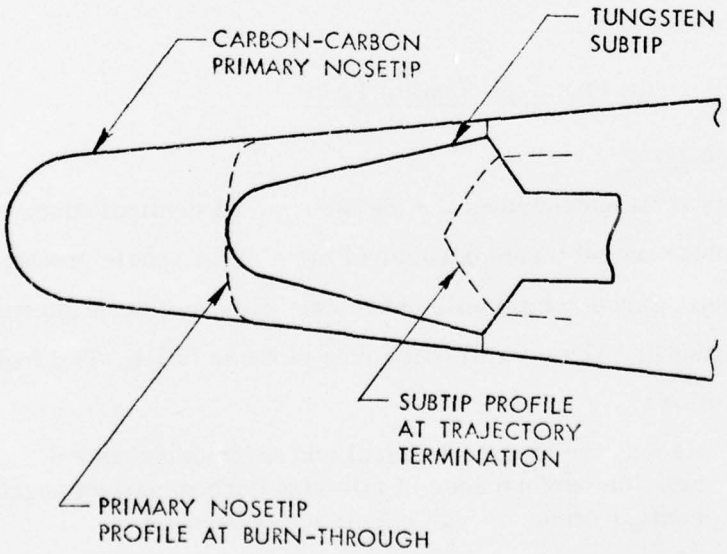

Figure 37: Erosion-Resistant Design Concept

3. Evaluate the relative development of turbulent shapes of each material during high pressure ablation.

4. Evaluate the ablation and thermostructural performance of an erosion-resistant ABM subtip design.

2.7.2 Test Method

Two model configurations as shown in Figures 38 and 39, respectively, were tested. Each configuration was tested twice, using a different carbon-carbon outer, or primary, tip for each test. Each model was exposed to a high pressure rocket exhaust at Pad 1-52-C of the Air Force Rocket Propulsion Laboratory (AFRPL) at Edwards Air Force Base, California. The high pressure exhaust was developed by combusting benzonitrile and liquid oxygen propellants at an oxygen-to-fuel mixture ratio of 2.8. The maximum model stagnation pressure for each test was approximately 160 atmospheres. Each model was positioned initially in the exhaust one inch aft of a 4.5-inch diameter nozzle as shown in Figure 40.

Because of high bending loads which would result from model insertion at full stagnation pressure, it was necessary to insert the models on the flow centerline during the start-up of the rocket engine before steady-state operating pressure was reached. A polyethylene bag was used to protect the models from the nozzle coolant flow during the start-up transient.

Description of Tests

Two models of a clear air advanced terminal interceptor nosetip configuration were tested, and two models of a weather-resistant configuration were tested. Each model had a different carbon-carbon outer tip as discussed in Section 2.7.3. Table 24 gives the matrix of concepts and materials that were tested.

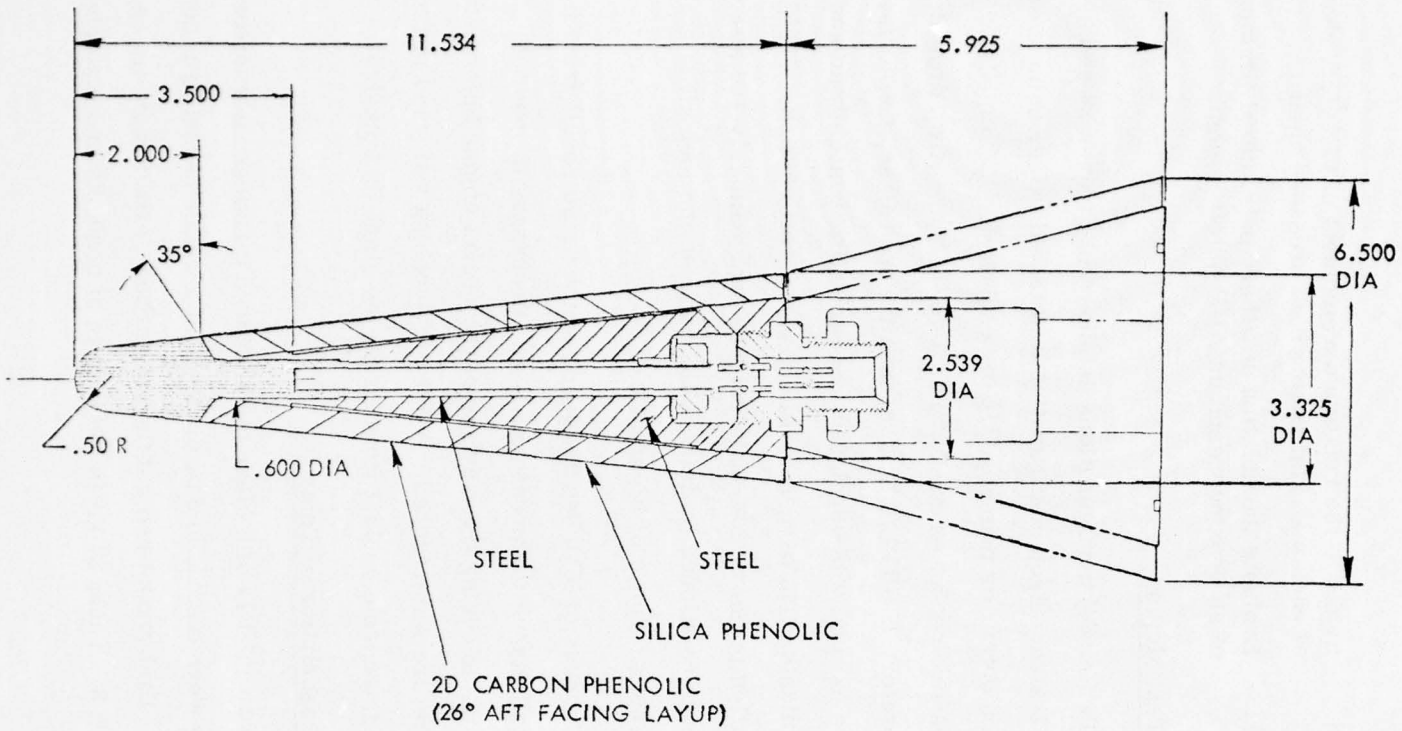

Figure 38: Carbon-Carbon Plug Nosetip RPL Test Model

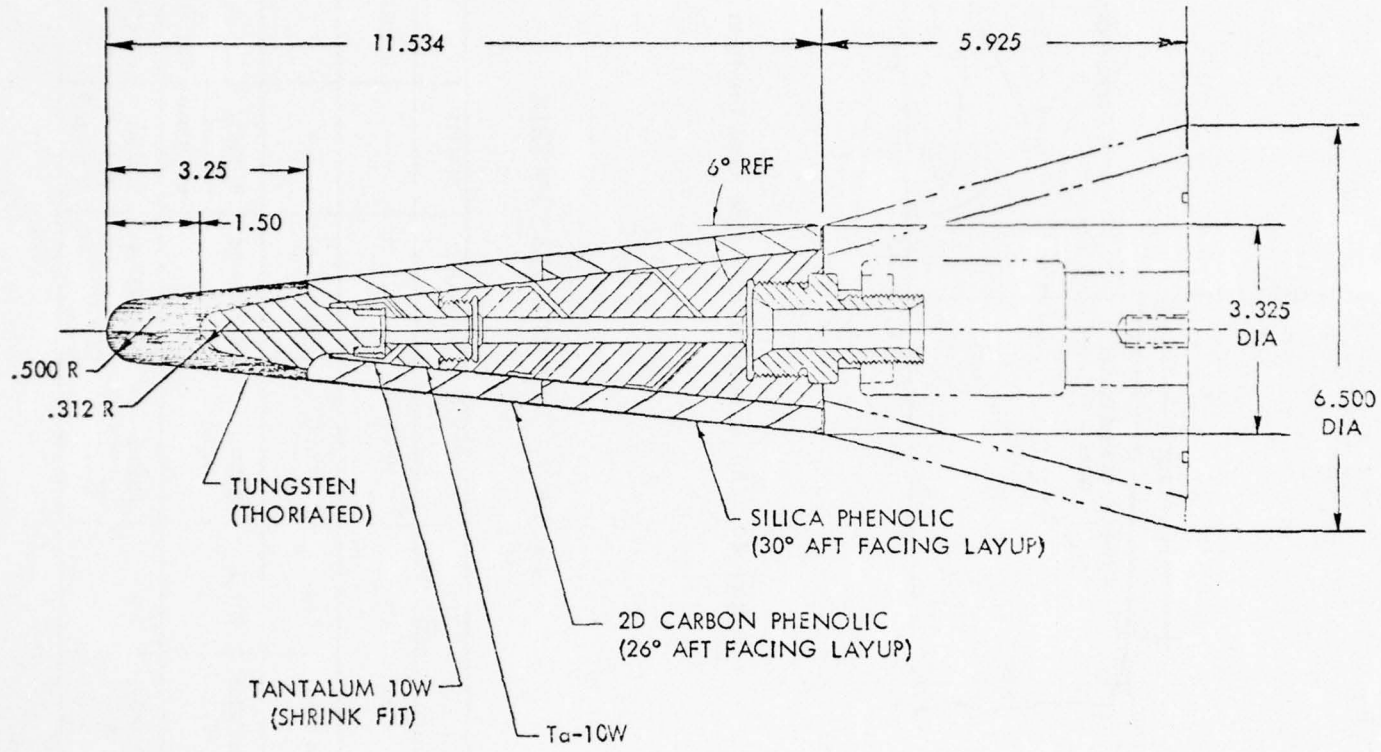

Figure 39: Carbon-Carbon Shell Over Tungsten Subtip - RPL Test Model

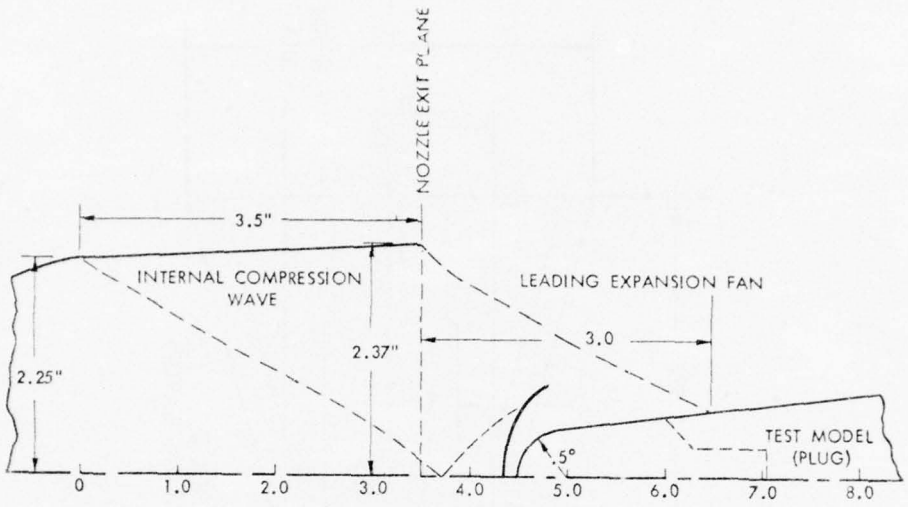

Figure 40: 155 Atmosphere Nozzle Test Configuration

TABLE 24: AIM RPL TEST MATRIX

MODEL S/N	RPL TEST NO.	CONCEPT	PRIMARY TIP	SUBTIP	REMARKS
SK 41966 -1	205	PLUG	T50-221-44	---	Baseline Material
SK 41966 -3	206	PLUG	T50-112-40	---	
SK 41966 -1	207.2	SHELL SUBTIP	T50-111-55	W-ThO_2 (Swaged & Forged)	
SK 41965 -3	208	SHELL SUBTIP	T50-221-44	W-ThO_2 (Swaged & Forged)	Baseline Material

The first two models were tested to assess ablation and thermostructural performance of the carbon-carbon only. These tests were terminated prior to complete loss of the carbon-carbon, and the remaining material was therefore available for post-test analyses. These models were exposed to high pressure for only two seconds.

The second two models were tested for ablation, thermostructural, and removal performance of the carbon-carbon after exposure of the tungsten subtip. Then the thermostructural performance of the tungsten subtip was tested during a 2-second exposure after removal of the outer carbon-carbon tip. To maintain peak stagnation pressure on the subtip after burnthrough and removal of the carbon-carbon, the models were moved forward 1.5 inches by the remotely-operated axial model positioner. Removal of carbon-carbon was observed on closed circuit television which was monitored in the control room. When the removal was observed, the AFRPL test engineer manually activated the forward motion of the sting. A timed override was also used to initiate forward motion in the event that removal could not be seen on the television.

Test Conditions Selection

Table 25 shows the test conditions that were planned for all models. Based on the trajectory analyses described in Reference 1, the 160 atmosphere test condition provided a good simulation of the stagnation pressure to be encountered in an advanced intercept mission. Figure 41 shows a comparison of the stagnation pressure history for the RPL test condition and typical intercept mission. The decay from peak pressure in the RPL test as shown in Figure 41 was the effect of tip recession in the flowfield while the model remained in fixed position.

TABLE 25: TEST CONDITIONS

	PRIMARY
Propellants	C_6H_5CN/LOX
Mixture Ratio (O/F)	2.8
Model Stagnation Pressure, Atm	155-170*
Mach Number	1.83
Nozzle Exit Diameter, In	4.74
Total Temperature, ^{o}R	7,165
Total Enthalpy, Btu/Lb	3,980

*Calibration measurements of this test condition have not been completed

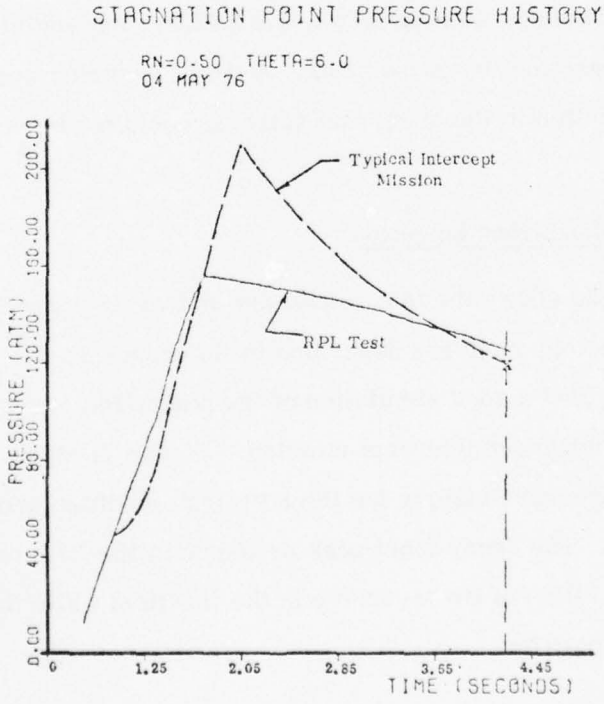

Figure 41: Stagnation Pressure Comparison for RPL Test and Typical Intercept Mission

AD-A033 540 PROTOTYPE DEVELOPMENT ASSOCIATES INC SANTA ANA CALIF F/G 11/4
EVALUATION OF CARBON-CARBON COMPOSITE NOSETIP MATERIALS.(U)
OCT 76 J R STETSON, J C SCHUTZLER DAAG46-75-C-0099
UNCLASSIFIED PDA-TR-1042-00-09 AMMRC-CTR-76-34 NL

2 OF 2
ADA033540

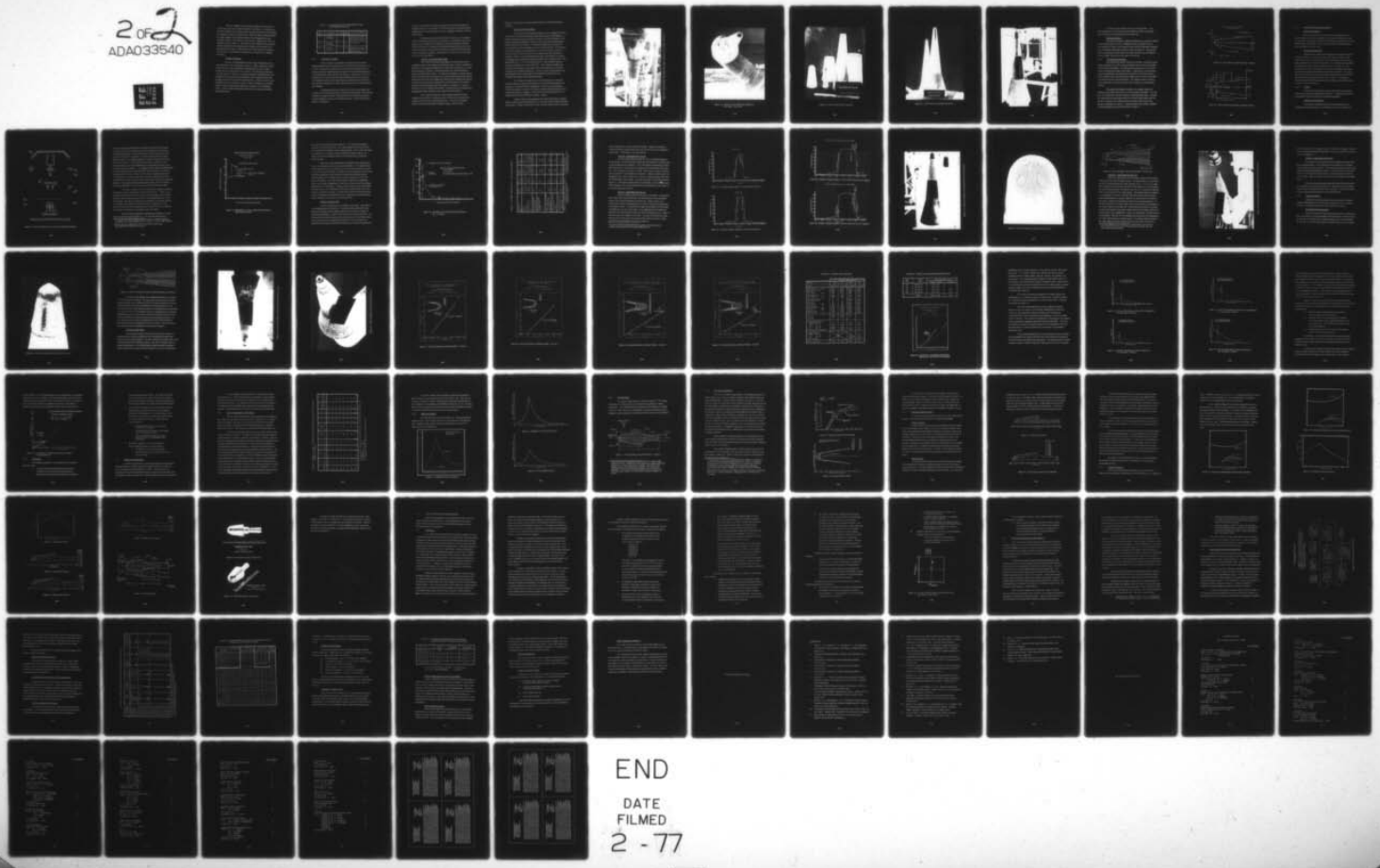

END

DATE
FILMED
2 -77

This test condition required that the model be inserted prior to the time that steady-state chamber pressure was achieved. Therefore each model was inserted into the exhaust after the engine had started and stabilized at a chamber pressure less than 600 psi. After the model reached centerline, the engine pressure was increased rapidly to its 3000 psig steady-state operating condition. The rise time to steady-state conditions was about one second as shown in Figure 41. Note that this start transient also provided an excellent simulation of the pressure history during the boost phase of the typical intercept mission. Total exposure time of the model was measured from the time the model entered the exhaust (2.5 inches prior to reaching centerline).

Flowfield Calibration

Because of the installation of a new nozzle configuration at RPL, new calibrations of the flowfield were required. AFRPL conducted a series of heat flux and pressure calibrations using oxygen-free copper (OFHC) models with nose radii from 0.5 to 2.0 inches. All calibration models had cone half-angles of 7 degrees. Heat flux and pressure distribution data were obtained for at least seven inches downstream of the stagnation point using the same nozzle that was used for the nosetip tests. Although a series of six calibration tests were planned by AFRPL, various operating and scheduling problems were encountered that delayed the completion of the calibration series. Table 26 lists the calibration tests that were completed during the AIM program entry.

TABLE 26: CALIBRATION TESTS PERFORMED IN THE HIGH PRESSURE NOZZLE

RPI TEST NO.	TYPE OF CALIBRATION	NO. OF SENSORS	NOSE RADIUS	RESULTS/REMARKS
203	Pressure Distribution	4	0.75	Teflon glove removed prematurely; C_L data 3.0 inches from nozzle exit
204	Heat Flux Distribution	10	2.0	Data Obtained
210	Pressure Distribution	4	0.75	Teflon glove removed at Axial Station 1.5 inches from nozzle exit

2.7.3 Description of Models

Three materials were selected for testing from the fourteen different carbon-carbon materials that were evaluated in this program. The T50-221-44 material was selected as the baseline material because of the relatively complete engineering data package that was available and because several flight tests of the material were planned. A fine-weave T50-112-40 material was also selected for full-scale evaluation because this material had exhibited excellent strength and ablation characteristics in the 50 Megawatt and HIP screening tests. Plug configuration tests were planned for these two materials.

An additional fine-weave material (T50-111-55) was selected for testing in a shell configuration with an erosion-resistant subtip. This material provided the maximum number of unit cells across the shell wall thickness. A shell configuration model of the baseline material, T50-221-44, also was tested for comparison.

The tests, as planned, provided an evaluation of the thermostructural and ablation responses of the baseline T50-221-44 material in both plug and shell configurations, and comparisons of two other candidate materials to the baseline material.

Materials processed from Thornel 75 yarns were not considered for RPL testing because the yarn was currently out of production, and consequently, not a candidate for development of advanced interceptor nosetips. None of the fine-weave Thornel 400 materials exhibited ablation rates as low as those of the fine-weave Thornel 50 materials in AFFDL 50 Megawatt tests at the 75 atmosphere condition, and therefore, the former were not selected for full-scale testing either.

Carbon-Carbon Plug Model Design

The carbon-carbon plug design (Figure 38) was sized for clear-air ablation based on the advanced terminal interceptor trajectory described in Section 2.6. Recession calculations for this trajectory showed that a 1.5-inch plug overhang was required. Plug bending loads were carried through the shank to the substructure sleeve. The plug was assembled to a steel wand and all four thermocouples were placed on the carbon-carbon plug backface and led through the wand which also contained the thermocouple extension wire splices. This nosetip/instrumentation subassembly was then slipped into the primary structure and heatshield assembly and retained by a large nut. A key was provided to prevent rotation of the nosetip. All axial loads on the nosetip were transferred through a shoulder on the wand to the steel structure.

Each model was bolted to a steel adapter insulated with tape-wrapped silica phenolic. The adapter was a 5.9-inch long, 15-degree cone frustum common to both nosetip configurations. The base of the adapter bolted to the movable insertion mechanism (sting) of the RPL stand.

Figures 42 and 43 show the two plug models mounted on the RPL sting prior to testing.

ERN Concept Model Design

The carbon-carbon shell model (Figure 39) was configured for clear-air survival on the advanced terminal interceptor trajectory and adapted to a tungsten subtip to provide survivability in weather or dust environments. The tungsten subtip was configured to minimize nose shape change during carbon-carbon shell removal in weather. The maximum diameter was selected to provide adequate erosion shielding of the structural attachment. The shell was retained by bonding in the aft region where a step in the carbon-carbon provided a longer bond-line in shear; and the tungsten subtip was retained by a threaded tantalum, 10 percent tungsten alloy sleeve shrink-fitted to the shank. The tungsten subtip shank and the internal diameter of the tantalum sleeve were dimensional for a 0.1 to 0.5 mil interference fit. This assembly required heating the tantalum sleeve to at least 350^{O}F. The completed assembly provided retention strength for axial loads of about 1000 pounds in the forward direction for the nominal interference. Thus the stress concentrations in the brittle tungsten which would result from threading the subtip itself were completely eliminated by this attachment design.

The subtip was forged from a 1.00-inch diameter, two-percent thoriated tungsten swaged bar purchased from Schwarzkopf Development Corporation to a certified chemical composition. The bar was upset-forged to 1.250-inch diameter to improve the transverse tensile strength associated with tungsten extrusions or swagings. Fabrication of the subtip subassembly was performed by Northwest Industries of Albany, Oregon.

Figure 44 shows the components of the ERN model before assembly. Figure 45 shows the fully assembled T50-111-55 shell model mounted on the RPL sting adapter. Figure 46 shows the T50-221-44 model mounted in the test facility.

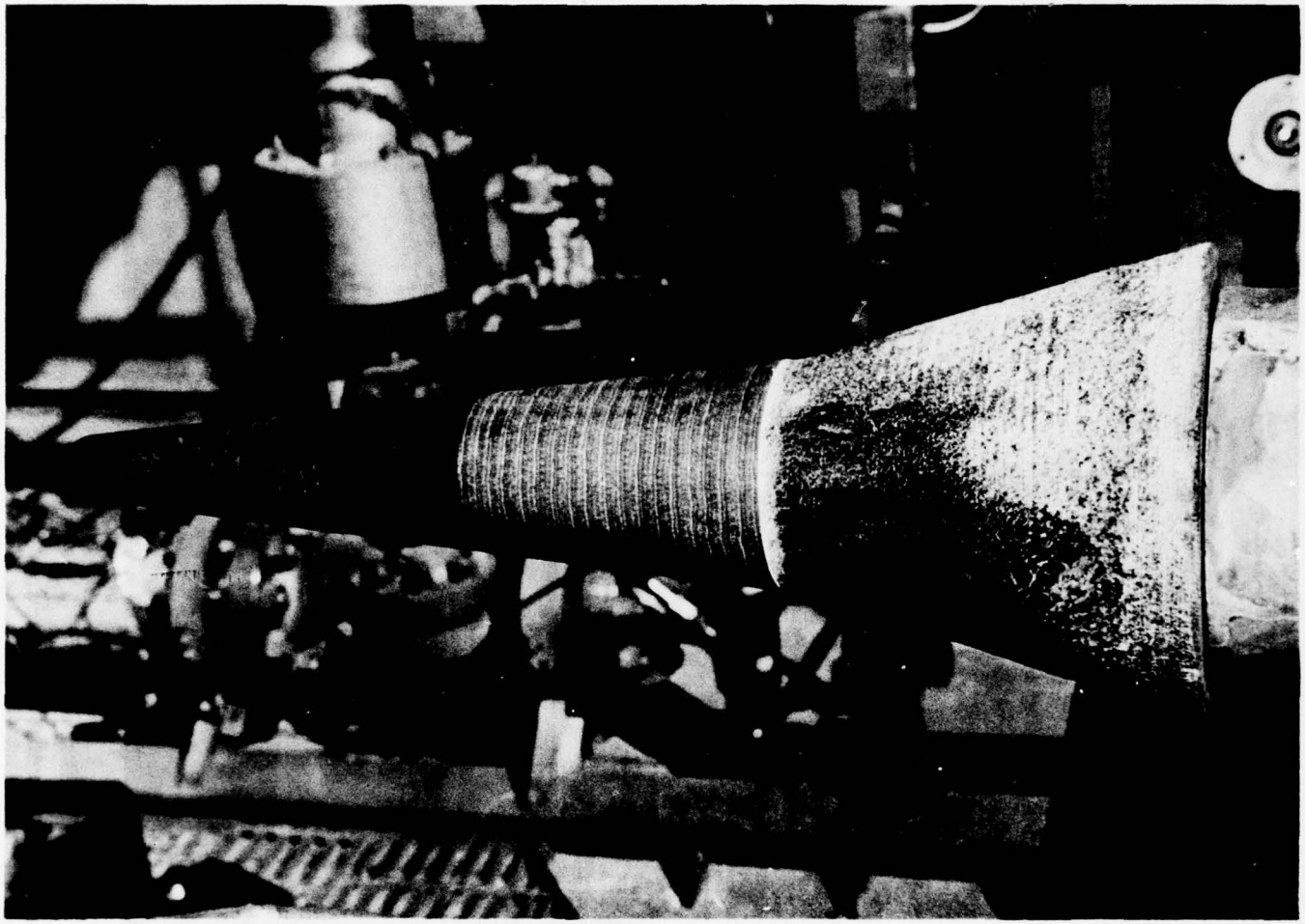

Figure 42: Carbon-Carbon Plug Model and Adapter Mounted on RPL Sting - Side View

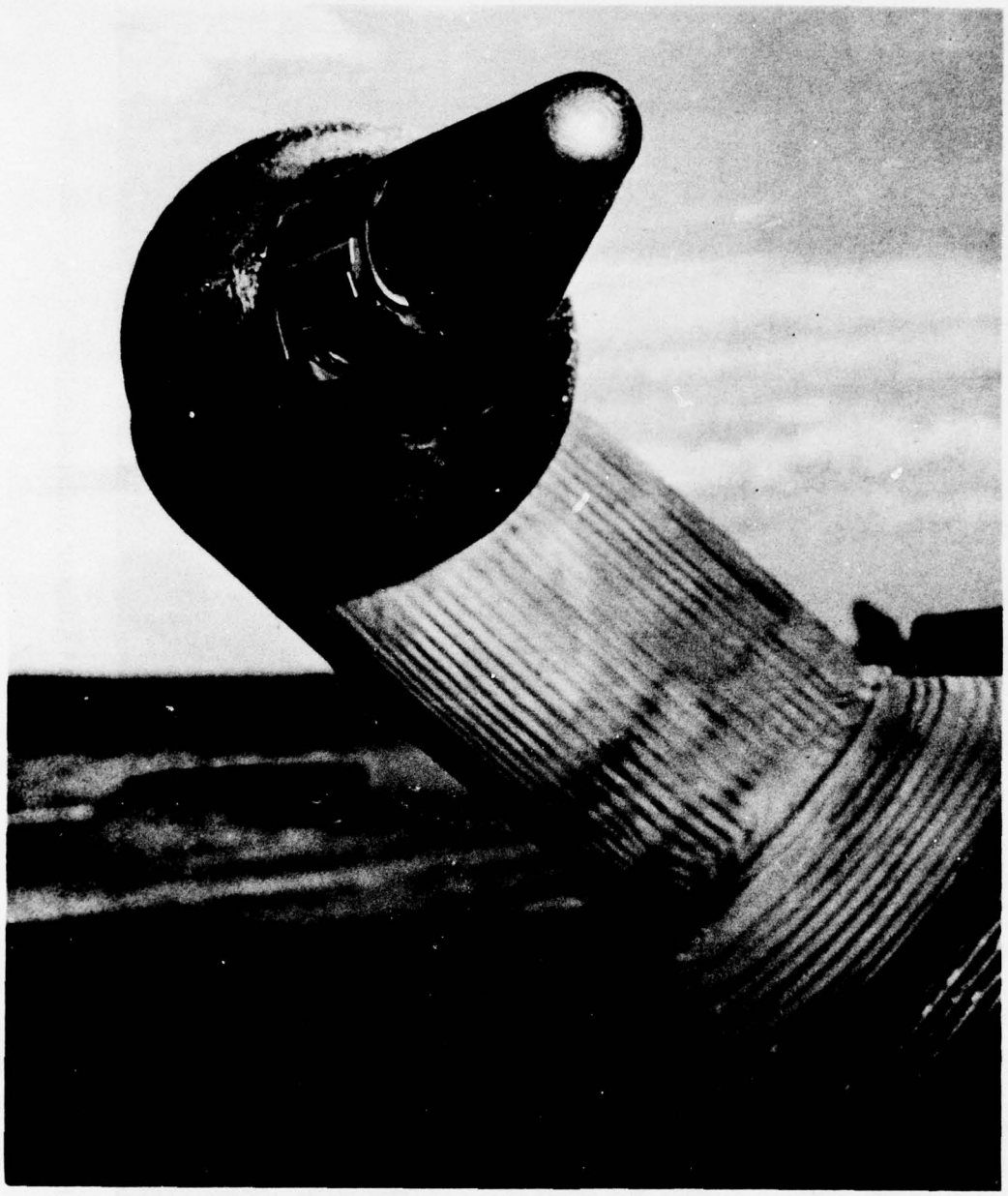

Figure 43: Carbon-Carbon Plug Model Mounted on RPL Sting - Front View

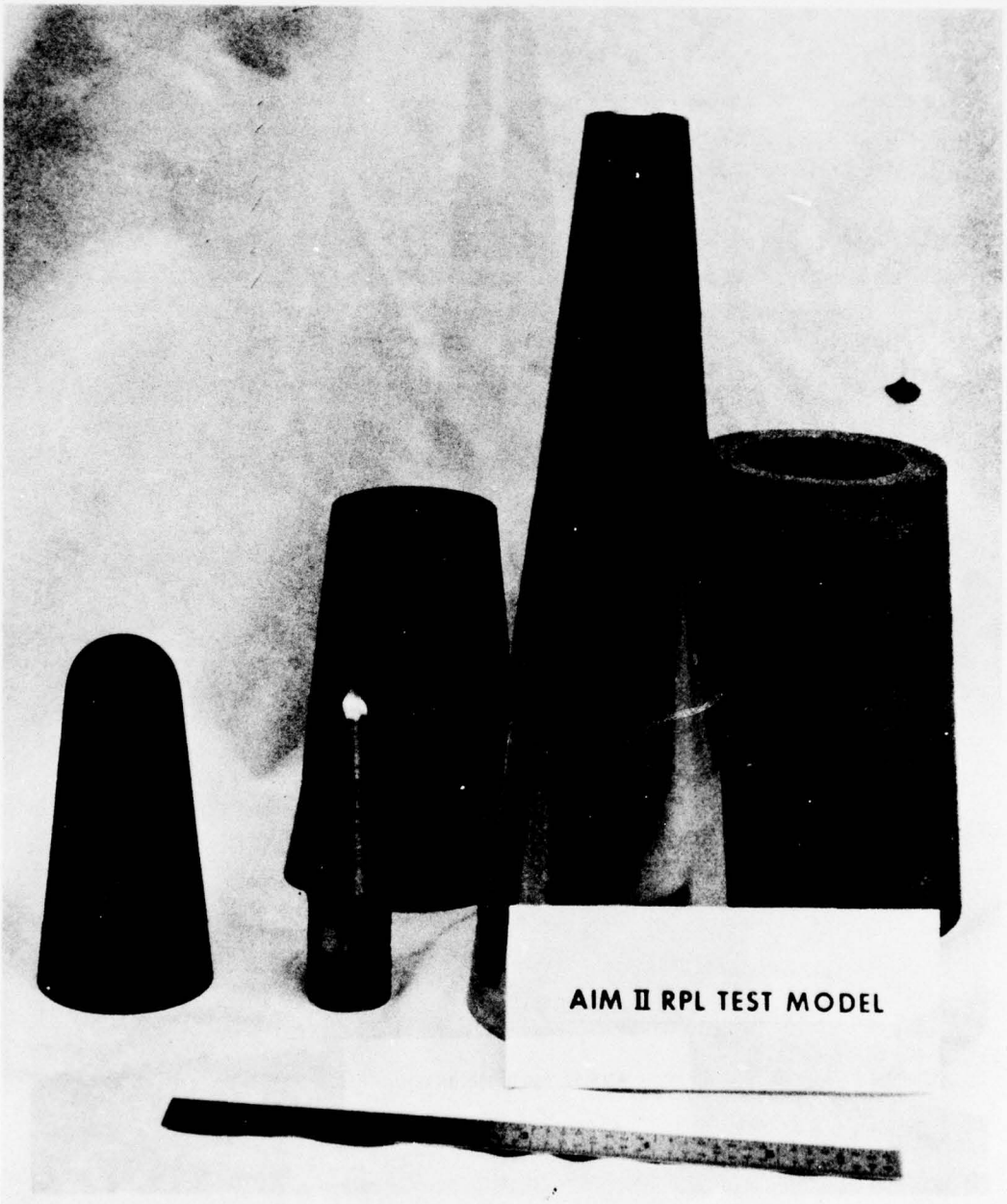

Figure 44: ERN Concept Model Components

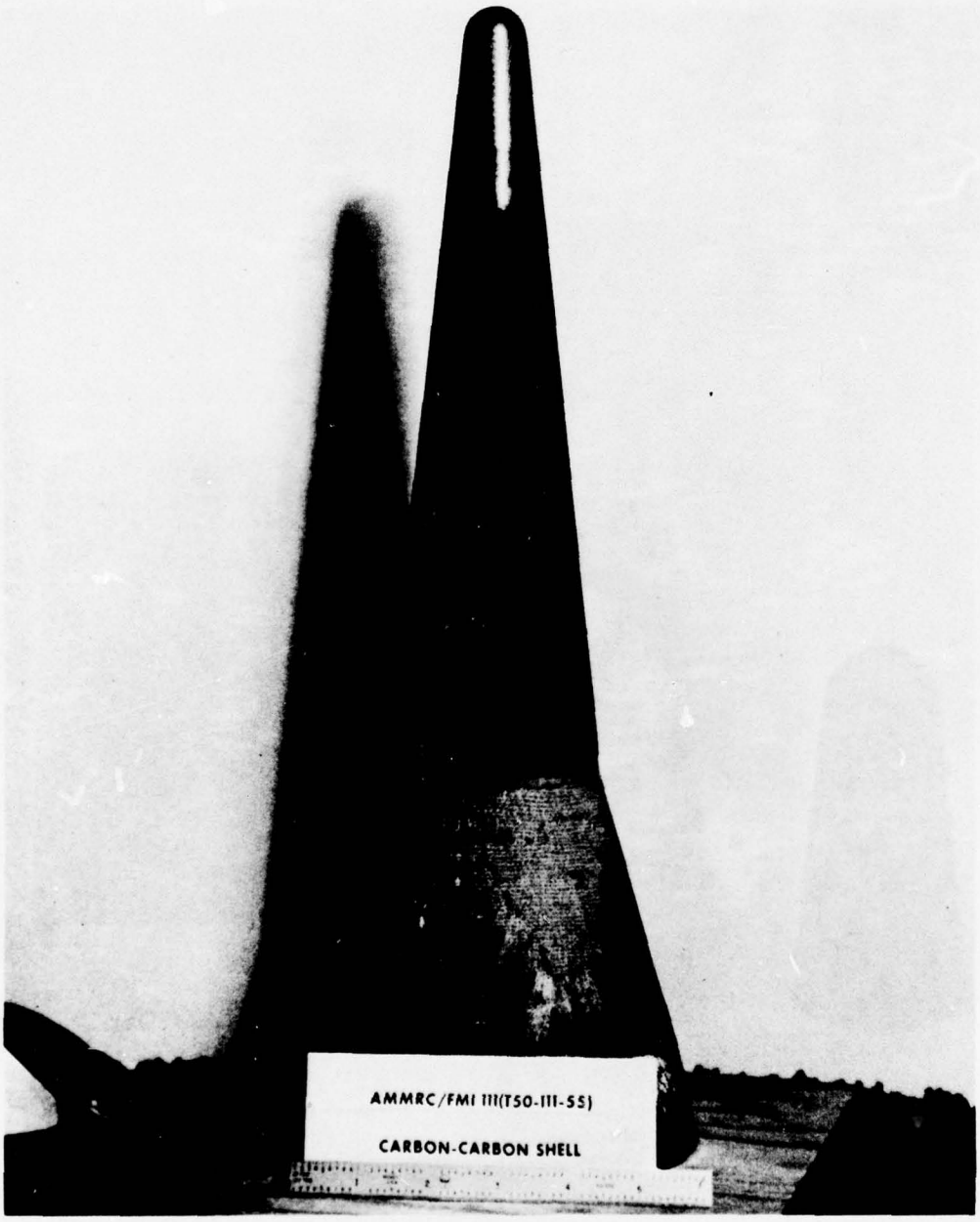

Figure 45: ERN Concept Shell Model T50-111-55

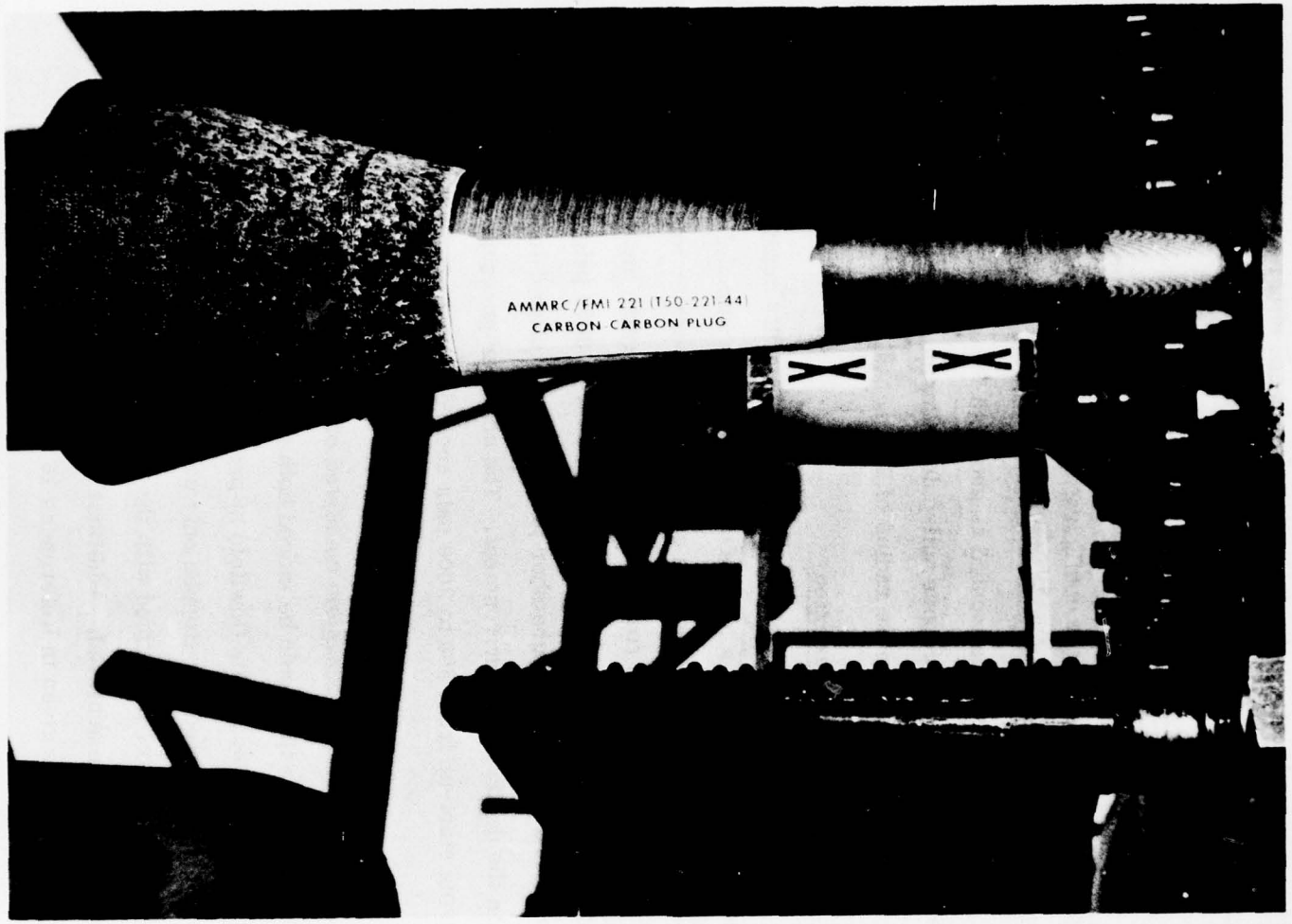

Figure 46: ERN Concept Model T50-221-44

The ERN concept nosetips each had ten thermocouples. Four thermocouples were located between the heatshield and either the tungsten subtip backface or the tantalum sleeve (See Figure 39).

Calibration Models

Heat flux and pressure calibration models were provided by AFRPL. The pressure models were of the configuration shown in Figure 47 with a nose radius of 0.75 inch. Each pressure model used four Kulite fast-response type "IS" pressure transducers located as shown in Figure 47. The heat flux model was instrumented with copper null-point calorimeters at the locations shown in Figure 48 and had a nose radius of 2.0 inches.

2.7.4 Test Facility Description

The ABRES RPL Reentry Nosetip Test Facility consisted of rocket engine test stand 1-52-C with a hot gas combustor and a remotely-controlled model insertion mechanism. The high enthalpy gas generator was a 50,000-pound thrust-equivalent liquid rocket engine. Liquid oxygen and benzonitrile (C_6H_5CN) propellants were burned in the combustor at 3000 psig pressure. Both the mixture ratio and the chamber pressure were closed-loop controlled to maintain the desired test environment. The chamber pressure could be varied during start-up from 500 to 3000 psia according to a predetermined program.

The insertion mechanism consisted of a rotating, radial arm mounted on a carriage that could be moved both axially and radially. The test item was swept in and out of the flowfield at preprogrammed rates. Although the engine could be started and stopped only with the model holder out of the stream, these tests were performed with the model in place before high pressure conditions are achieved. Additional details of the facility capability and instrumentation are given in References 16 and 17.

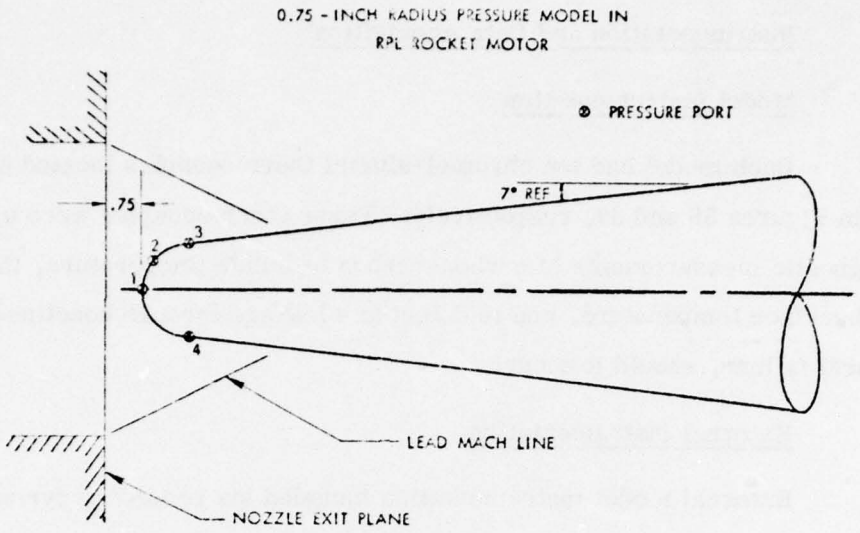

Figure 47: RPL Pressure Calibration Model (Typical)

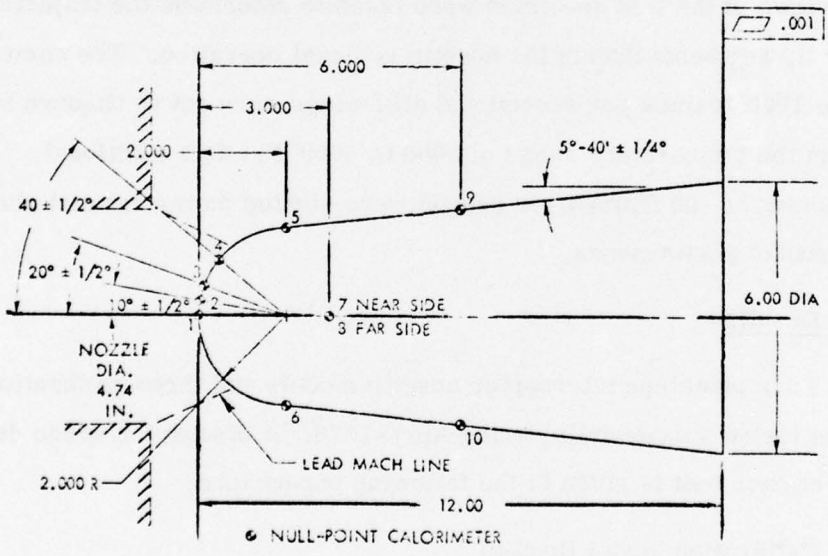

Figure 48: RPL 2.00-Inch Nose Radius Calorimeter Model

2.7.5 Instrumentation and Data Acquisition

Model Instrumentation

Each model had ten chromel-alumel thermocouples located as shown in Figures 38 and 39, respectively. These thermocouples were used for diagnostic measurements of carbon-carbon backface temperature, the heat-shield backface temperature, and to detect gas leakage through bondlines or structural failure, should it occur.

External Instrumentation

External model instrumentation included six recording pyrometers to measure surface temperature and eight motion picture cameras. High speed motion picture coverage of each test was provided by six color motion picture cameras focused on the test specimen. The viewing orientation (angle and elevation) of each camera was defined as shown in Figure 49. Three orthogonal views of the test specimen were taken to determine the trajectory of the outer tip segments during the nosetip removal operation. The camera speeds were 1000 frames per second and all f-stops were set to observe surface detail in the temperature range of 5000 to 6000^{o}F. Two additional cameras running at 400 frames per second were sighted on the exhaust plume to observe rocket performance.

2.7.6 Results

Four prototype interceptor nosetip models and three calibration models were tested successfully during April 1976. A discussion of the data and results of each test is given in the following paragraphs.

Calibration Model Results

Two pressure calibrations and one heat flux calibration were performed as shown in Table 26. The teflon glove that was to protect each

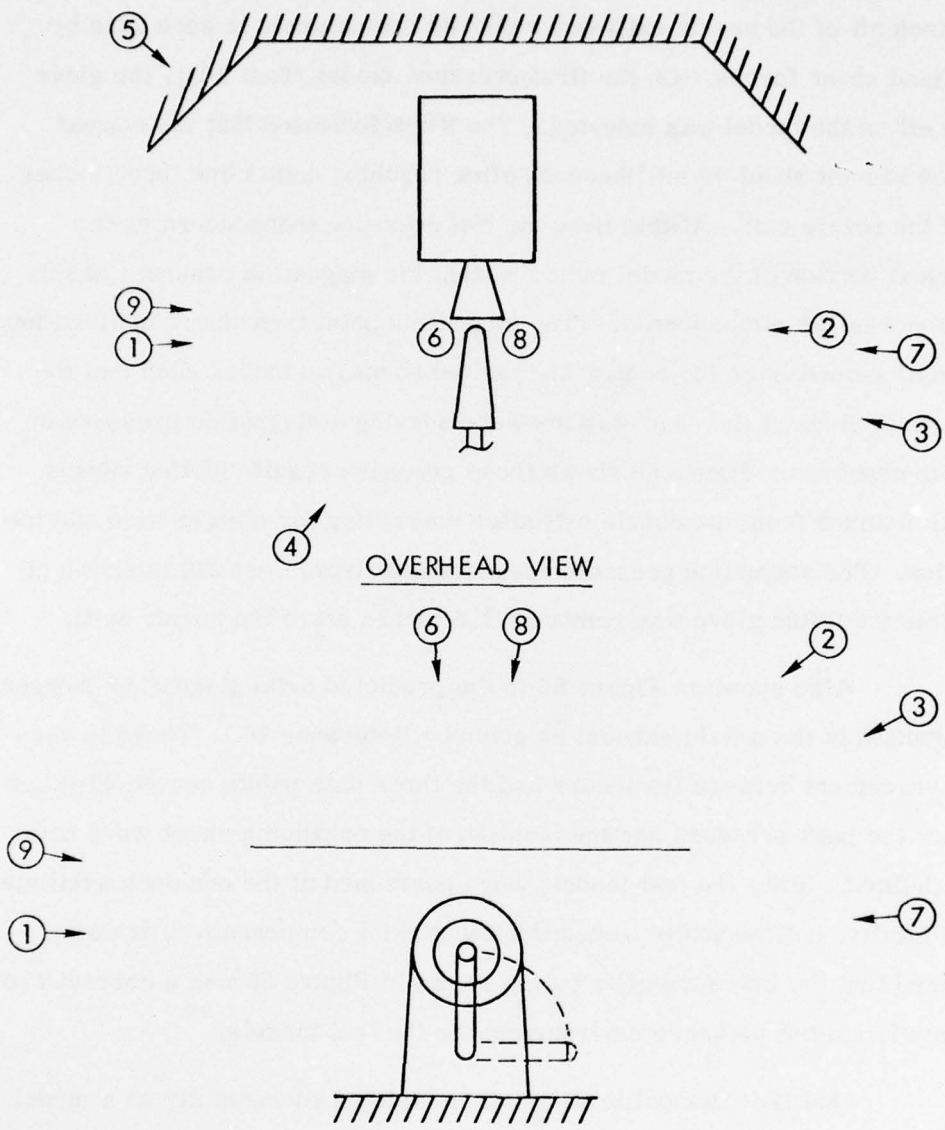

Figure 49: RPL Test Stand 1-52-C Camera Locations and Numbers

pressure model during insertion to the desired test station in the exhaust (1.0 inch aft of the nozzle exit) was removed prematurely in each case by undefined shear forces. On the first pressure model (Test 203), the glove came off as the model was inserted. The films indicated that the copper started to melt about 40 milliseconds after reaching centerline three inches aft of the nozzle exit. At this time the two pressure transducers on the spherical portion of the model indicated that the stagnation pressure at this location was 123 atmospheres. (The stagnation point transducer malfunctioned). One-half second later the copper had melted about two inches such that the transducer lines at the rear stations were sensing a stagnation pressure of 140 atmospheres. Figure 50 shows these pressure results plotted versus actual distance from the nozzle exit after correcting for sting motion and model ablation. The stagnation pressure measurement from Test 210 is shown at the time the teflon glove was removed (1.5 inches aft of the nozzle exit).

Also shown in Figure 50 is the predicted axial stagnation pressure distribution in the nozzle exhaust as given by Reference 16.* There is very good agreement between the theory and the three data points shown, although neither the peak pressure nor the location of the enhancing shock wave have been defined. Since the test models were positioned at the one-inch axial station initially, but thereafter receded without axial compensation, it was assumed that the pressure distribution shown in Figure 50 was a correct representation of the pressure environment for the test models.**

One heat flux calibration was completed successfully on a model with a 2.0-inch nose radius (Figure 48). The heat flux distribution as

* The variation of model stagnation pressure shown in Figure 50 assumed a constant shock stand-off distance of 0.3 inch for a 1.0 inch radius sphere.

**Further pressure calibrations of this nozzle will be performed and reported by AFRPL later this year.

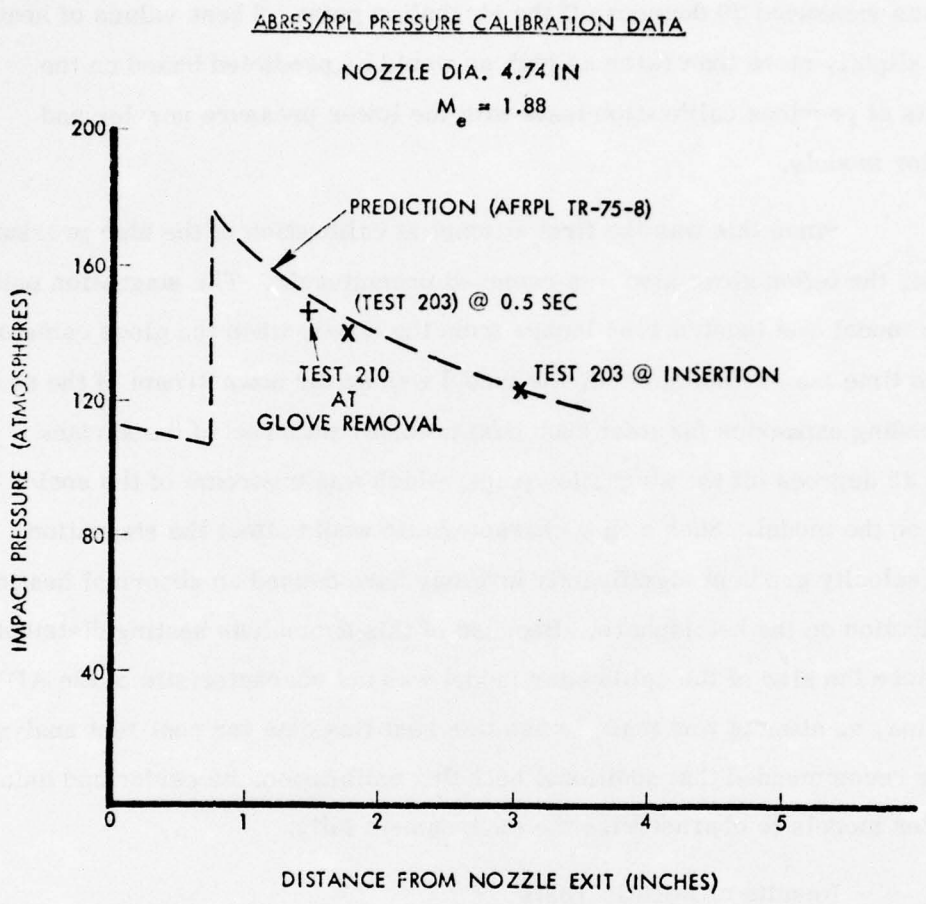

Figure 50: ABRES/RPL Pressure Calibration Correlation - High Pressure Nozzle

measured by this model is shown in Figure 51. The measured stagnation heat rate was 18,000 Btu/ft^2-sec, and a peak heating rate of 23,000 Btu/ft^2-sec was measured 20 degrees off the stagnation point. These values of heating were slightly more than twice as high as would be predicted based on the results of previous calibration tests with the lower pressure nozzles and smaller models.

Since this was the first attempt at calibration of the high pressure nozzle, the teflon glove also was removed prematurely. The stagnation point of the model was located 1.65 inches from the nozzle when the glove came off. By the time the surface melted, the model was so far downstream of the nozzle, the leading expansion fan (test rhombus) probably intersected the surface about 35 degrees off the stagnation point, which was upstream of the sonic point on the model. Such a flow characteristic would affect the stagnation point velocity gradient significantly and may have caused an abnormal heating distribution on the hemisphere. Because of this anomalous heating distribution and since the size of the calibration model was not characteristic of the AIM nosetips, no attempt was made to use this heat flux data for post-test analysis. It was recommended that additional heat flux calibrations be performed using smaller models to characterize the environment fully.

Results of Nosetip Tests

All four nosetip tests were completed successfully. Both carbon-carbon plug models survived intact. The carbon-carbon shell models were removed as intended and both tungsten subtips survived without evidence of thermostructural failure. Table 27 summarizes the results of each test. The data given in table include exposure time of the primary tip and subtip, steady-state recession rates as measured from film data, total recession of the primary tip and subtip, and sidewall recession at the forward joint between the

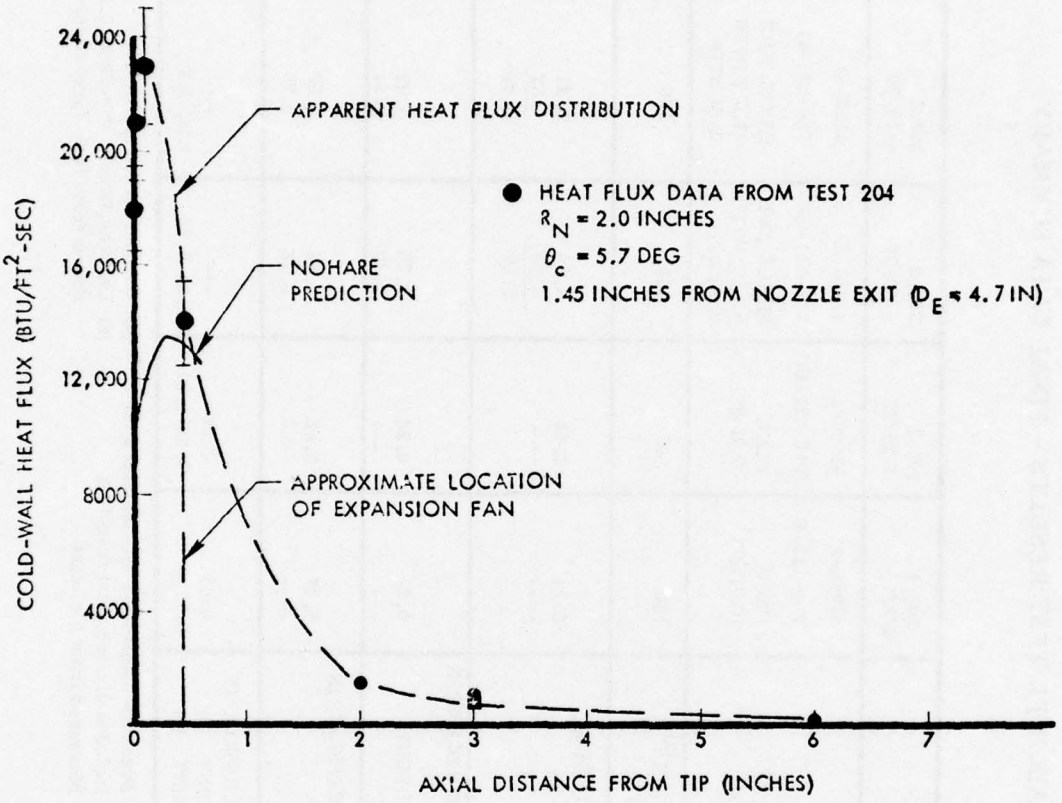

Figure 51: Measured Cold-Wall Heat Flux Distribution - R_N = 2.0 Inches

TABLE 27: AIM/RPL TEST RESULTS - FINAL DATA SUMMARY

RPL TEST NO. DATE	205.1 4/8/76	206.1 4/20/76	207.2 4/21/76	208.1 4/28/76
MODEL	41966-3	41966-1	41965-1	41965-3
MATERIAL	T50-112-40	T50-221-44	T50-111-55	T50-221-44
CONFIGURATION $R_N = 0.5$, $\theta_c = 6^o$	PLUG (O/H=2")	PLUG (O/H=2")	SHELL (O/H =1.5") WITH W SUBTIP	SHELL (O/H =1.5") WITH W SUBTIP
PEAK STAGNATION [a] PRESSURE, ATM	160	160	160	160
EXPOSURE TIME (SEC) *PRIMARY TIP* (b) SUBTIP	2.24 ----	2.44 ----	4.94 0.58 5.52	5.21 .57 5.78
STEADY-STATE RECESSION RATE, IN/SEC (c) (CARBON/CARBON) (TUNGSTEN)	0.25 ----	0.26 ----	0.25 0.43	0.23 0.41
TOTAL TIP RECESSION, IN PRIMARY TIP SUBTIP	0.47 ----	0.62 ----	1.50 0.31	1.50 0.29
SIDEWALL RECESSION, IN FORWARD JOINT (d) FORWARD SKIRT (e)	0.07 0.11-0.19	0.09 0.13-0.21	--- 0.24-0.28	--- 0.22-0.26

NOTES:
(a) Pressure calibration not completed yet
(b) Includes 0.7 sec start transient
(c) Measured from film data
(d) Carbon-carbon recession
(e) Carbon-phenolic recession 0.25 inch downstream from forward joint

carbon-carbon and the carbon-phenolic heatshield. Figures 52 through 55 show the chamber pressure history for each test with the times of significant events noted. A discussion of each test follows:

Test 205 - Plug Model (T50-112-40)

The first plug model was tested for only 2.2 seconds because of the uncertainty of predicted carbon-carbon and carbon-phenolic recession rates at this uncalibrated test condition.* The model ablated symmetrically and the films showed that a turbulent biconic shape was developed shortly after insertion. The tip ablated just under 0.5 inches. There was no evidence of thermostructural failure of mechanical loss of material. Figure 56 shows a post-test photograph of the model. Figure 57 is a close-up of the tip region which shows the smooth nature of the surface. The post-test shape of the model is shown in Figure 58. Although the nosetip ablated symmetrically, there was some asymmetric ablation on the forward carbon-phenolic heatshield due to the motion of the model during entry and exit.

Test 206 - Plug Model (T50-221-44)

The second plug model was tested for 2.44 seconds. The exposure time of this model was extended only 0.2 second because of the asymmetric nature of the heatshield ablation on the first test. Again, however, the carbon-carbon ablated symmetrically and smoothly, without thermostructural or mechanical losses. A smooth biconic shape was developed at a solid angle of 60 degrees to the axis of the model. (It is significant that this angle was identical to the angle measured from the AFFDL 50 Megawatt tests.) Figure 59 shows the post-test condition of the model. The post-test profile and surface texture were the same as for the previous model tested, except for a slight increase in tip and sidewall recession (See Table 27).

*The pretest analysis indicated that the maximum exposure time for carbon-carbon should be 3.0 seconds (Reference 18).

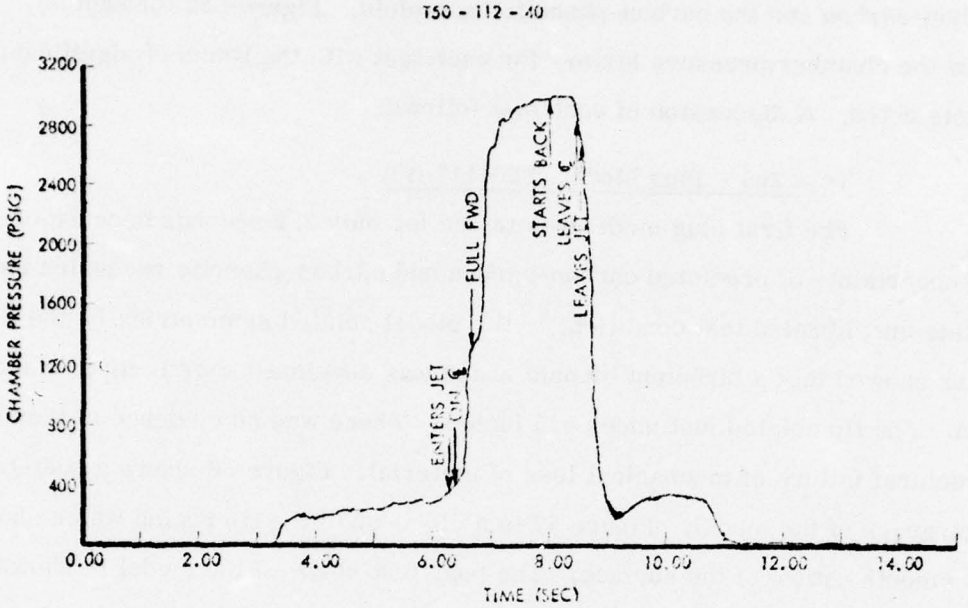

Figure 52: Chamber Pressure History, Test 205 (T50-112-40)

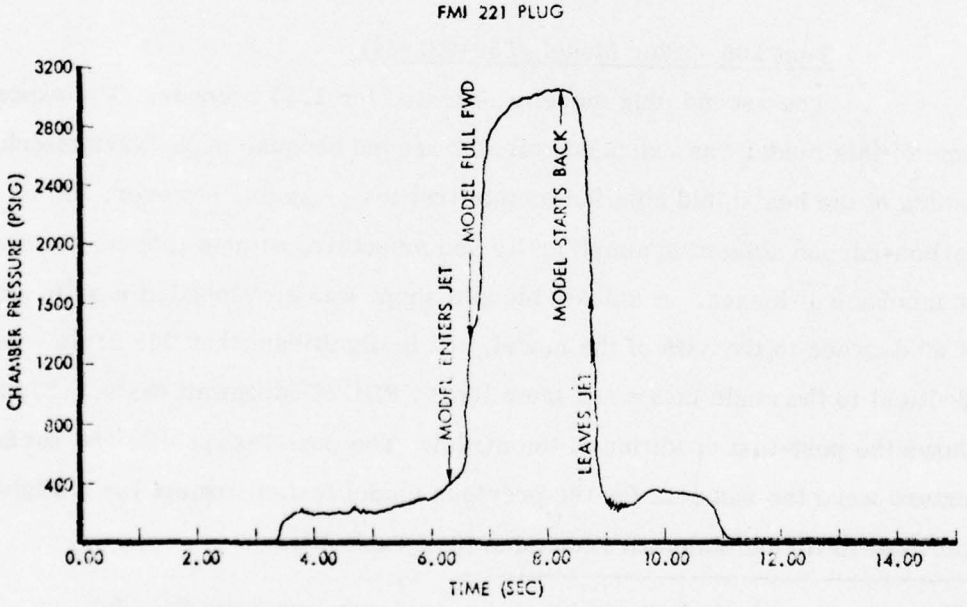

Figure 53: Chamber Pressure History, Test 206 (T50-221-44)

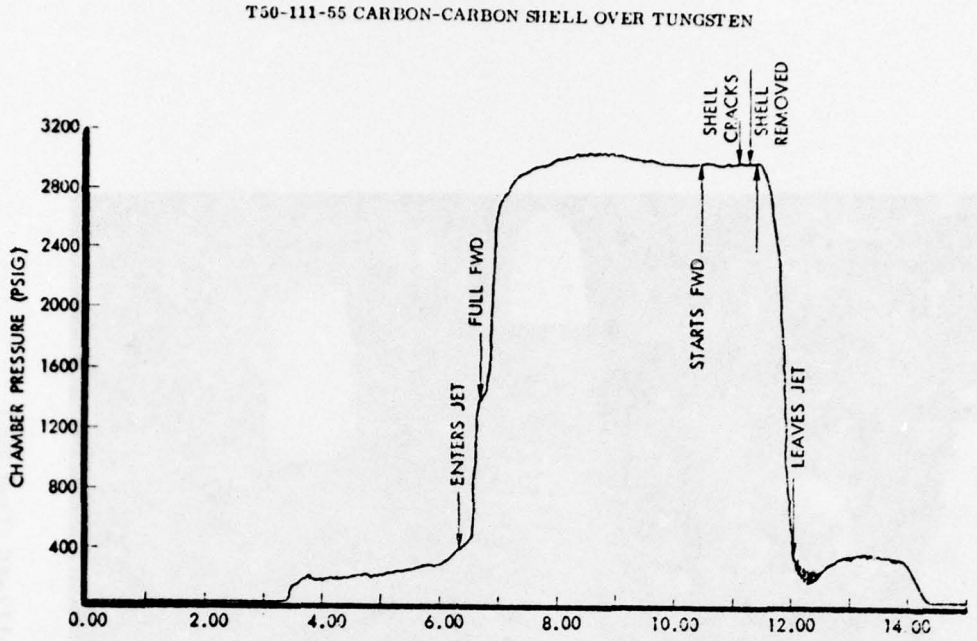

Figure 54: Chamber Pressure History, Test 207 (T50-111-55 over Tungsten)

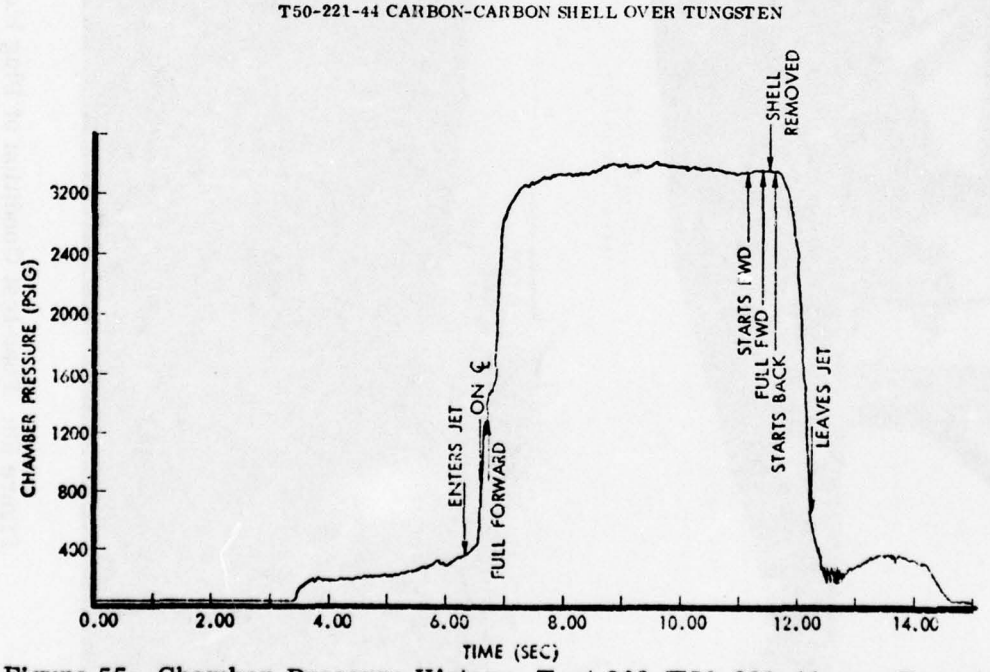

Figure 55: Chamber Pressure History, Test 208 (T50-221-44 over Tungsten)

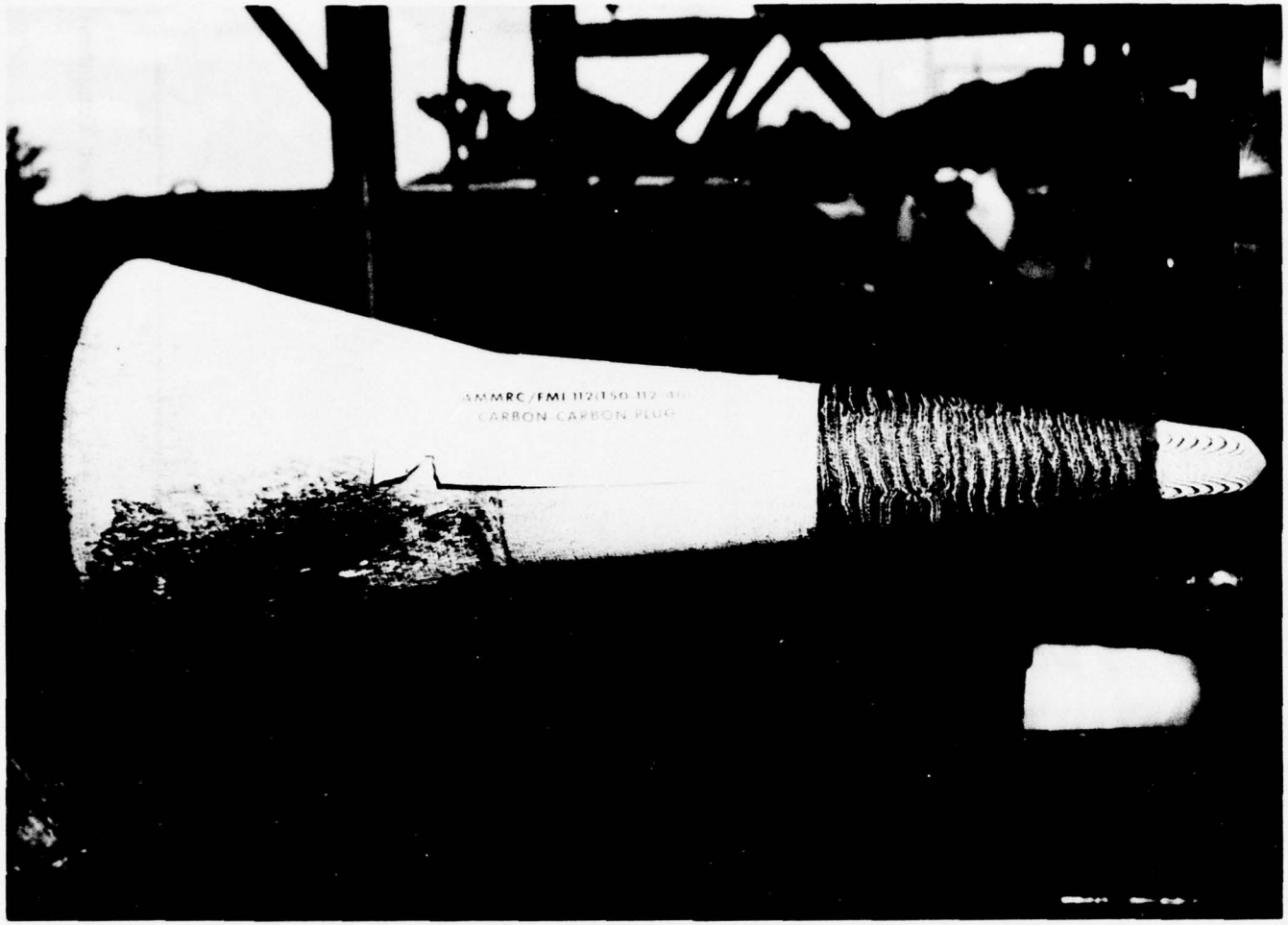

Figure 56: Post-test Condition of Plug Model T50-112-40 (Test 205)

Figure 57: Post-test Surface of Plug Model T50-112-40

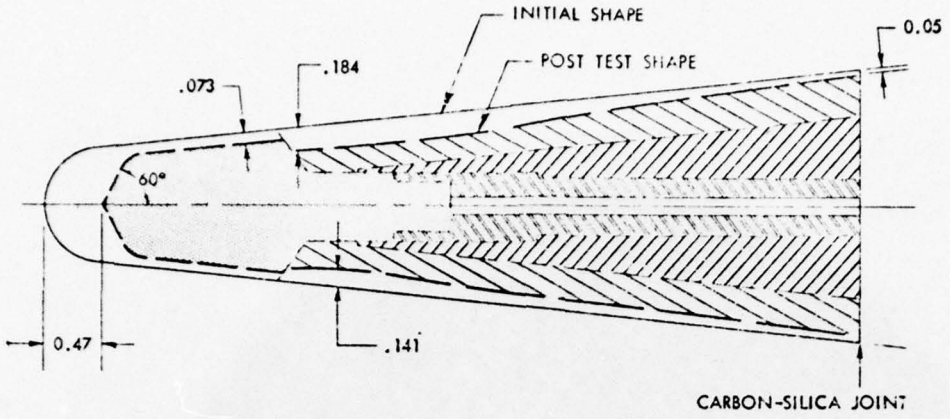

Figure 58: Post-test Shape Test 205 (Plug Model - T50-112-40)

Test 207.2 - Shell Model (T50-111-55)

This was the first test of the ERN design concept with the carbon-carbon shell to be removed during the test. The first attempt to complete this test (207.1) was aborted due to a faulty pressure switch. There was no significant heating of the model during the aborted test, and the second attempt was completed without incident. The primary tip survived 4.9 seconds of exposure before it was removed by the exhaust gases. The tungsten subtip was exposed for an additional 0.6 second. The film data showed that the carbon-carbon ablated symmetrically in a biconic shape for 4.8 seconds after the insertion until about 1.3 inches of recession had occurred at the recession point.* At this time a thin layer of carbon-carbon on the cone sidewall corresponding to a few layers of fibers was stripped off. This phenomenon probably was related to initial burn-through of the carbon-carbon shell near the tangent point of the subtip's sphere-cone configuration. About 0.15 second later, the shell removal was completed. Removal of the remaining shell material was accomplished in less than 0.002 second (two camera frames). The tungsten ablated smoothly also with a slight asymmetry visible on the side that left the exhaust last.

* The model started to move forward 0.8 second before shell removal. This occurred because the actual carbon-carbon recession rate was lower than initial predictions.

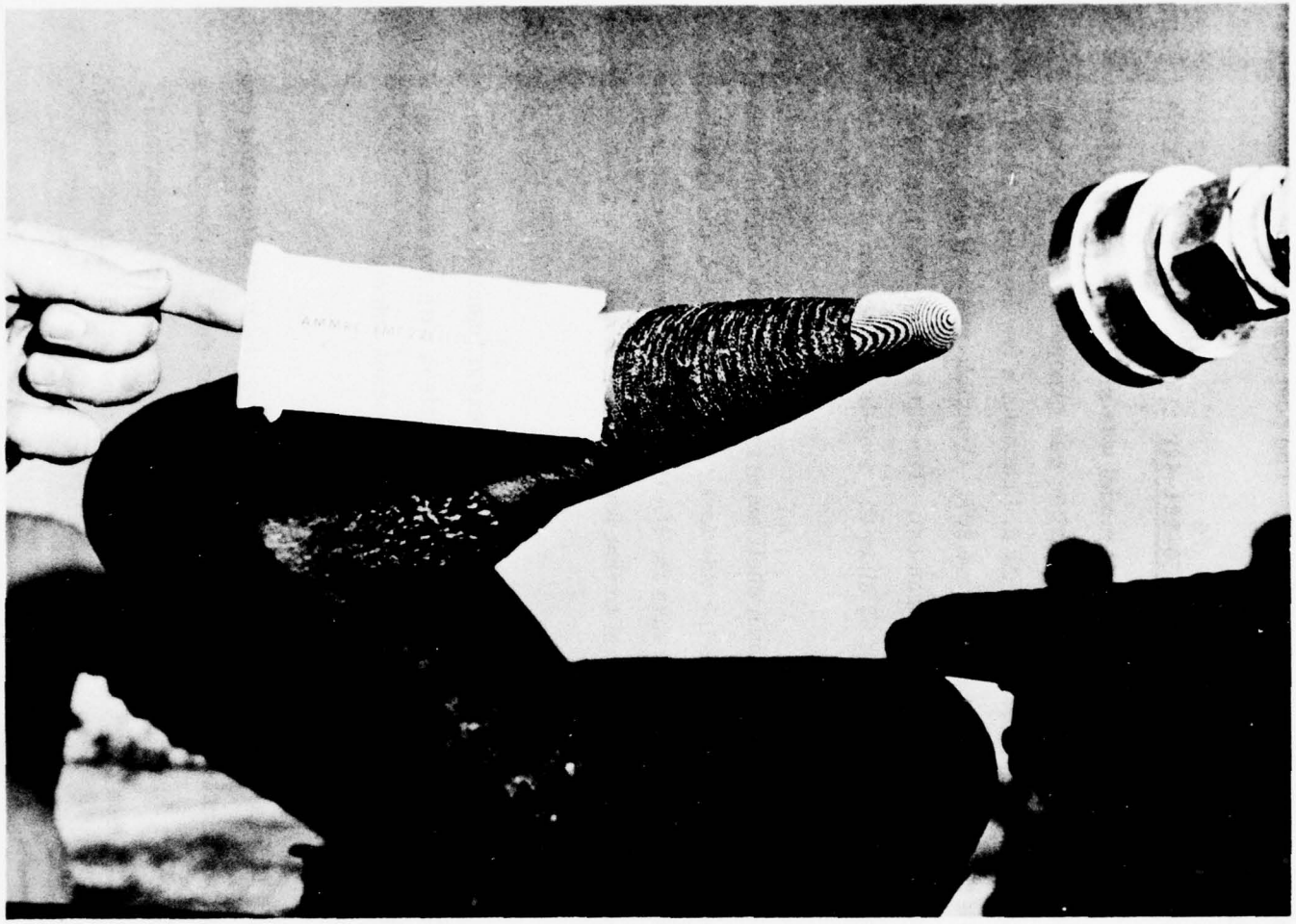

Figure 59: Post-test Condition of Plug Model T50-221-44 (Test 206)

Post-test inspection of the tungsten showed no evidence of cracking. Figure 60 shows a post-test photograph of the model. The post-test profile of the model is shown in Figure 61.

Test 208 - Shell Model (T50-221-44)

The second test of the shell model was similarly successful with nearly identical results. The carbon-carbon was exposed for 5.2 seconds before complete removal occurred. At 5.0 seconds a few layers of fiber were stripped off the sidewall similar to test 207. Complete removal occurred in less than 0.002 second (2 camera frames). The tip recession at this time was 1.2 inches. Figures 62 and 63 show the post-test condition of the subtip model.

The 221 carbon-carbon shell apparently survived longer becuase its recession rate was lower during this test. Because of this, the tungsten exposure time was slightly less than for the third test. The post-test profile of this model was nearly identical to that for the third test.

2.7.7 Post-test Analysis

Analysis of the results included the measurement of recession histories and profiles for each model and a comparison with the recession predicted by thermochemical theory for the RPL rocket exhaust.

Recession Rate Measurements

Figures 64 through 67 show the recession histories and shape profiles of the tip for each test as measured from the film data. Table 28 shows the analysis of the digital data from which exposure times were determined for each test. These times are quoted in seconds measured from the signal.

Figure 60: Post-test Condition of Shell Model (T50-111-55)

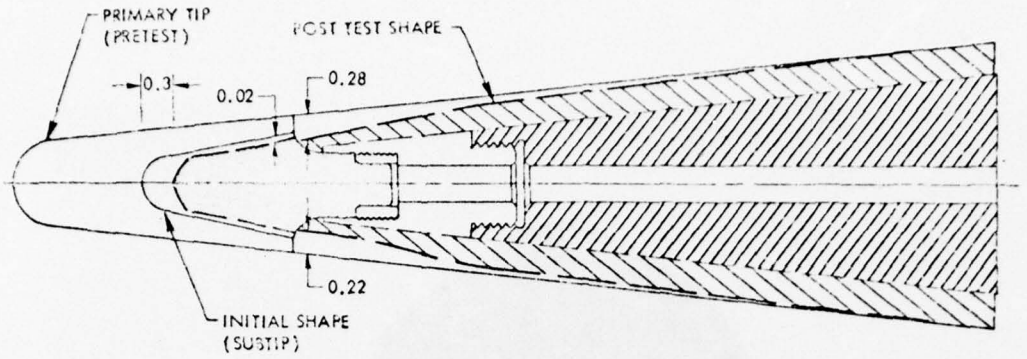

Figure 61: Post-test Contours of Carbon-Carbon/Tungsten Shell Models

The steady-state ablation rates obtained from Figures 64 through 67 are summarized in Table 29. This table shows that the measured instantaneous recession rates varied from 0.21 to 0.28 inch per second for the four carbon-carbon tips without any discernible trend among the three weaves. The mean of all the carbon-carbon recession rate measurements was just under 0.25 inch per second. The estimated accuracy of this measurement technique using film data was $\pm$ 10 to 15 percent. Since the variation of recession rate between materials was of the same order as the measurement accuracy, it was concluded that there was no significant effect of the weave spacing of these three materials on ablation rate at these pressures. Thus, all three of the materials performed excellently in high pressure ablation.

Comparison with Theory

The recession histories of all four tests are shown in Figure 68 together with the recession predicted by the PDA NOHARE computer code based on the actual test conditions. The flow conditions in the RPL facility were calculated using the PDA NOHARE computer code with the NONAIR option described in Reference 19. The NONAIR option utilized complete freestream rocket exhaust thermophysical properties obtained from the One-Dimensional

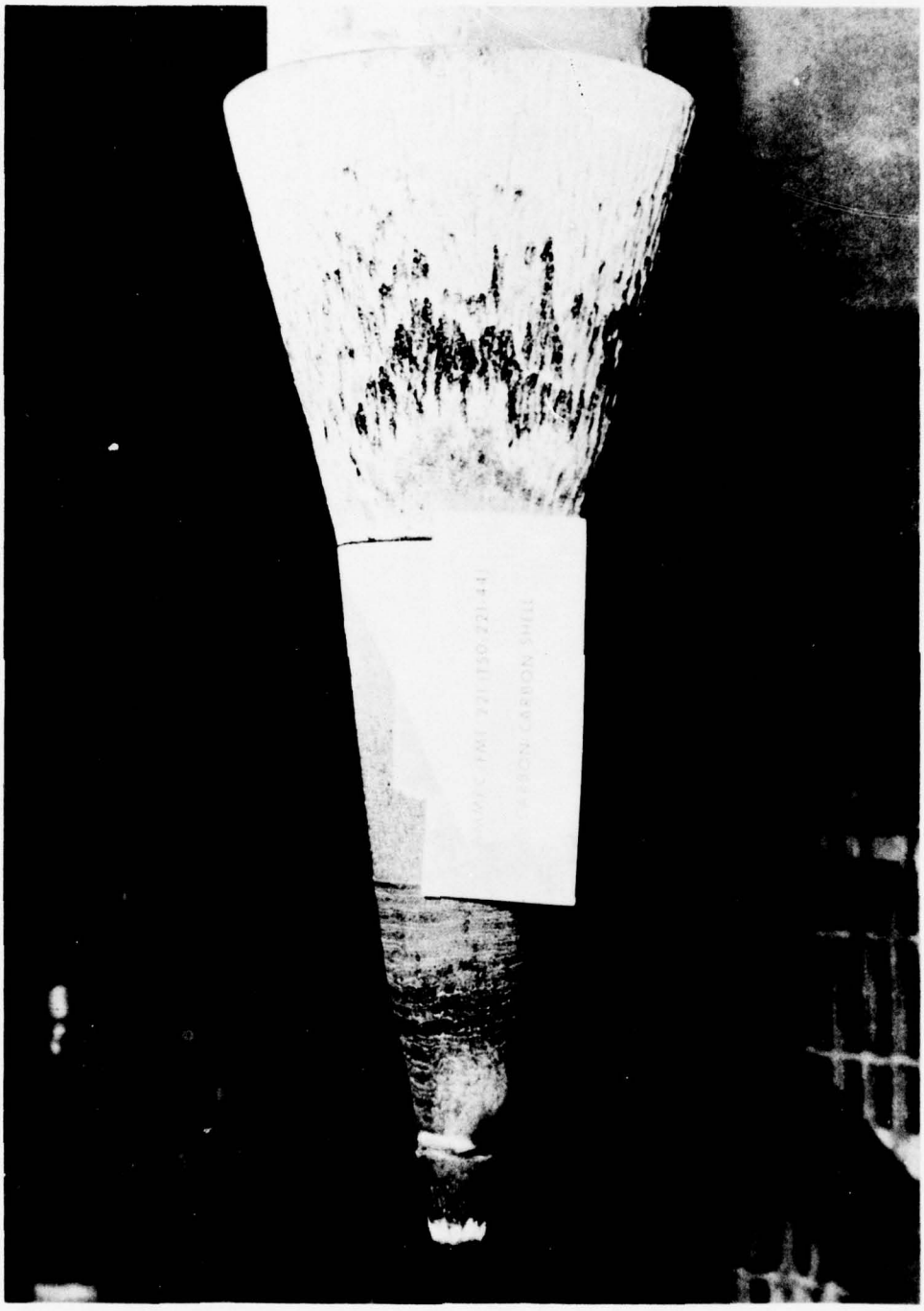

Figure 62: Post-test Condition of Shell Model T50-221-44 (Test 208)

Figure 63: Post-test Surface of Shell Model T50-221-44

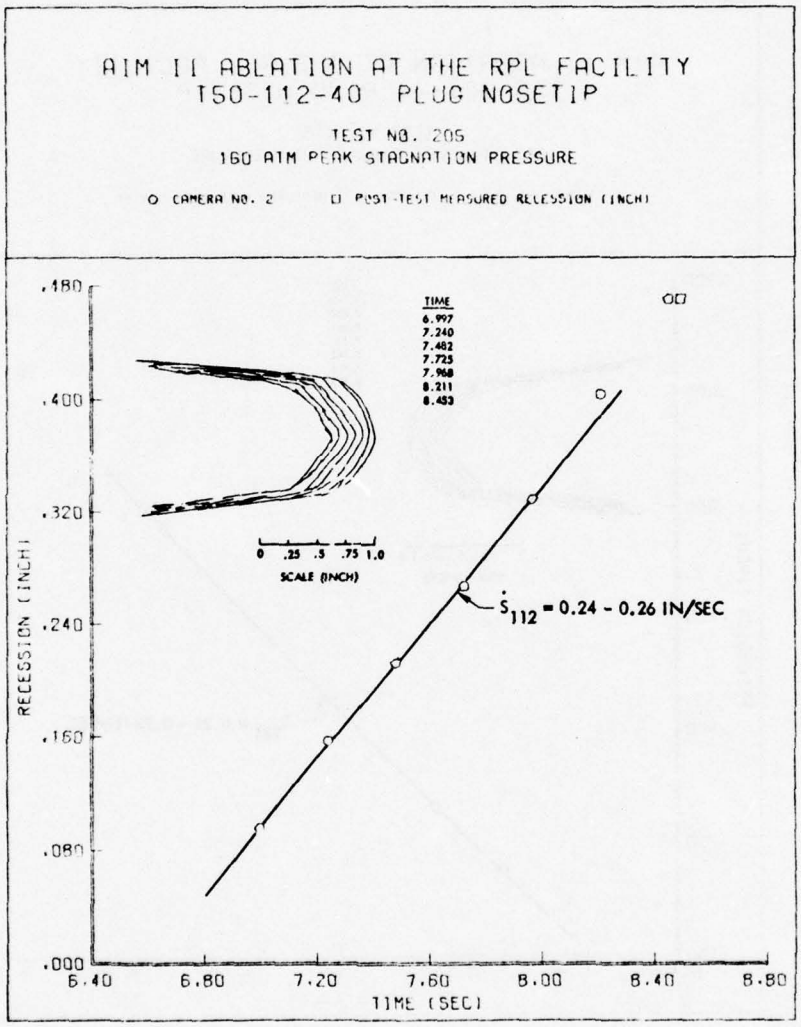

Figure 64: Recession History and Shape Profiles - Test 205

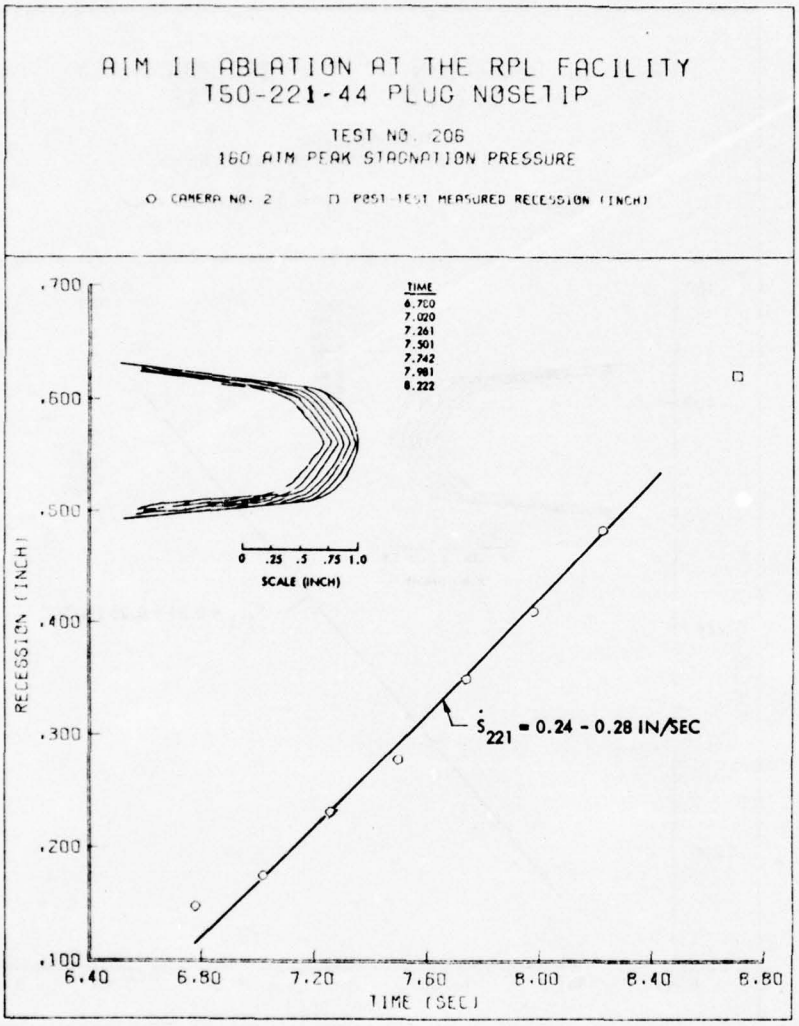

Figure 65: Recession History and Shape Profiles - Test 206

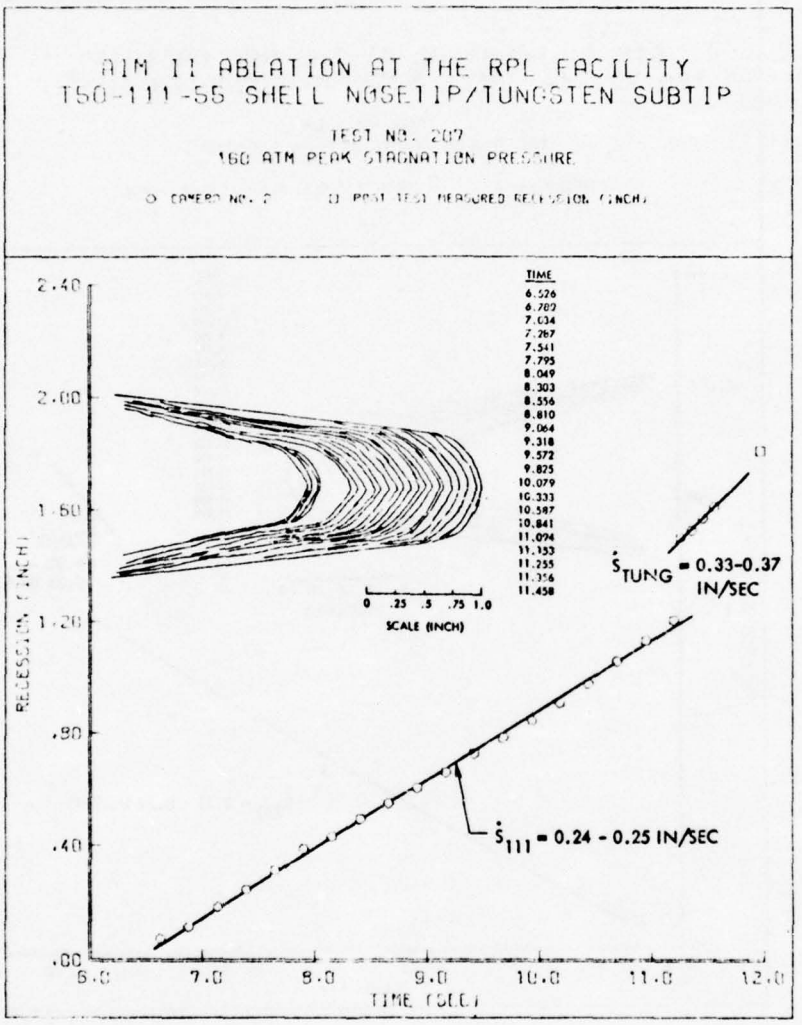

Figure 66: Recession History and Shape Profiles - Test 207

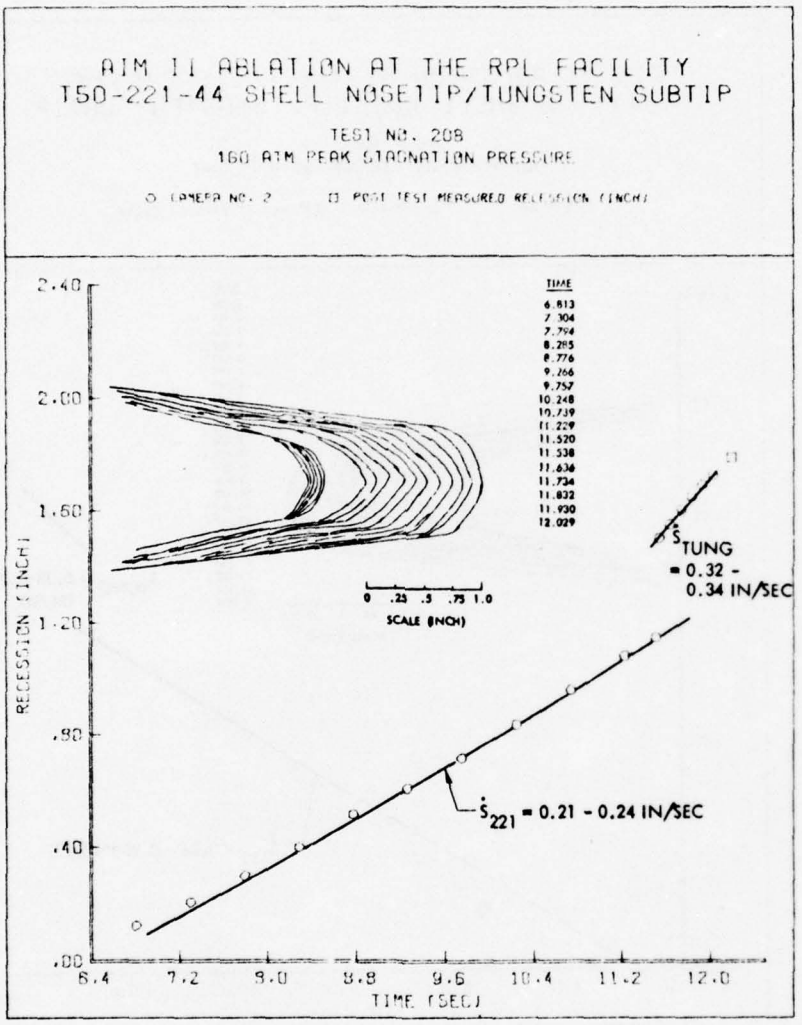

Figure 67: Recession History and Shape Profiles - Test 208

TABLE 28: AIM/RPL DATA ANALYSIS

	FACILITY EVENT TIME (SEC)			
TEST NO.	205	206	207.2	208
MODEL	112 PLUG	221 PLUG	111 SHELL	221 SHELL
Model Enters Jet (T_1)	6.307	6.307	6.323	6.325
Model Starts Forward	6.394	6.381	6.443	6.445
Model on ℄	6.454	6.414	6.543	6.625
P_{c_2} > 600 psi (T_2)	6.587	6.567	6.556	6.571
Model Full Forward	6.660	6.660	6.710	6.698
P_{c_2} > 2800 psi (T_3)	7.392	7.113	7.175	7.184
Model Starts Forward			10.450	11.170
Model Full Forward			10.703	11.430
Shell Cracks			11.11	11.310
Shell Removed (T_4)			11.257	11.534
Model Starts Back	8.025	8.251	11.362	11.610
P_c Starts Down (T_5)	8.484	8.517	11.502	11.790
P_c < 1500 (T_6')	8.724	8.770	11.841	12.101
Model Leaves ℄	8.497	8.704	11.968	12.189
Model Leaves Jet (T_5)	8.550	8.744	12.021	12.242
T_1 Failed	7.925	8.105	11.076	---
T_2 Failed	7.905	7.712	---	---
Carbon-Carbon Exposure:				
Transient ($T_3 - T_1$)	1.085	0.806	0.852	0.859
Full P_c ($T_5 - T_3$)	1.092	1.404	4.082	4.350
Exit ($T_6 - T_5$)	0.066	0.227	---	---
Total Carbon-Carbon Exposure	2.243	2.437	4.934	5.209
Tungsten Exposure:				
Full P_c ($T_5 - T_4$)			0.245	0.256
Exit ($T_6 - T_5$)			0.339(T_6')	0.311
Total W Exposure			0.584	0.567
TOTAL TEST TIME	2.243	2.437	5.518	5.776

TABLE 29: RANGE OF MEASURED RECESSION RATES

TEST NO.	MODEL NO.	RECESSION RATE (IN/SEC	
		CARBON-CARBON	TUNGSTEN
205	T50-112-40	0.24 - 0.26	---
206	T50-221-44	0.24 - 0.28	---
207	T50-111-55	0.24 - 0.25	0.35
208	T50-221-44	0.21 - 0.24	0.33
	MEAN	0.245 ± 0.035	0.34

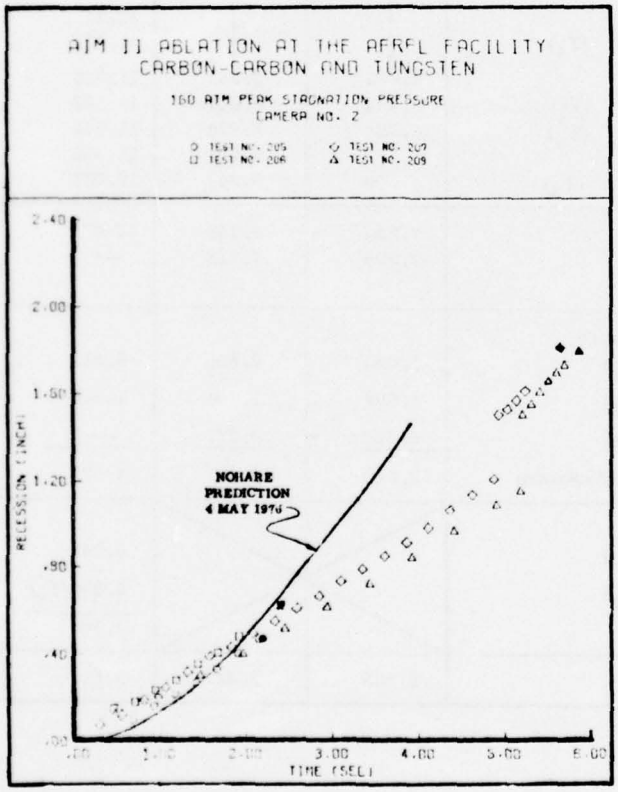

Figure 68: Comparison of Predicted and Measured Recession for all Carbon-Carbon Models

Equilibrium (ODE) computer program over the full test pressure and temperature range. The program calculated the complete local flow properties including molecular weight, density, entropy, viscosity, gas enthalpy, and temperature. The analysis assumed an oxidizer-to-fuel mixture ratio of 2.8 for the liquid oxygen/benzonitrile (C_6H_5CN) propellant system. Since the new 4.7-inch diameter nozzle was used for these tests, the Mach number, pressure and total enthalpy for the new propellant system were assumed distribution calculations (See Table 25).

The pressure distribution predicted for the initial primary tip configuration, a 0.50-inch nose radius, six-degree cone, is shown in Figure 69. The subtip pressure distribution for 0.313-inch nose radius, 14-degree cone appears in Figure 70.

The heat flux distributions for the test models are shown in Figures 71 and 72 for primary tip and subtip configurations, respectively. These heat flux distributions assumed a boundary layer transition at a Reynolds number based on momentum layer thickness of 215 (the so-called "PANT" criterion). This resulted in turbulent flow occurring just a few degrees off the hemispherical stagnation point and downstream thereafter. The turbulent heating was gradually reduced downstream of the intersection of the lead Mach line with the model (See Figure 40) to one-quarter of the predicted freestream value.

The recession prediction for the carbon-carbon was also calculated with the NOHARE code using the NONAIR option with carbon thermochemistry in the RPL exhaust gas exhaust gas environment. The Graphite Surface Kinetics Computer Program (GASKET) described in Reference 20 was used to calculate

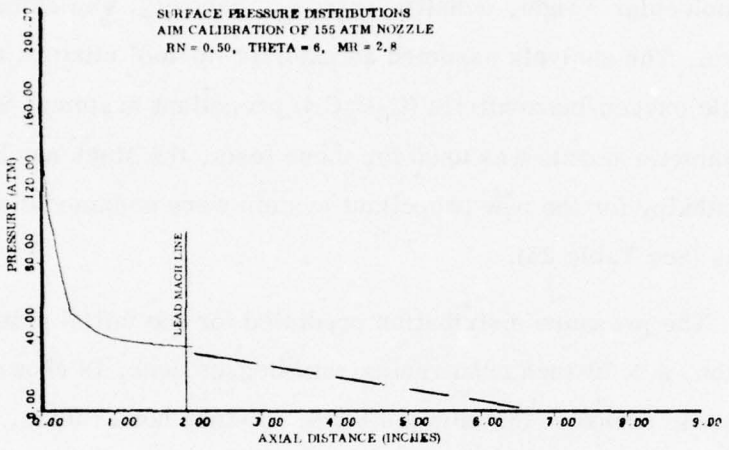

Figure 69: Pressure Distribution, Primary Tip Configuration - 155 Atmosphere Condition

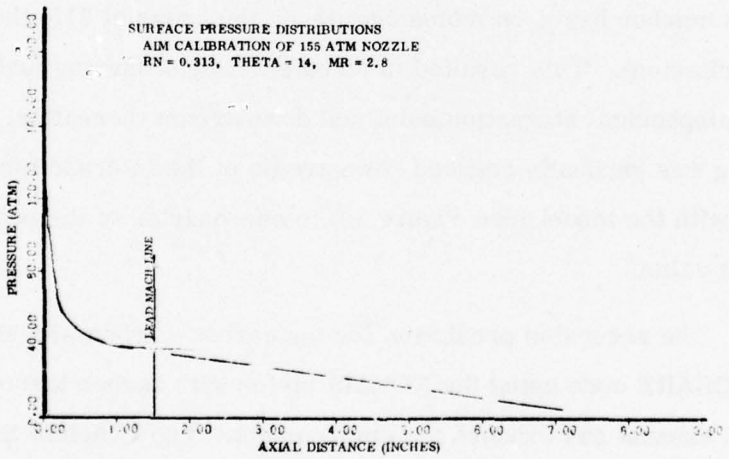

Figure 70: Pressure Distribution, Subtip Configuration - 155 Atmosphere Condition

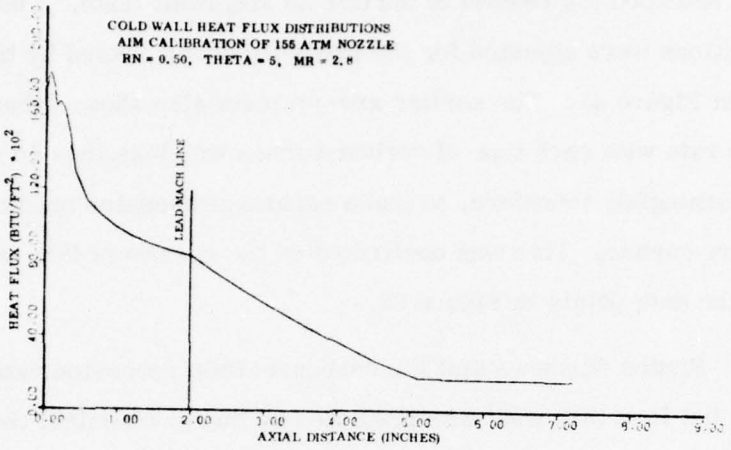

Figure 71: Heat Flux Distribution, Primary Tip Configuration - 155 Atmosphere Condition

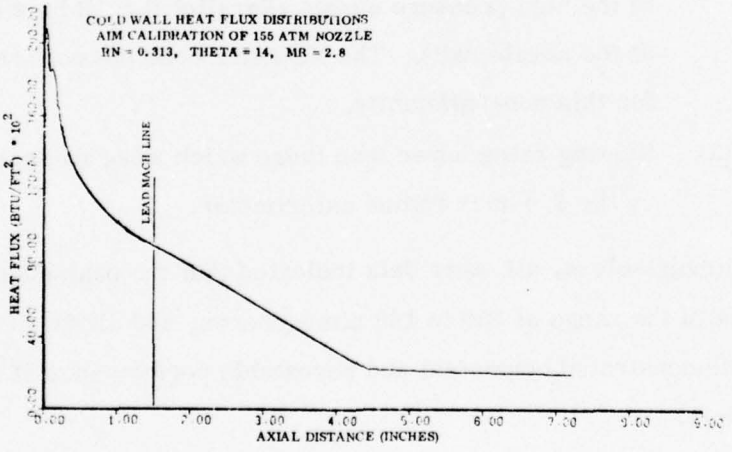

Figure 72: Heat Flux Distribution, Subtip Configuration - 155 Atmosphere Condition

the rate-limited reaction rates of the carbon with the exhaust products. A turbulent ablation roughness height of 0.020 inch was assumed for all carbon-carbons based upon the results of earlier 50 Megawatt tests. The stagnation point conditions were adjusted for the pressure decay caused by tip recession as shown in Figure 41. The earlier arc-jet tests also showed that the variation of ablation rate with each type of carbon-carbon was less than 10 percent. It was not meaningful, therefore, to make separate recession predictions for each carbon-carbon. This was confirmed by the results of this test series as shown by the data points in Figure 68.

Figure 68 shows that the carbon-carbon recession rates were repeatable but less than what was predicted by thermochemical theory for RPL. The probable reasons for the difference between predicted and measured recession were:

(1) Incorrect surface reaction kinetics that produced lower reaction rates with the exhaust.

(2) Axial and radial pressure gradients in the flowfield of the high pressure nozzle (Parallel flow did not exist at the nozzle exit). The NOHARE code did not account for this non-uniformity.

(3) Heating rates lower than those which were measured by the 2.0-inch radius calorimeter.

Nevertheless, all other data indicated that the peak stagnation pressure was in the range of 150 to 160 atmospheres, and all four carbon-carbon tips demonstrated consistent and repeatable performance at these pressure levels.

The theoretical stagnation point recession histories for the tungsten subtip were also calculated by the PDA NOHARE code using equilibrium thermochemical data for tungsten from the ODE code. These results are

shown in Figure 73. These calculations were only approximate, since tungsten ablation rates are very sensitive to sidewall heating effects and to the amount of preheat received through the carbon-carbon before its removal. Because of this, the actual recession of the tungsten as shown by the data points of Figure 73 was higher than the prediction for these short exposure times.

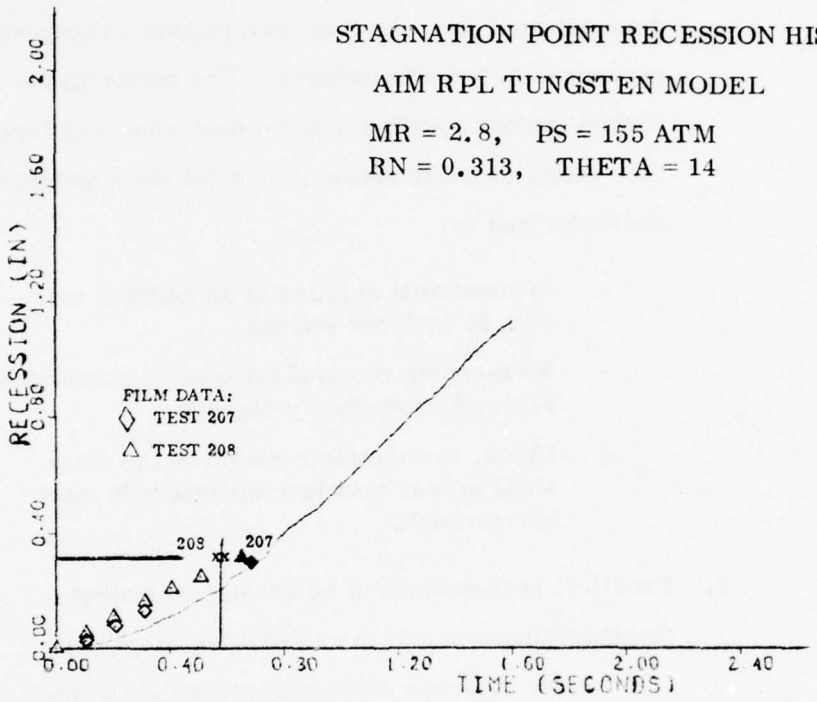

Figure 73: Comparison of Predicted and Measured Tungsten Recession Histories

2.7.8 Conclusions

The following conclusions were made based on the results of these four tests:

1. Prototype full-scale advanced interceptor nosetip designs have been demonstrated successfully in a high pressure environment characteristic of advanced

terminal intercept requirements. The design components that were evaluated successfully included carbon-carbon plug and shell primary nosetips, a tungsten subtip, phenolic carbon forward skirts and a tantalum forward substructure.

2. Three AMMRC/FMI fine-weave carbon-carbon materials demonstrated good ablation performance at stagnation pressures to 160 atmospheres. The performance of the carbon-carbon nosetips was not discernably different from the results of lower pressure arc-jet tests and was characterized by:

   - Symmetrical ablation at an average rate of 0.25 inch per second
   - No thermostructural failures or mechanical removal of surface material
   - Clean, symmetric removal of the outer shell in less than two milliseconds after burnthrough.

3. Excellent performance of an erosion-resistant thoriated tungsten subtip was demonstrated by:

   - No evidence of thermostructural failure
   - Symmetric ablation at an average rate of 0.34 inch per second.

2.8 SAMS Nosetip Experiment

An FMI 221 (T50-221-44) carbon-carbon nosetip was fabricated by PDA and delivered to Sandia Corporation for flight testing on a Sandia-Air Force Materials study (SAMS) flight test vehicle. The properties of the material and the ablation and thermal stress responses were predicted by PDA for AMMRC to support the flight test. Sandia specified the nosetip configuration.

A pretest ablation analysis predicted a total nosetip recession of approximately 0.8 inch, and showed that the radioactive source locations specified by Sandia would result in good definition of the recession history from telemetered data. The computed thermal stresses were low compared to predicted material strengths using conservative linear elastic analysis methods. The following sections describe the analysis of the SAMS design.

2.8.1 Material Description and Properties

The 221 carbon-carbon material was produced by Fiber Materials, Inc. (FMI). The preform was woven on 0.040 x 0.023 inch X, Y, Z centers with two Thornel 50 varns per X and Y site and one Thornel 50 yarn per Z site. The preform was densified with Ashland A240 pitch to a composite density of 1.9 gm/cc. The nosetip was excised from FMI billet number 551.

The material properties used for thermostructural analysis of the nosetip are given in Table 30. No engineering properties had been measured on the material at the time the analysis was performed. Therefore, all properties were estimated from similar materials or calculated as explained below. Thermal conductivities in the Z and X (or Y) directions were estimated by comparision with GE 223 carbon-carbon. This material had identical reinforcement yarn constituents and was pitch-densified to the same density. The latter material had filament volume fractions of 13 percent and 22 percent in the X and Z directions, respectively, while the AMMRC 221 material filament volume fractions were 14 percent and 12 percent. Since the principal difference between the two materials was the volume fraction of filament reinforcement, the thermal conductivity of the 221 in all directions was taken to be equal to the conductivity of 223 in the X direction, as given in Reference 21. This was a reasonable approximation since the X direction filament volume fraction of 223 approximated the 221 filament volume fraction in all directions.

TABLE 30: AMMRC 221 3DCC, MATERIAL PROPERTIES FOR SAMS FLIGHT ANALYSES
Density = 1.90 gm/cc

Temp (°F)	E_x (1) (10^6 psi)	E_z (1) (10^6 psi)	σ_x (1) (ksi)	σ_z (1) (ksi)	$\left(\frac{\Delta L}{L}\right)_x$ (1) (10^{-3} in/in)	$\left(\frac{\Delta L}{L}\right)_z$ (1) (10^{-3} in/in)	ν_{xy} (2)	ν_{xz} (2)	ν_{zx} (3)	K_x (4) $\left(\frac{\text{Btu-in}}{\text{hr ft}^2\,^\circ\text{F}}\right)$	K_z (4) $\left(\frac{\text{Btu-in}}{\text{hr ft}^2\,^\circ\text{F}}\right)$
70	8.5	7.5	20	18	0	0	.05	.05	.04	557	557
1000	8.5	7.5	20	18	-0.29	-0.26	.05	.05	.04	365	365
2000	8.5	7.5	20	18	0.45	5.16	.05	.05	.04	274	274
3000	8.5	7.5	26	22	1.68	1.78	.05	.05	.04	223	223
4000	5.8	5.0	40	33	3.28	3.46	.05	.05	.04	218	218
5000	3.1	2.5	--	--	4.88	5.14	.05	.05	.04	218	218
6000	0.40	0.2	--	--	6.48	6.82	.05	.05	.03	218	218
7000	0.40	0.2	--	--	8.08	8.50	.05	.05	.03	218	218

(1) Computed from constituent properties and preform geometry with PDA CCCELL Code (Ref. 6, 22)
(2) Estimated
(3) Calculated from $\nu_{zx} = \frac{E_z}{E_x} \nu_{xz}$
(4) Assumed equal to GE 223 x-direction thermal conductivity (Ref. 21)

The elastic moduli, tensile strengths and thermal expansions of the 221 material were computed from the PDA CCCELL code. This code calculated the properties of a three-dimensional unit cell with appropriate boundary conditions of compatibility and equilibrium (References 6, 22). The properties of ATJS graphite were used for the matrix and the properties of Thornel 50 yarns from Reference 23 were used for the reinforcement.

2.8.2 Flight Environment

The flight trajectory is shown in Figure 74. The ground-launched missile reaches a peak velocity at burn-out of 10,400 fps at 12,600 feet altitude. Stagnation point pressure and total enthalpy histories are given in Figures 75 and 76, respectively.

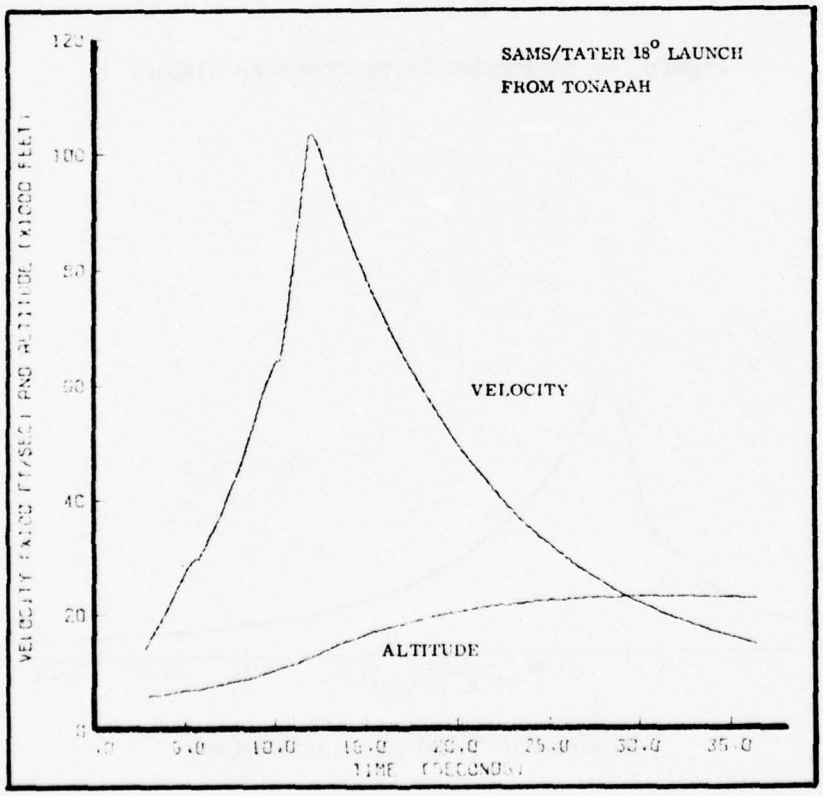

Figure 74: Altitude and Velocity Histories

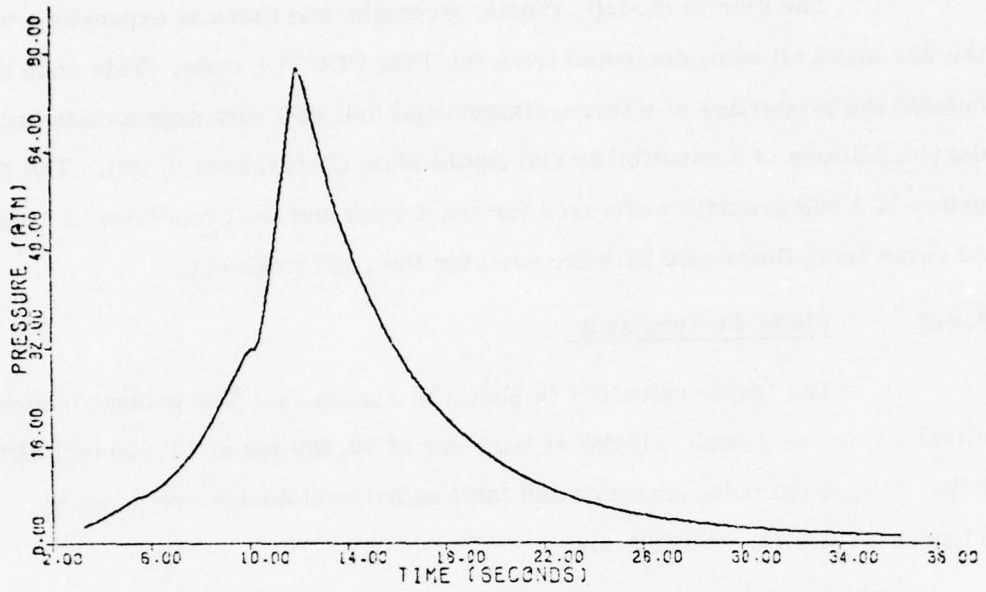

Figure 75: Stagnation Point Pressure History

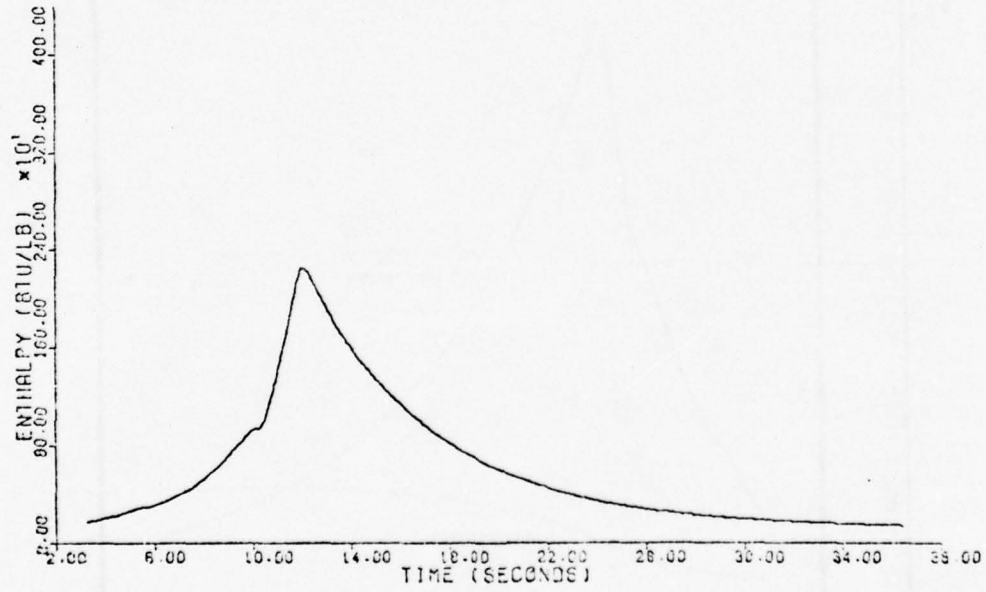

Figure 76: Total Enthalpy History

2.8.3 Nosetip Design

The nosetip design analyzed is shown in Figure 77.* The design and radioactive ablation gage source locations were specified by Sandia Corporation. It was assumed that the nosetip would be attached to the SAMS vehicle by a split collette, and consequently, the axial aerodynamic pressure loads were reacted primarily at the radius forward of the 0.700-inch diameter.

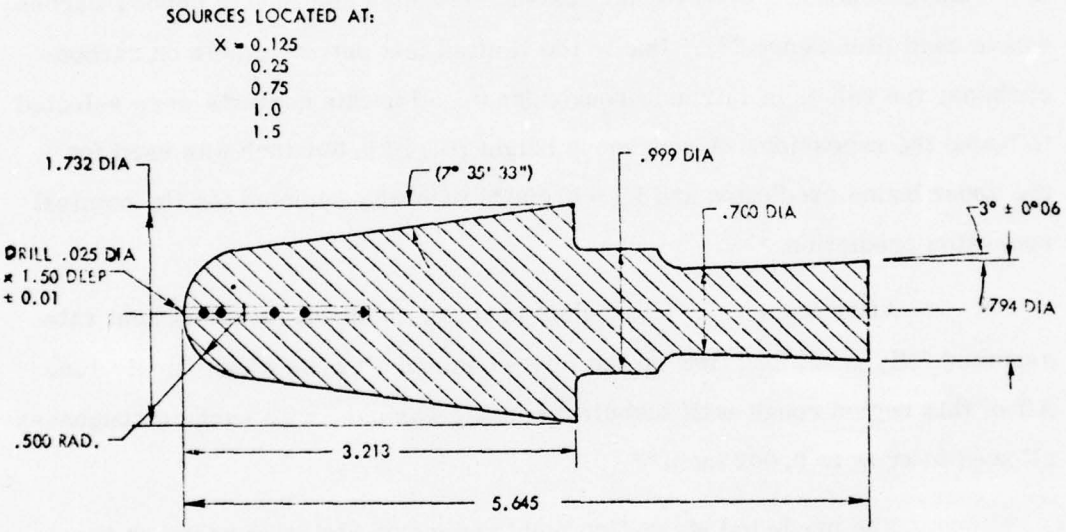

Figure 77: Nosetip Design Analyzed and Source Locations

* The thermostructural analysis was performed for a nosetip initial radius of 0.5 inch. Subsequent to this analysis, the initial radius was changed to 0.65 inch at the request of Sandia. The effect of this radius change on thermostructural response of the nosetip was negligible. However, the recession predictions were repeated for the revised nose radius of 0.65 inch and are shown in Figures 78 and 79.

2.8.4 Recession Calculations

Recession and shape change histories of the SAMS nosetip with an initial radius of 0.65 inch were predicted using the PDA Nosetip Heating and Recession (NOHARE) computer program described in Section 2.6. The predicted recession and shape history of the nosetip is strongly dependent upon the time and location of boundary layer transition, which in turn is a function of boundary layer thickness, wall temperature and intrinsic surface roughness of the material. Recent correlations of HEARTS flight tests of carbon-carbon nosetips have indicated that the intrinsic roughness may vary from 0.00015 to 0.001 inch, depending upon the processing variables and type of carbon-carbon weave used (Reference 24). Due to the limited test data available on carbon-carbons, the values of intrinsic roughness used for this analysis were selected to bound the recession. A roughness height (K_i) of 0.001 inch was used for the upper bound prediction and K_i = 0.00025 inch was selected for the nominal recession prediction.*

After transition to turbulent heating, the local turbulent heat rate assumed fully-scalloped flow on the fore-cone and aft cone where applicable. Aft of this region rough-wall turbulent heating was used with surface roughness allowed to grow to 0.002 inch.**

The predicted stagnation point recession histories based on these calculations are shown in Figure 78 for the upper bound and "nominal" roughness heights, respectively. Figure 79 shows the predicted shape profiles for the upper bound recession case.

* A value of K_i = 0.00015 gave a good correlation of flight test results for a GE 223 carbon-carbon nosetip (Reference 24). However, transition experiments in the AFFDL 50 Megawatt arc-jet indicate that FMI 221 transitions at a lower pressure than does GE 223 due to different processing, and therefore implicitly has a higher intrinsic roughness.

** Subsequent to this analysis, the roughness model was changed to 0.020 inch; however, this change should have a negligible effect on the predicted recession.

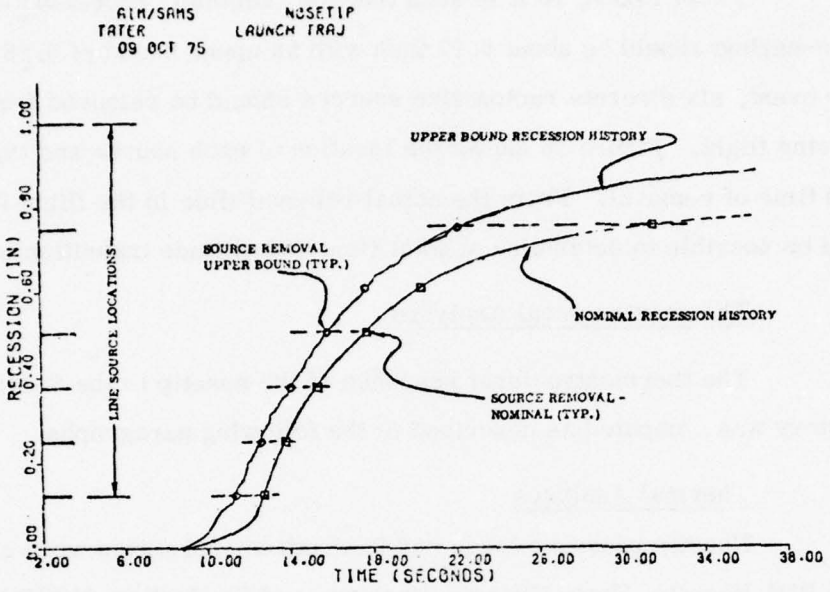

Figure 78: Stagnation Point Recession History

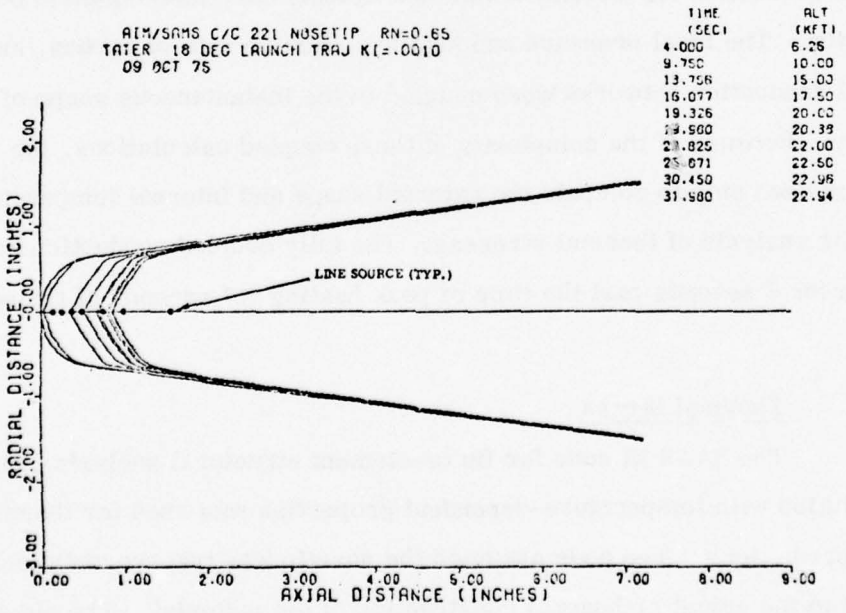

Figure 79: Nosetip Ablation Profiles

From Figure 78 it is seen that the "nominal" recession of the carbon-carbon should be about 0.77 inch with an upper bound of 0.88 inch. In either event, six discrete radioactive sources should be removed from the tip during flight. Figure 78 shows the location of each source and the predicted time of removal. From the actual removal time in the flight test, it should be possible to determine at what time and altitude transition occurred.

2.8.5 Thermostructural Analyses

The thermostructural response of the nosetip to the SAMS/TATER trajectory was computed as described in the following paragraphs.

Thermal Analyses

Nosetip pressure loads and in-depth temperatures were computed by the PDA Nosetip, Shape Change, Erosion, and Conduction (NOSEC) code. This code computed the local flowfield and heating environment, ablation and internal conduction for an anisotropic two-dimensional axisymmetric body of revolution. The local pressure and heating, ablation rate of carbon, and internal conduction networks were coupled to the instantaneous shape of the body. Because of the complexity of these coupled calculations, the NOSEC code was used only to compute the external shape and internal temperature fields for analysis of thermal stresses. The fully coupled conduction solution was run for 5 seconds past the time of peak heating (17 seconds of trajectory time).

Thermal Stress

The SAAS III code for finite-element structural analysis of solids of revolution with temperature-dependent properties was used for thermal stress predictions. The code assumed the nosetip was transversely isotropic as opposed to the actual orthogonal construction of the material. The elastic and

strength properties in the X- (or Y-) reinforcement direction was assumed for the isotropic plane. The ablated shape, internal temperature distribution and boundary pressures were read for each time point analyzed from tapes generated by the thermodynamic ablation code. A typical finite-element mesh is shown in Figure 80 for the critical (maximum stress) time. A plot of isotemperature contours is given in Figure 81 for the same trajectory time.

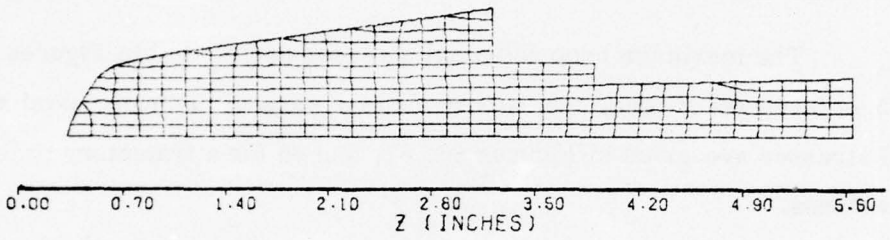

Figure 80: Finite Element Mesh

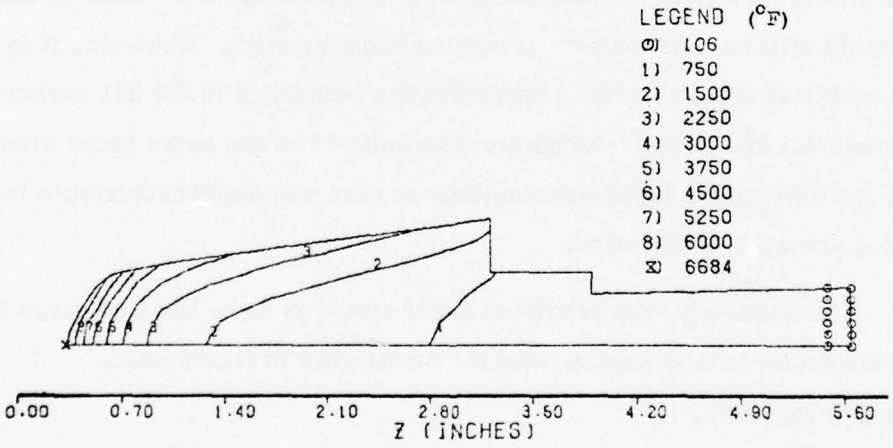

Figure 81: Iso-Thermal Contours at 12.6 Seconds

The tensile thermal stresses were maximum along the nosetip centerline, and the principal stresses in this region were aligned with the nosetip coordinates (axial, radial, and circumferential) due to symmetry. The axial and hoop (circumferential) stresses along the centerline are plotted in Figures 82 and 83, respectively, as functions of temperature for several flight times. The plots show the critical stress conditions (relative to the predicted strengths) to occur about 12.4 seconds after launch, or just after booster burn-out.

The maximum hoop and axial stresses are plotted in Figures 84 and 85 as functions of time. Iso-stress contour plots of the hoop, axial and radial stresses are given in Figures 86, 87, and 88 for a trajectory time of 12.6 seconds.

The maximum stresses occurred in a region of the nosetip affected by the centerline instrumentation hole. In a perfectly linear elastic material with axisymmetric loading, the effect of a small centerline hole is to double the hoop stress locally at the hole boundary. In this case, the resulting hoop stress would still be less than the predicted hoop strength. However, it is not reasonable to expect a stress concentration that large in the 221 carbon-carbon material since the material heterogeneity is on the same order size as the hole and will enable local deformations at yarn and matrix interfaces to reduce the stress concentration.

In summary, the predicted flight stresses were low compared to the predicted material strengths, and the probability of thermostructural survivability was high.

2.8.6 Nosetip Fabrication

The nosetip was machined from billet number 551 of FMI 221 carbon-carbon manufactured and processed by Fiber Materials, Inc., Biddeford,

Maine. Final billet density was 1.92 gm/cc. The design drawing of the actual configuration is shown in Figure 89. (This configuration was supplied by Sandia after the preceding analysis had been completed.)

Prior to final machining of the external configuration the 0.025-inch diameter x 1.50-inch deep hole (Figure 89) was installed by electrical discharge machining (EDM) techniques. Past experience with drilling small holes to that depth had shown that EDM was necessary to preclude wandering and run-out of a deep hole in carbon-carbon. Several test holes were put into blank specimens of 221 by EDM and the specimens were x-rayed to verify that the holes were true. The final machined tip was x-rayed also. Figures 90 and 91 show photographs of the finished nosetip in profile and frontal views.

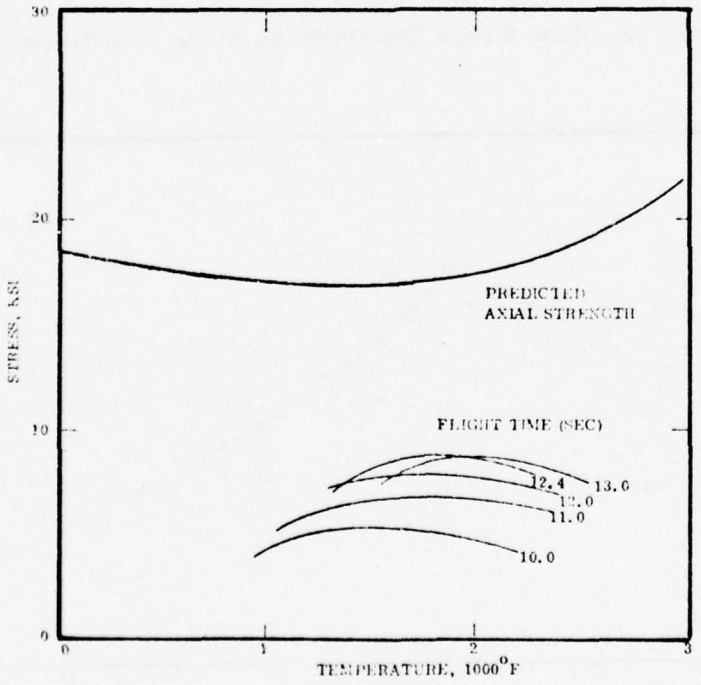

Figure 82: Axial Stress Distributions Along Nosetip Centerline

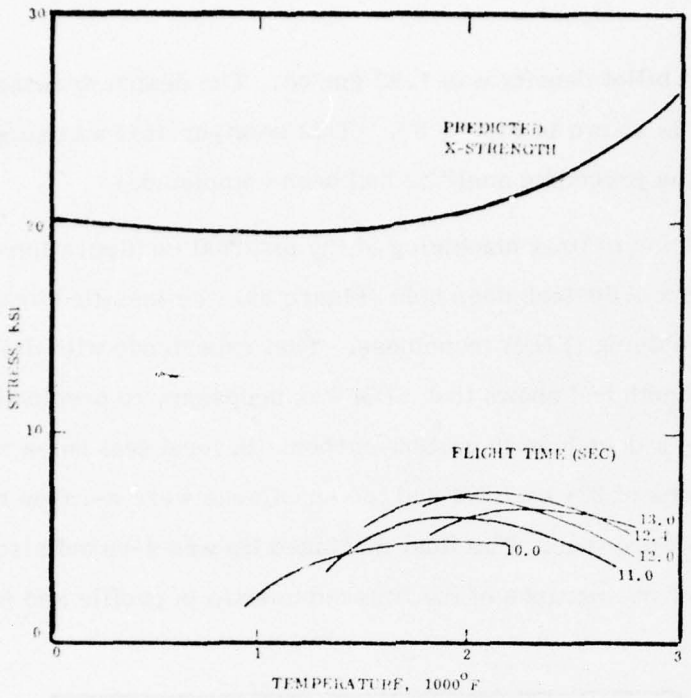

Figure 83: Hoop Stress Distributions Along Nosetip Centerline

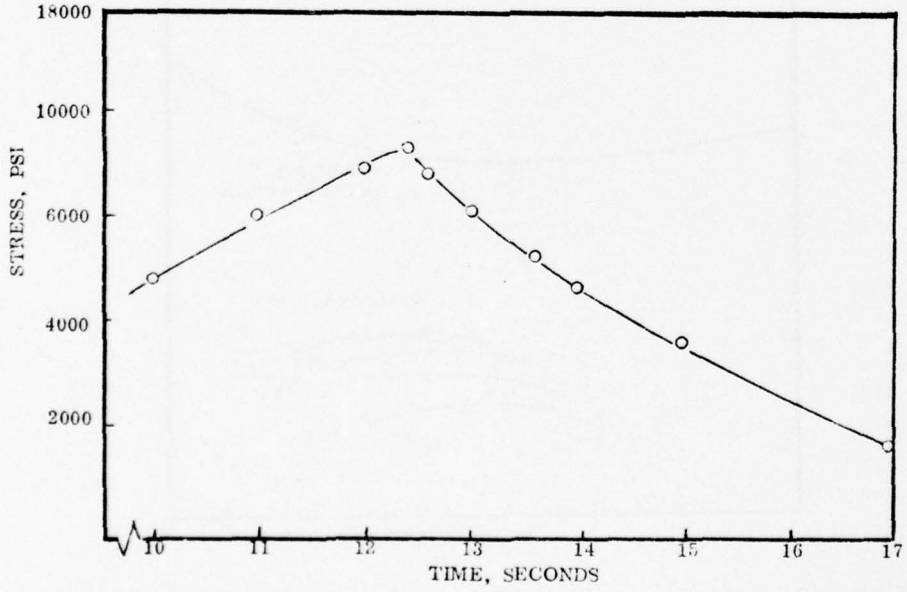

Figure 84: Maximum Hoop Stress History

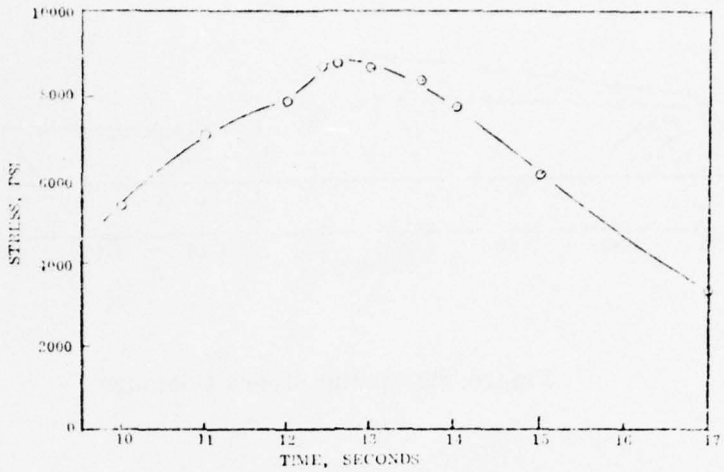

Figure 85: Axial Stress History

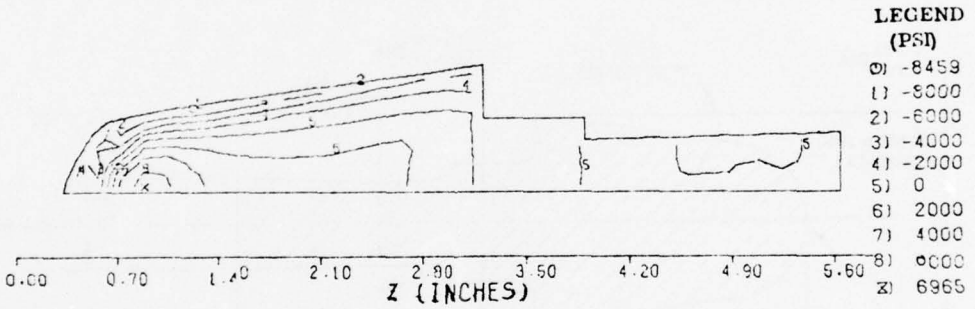

Figure 86: Hoop Stress Contours

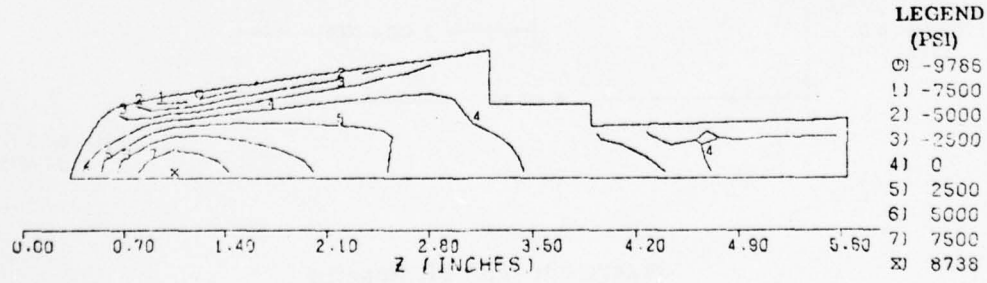

Figure 87: Radial Stress Contours

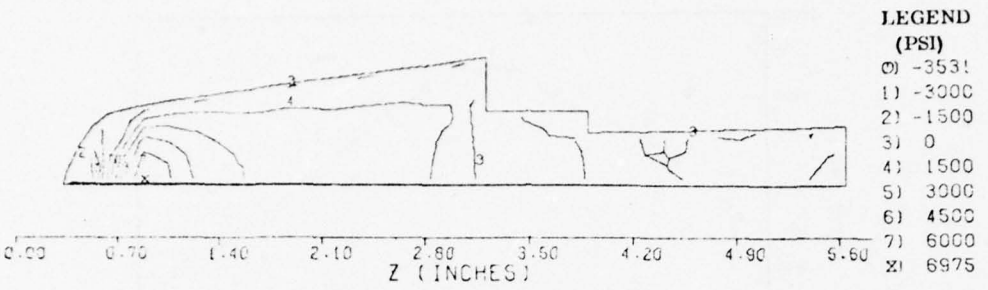

Figure 88: Radial Stress Contours

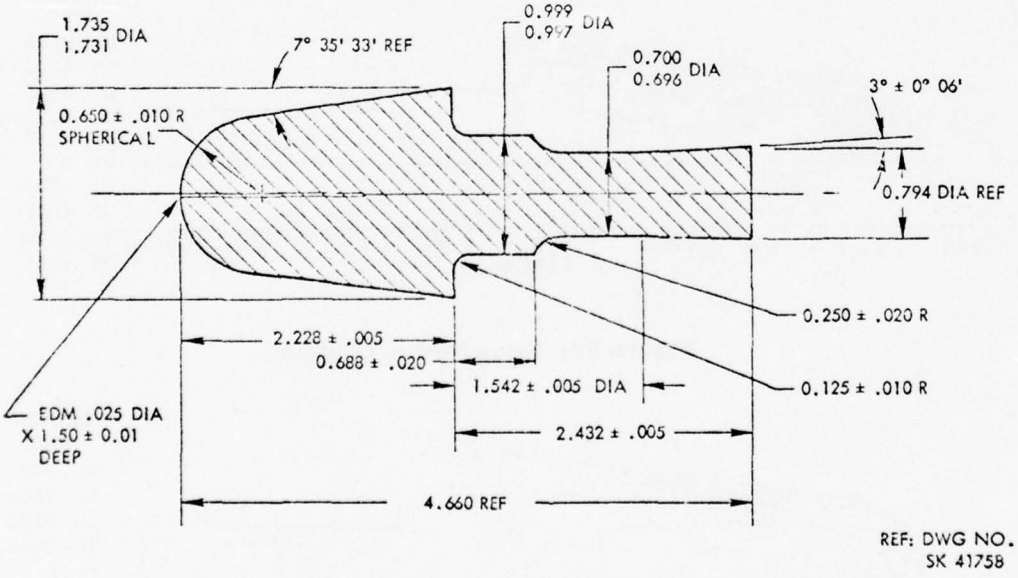

Figure 89: TATER Nosetip

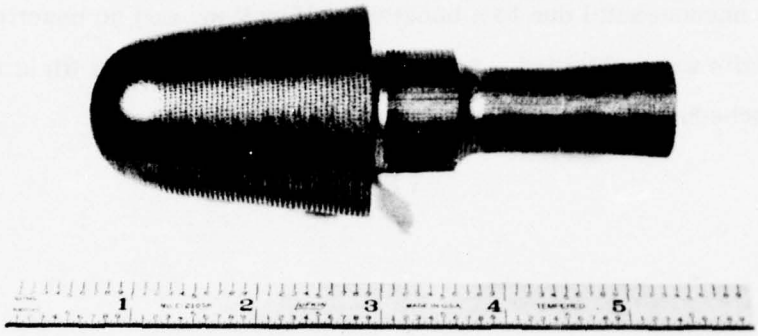

Figure 90: AIM/SAMS Nosetip, Profile View

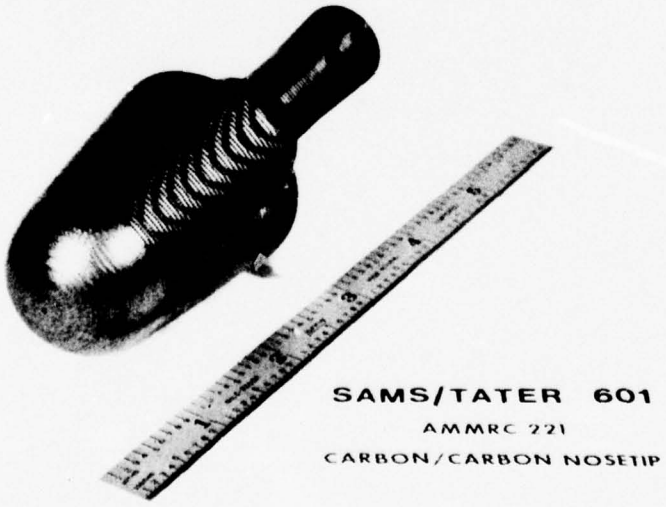

Figure 91: AIM/SAMS Nosetip, Frontal View

The finished nosetip was delivered to Sandia Laboratories, Albuquerque, New Mexico, in October 1975. The nosetip was mounted on a SAMS/TATER launch vehicle and a flight test was attempted in December. However, the flight was unsuccessful due to a booster malfunction, and no nosetip performance results were obtained. A repeat attempt to perform a flight test has not yet been scheduled.

3.0 CONCLUSIONS AND RECOMMENDATIONS

This section summarizes the conclusions from all the tests and analyses performed in this program. Recommendations for materials improvements are given, and a revised and updated intercepter nosetip development plan is recommended.

3.1 Conclusions

As a result of the work performed in the AIM II program, it can be concluded that carbon-carbon materials can be produced that satisfy the nosetip performance requirements of advanced terminal defense interceptor missiles. Specifically, the test results showed that fine-weave carbon-carbon materials produced from Thornel 50 yarns with orthogonal weave geometries having unit cell volumes on the order of 3×10^{-5} cubic inches or less, and processed with Ashland A240 pitch at impregnation pressures of 10,000 psi to densities of 1.9 grams per cubic centimeter will develop symmetric, stable nosetip shapes while undergoing turbulent ablation. This conclusion is based on test results from both subscale and full-scale models at stagnation pressures up to 168 atmospheres. In addition, tensile test results showed that these materials can be tailored, by weave configuration design, to yield tensile strengths over 35,000 psi in the axial direction.

Sufficient characterization data were obtained to perform nosetip preliminary design using one of the fine-weave materials (T50-221-44); and the ablation/shape change and thermostructural performance of three of the materials was verified in full-scale rocket exhaust tests with two basic nosetip design concepts. These tests showed that the AIM II fine-weave carbon-carbon materials can be incorporated into nosetip design concepts for advanced terminal defense interceptors and will remain symmetric through turbulent ablation at heating rates, pressures and total exposure times approximating the

conditions in anticipated ABM trajectories. The thermostructural survivability of monolithic thoriated-tungsten subtips on sudden exposure to the heating environment when the carbon-carbon primary nosetip is removed by ablation was also demonstrated in these tests. The tungsten survivability is attributed to the use of relatively small diameter (one inch) bars upset-forged to produce more equiaxial grain structure for improved transverse strength relative to stock extrusions or swagings.

The full-scale ground-test designs were based on requirements derived from analysis of a high performance advanced terminal interceptor mission both in clear air and in a very severe weather environment. It was concluded from this preliminary design exercise that stagnation point recessions on the order of 1.5 inches are experienced by the carbon-carbon materials in flights through clear air. In flights through weather, the stagnation point recession is minimized by the use of a tungsten subtip. However, for the severe conditions analyzed, even the dual material concept will produce total shape changes which exceed the limits imposed by some terminal stage control systems.

Evidence of good fiber-to-matrix bonding in the fine-weave carbon-carbon materials was derived from several of the test results: 1) on-axis tensile strength results showed that all of the Thornel 50 materials tested developed about sixty percent of theoretical strength. The one pitch-based yarn material (P-111-33) showed a fiber efficiency factor of about 100 percent indicating exceptional compatibility of the filaments with the in-situ matrix, 2) off-axis tensile tests of the T50-221-44 material showed the strengths in the 45^{o}-XY direction to be about 10,000 psi, and 3) no gross mass loss occurred on the ablating surfaces of the test models with the exception of some evidence of discrete mass loss in the HIP facility at the 168 atmosphere condition.

Specific technical conclusions from the results of both major tasks are individually stated in the following paragraphs.

The significant conclusions with respect to the medium and high pressure ablation performance of carbon-carbon materials are as follows:

1. The seven best performing carbon-carbons in the 50 Megawatt-75 atmosphere ablation tests all had average recession rates within 5 percent of each other and were as follows:

   T50-111-50
   T75-111-50
   T50-221-44
   T50-222-33
   T50-111-55
   T50-112-40
   P-111-33

   Therefore, it was concluded that all materials with unit cell volumes less than about 3×10^{-5} in^3 woven from Thornel 50 or Thornel 75 yarns and processed under the same conditions exhibited essentially the same ablation performance. The pitch-yarn material performed in the same category although it has a unit cell volume of about 4×10^{-5} in^3.

2. 50 Megawatt-75 atmosphere ablation test results and HIP 168 atmosphere ablation test results were consistent, and individual specimen results were repeatable to within 8 and 10 percent, respectively.

3. The current state-of-the-art analytical model for turbulent recession rate prediction was shown to be in good agreement with the 50 Megawatt-75 atmosphere

test results. A maximum roughness height of 0.010 inch yielded the best prediction of turbulent recession rate for the fine-weave AIM II carbon-carbon materials. The tests also showed evidence of unit cell volume effect on steady-state recession rates with the very coarse-weave materials receding about 25 percent faster than the very fine-weave materials. However, all materials with unit cell sizes less than about 3×10^{-5} in^3 ablated at approximately the same rates.

4. Some evidence of mechanical mass loss was observed on the ablating surfaces of the materials tested at the HIP facility at the 168 atmosphere condition. The frequency of mechanical mass loss occurrence (and the estimated contribution to total mass loss) was greater for the coarser weave materials. Mechanical mass loss effects for all materials were small relative to thermochemical recession rates. The increased mass loss rate of the coarser materials was less than the estimated repeatability of any given data point.

With respect to the strength tests, the significant conclusions are as follows:

5. Tensile tests conducted on six of the materials showed evidence of good matrix-to-filament bonding and filament straightness, with the Thornel filaments developing about 60 percent retention of the filament virgin strength, indicating a large improvement in matrix-to-filament bonding relative to the Thornel filaments. Test results showed that axial strengths on the order of 35,000 psi are attainable in the fine-weave materials.

6. The relative axial tensile strengths and steady-state recession rates for seven of the AIM II materials were compared, since these are the two most critical properties in the selection of nosetip materials. The strengths (Section 2.4) and average recession rates from the three test series (Section 2.2) were normalized relative to the data for T50-221-44 carbon-carbon. The results, plotted in Figure 92, showed only a small variation in average recession rate relative to the T50-221-44 material (less than $\pm$10 percent). The plot showed that materials with axial tensile strengths up to 60 percent greater than T50-221-44 may be available with no penalty in recession rate.

Preliminary design of flight intercepter nosetips indicated the following:

7. For a clear air intercept mission, a carbon-carbon plug nosetip with a 0.5 inch nose radius and a 2.0 inch overhang is representative of current ATI requirements.

8. An erosion-resistant nosetip concept investigated in this study which utilized a tungsten subtip under a carbon-carbon shell was found to extend the vehicle performance capability to natural weather environments.

The following conclusions were made based on the results of the full-scale prototype nosetip tests:

9. Three fine-weave carbon-carbon materials demonstrated good ablation performance at stagnation pressures to 160 atmospheres. The performance of the carbon-carbon nosetips was characterized by:

- Symmetrical ablation at an average rate of 0.25-inch per second
- No thermostructural failures or mechanical removal of surface material
- Clean, symmetric removal of the outer shell in less than two milliseconds after burn-through
- Results that were consistent with subscale specimen tests in arc-jets.

10. Excellent performance of an erosion-resistant thoriated tungsten subtip was demonstrated by:
    - No evidence of thermostructural failure
    - Symmetric ablation at an average rate of 0.34 inch per second.

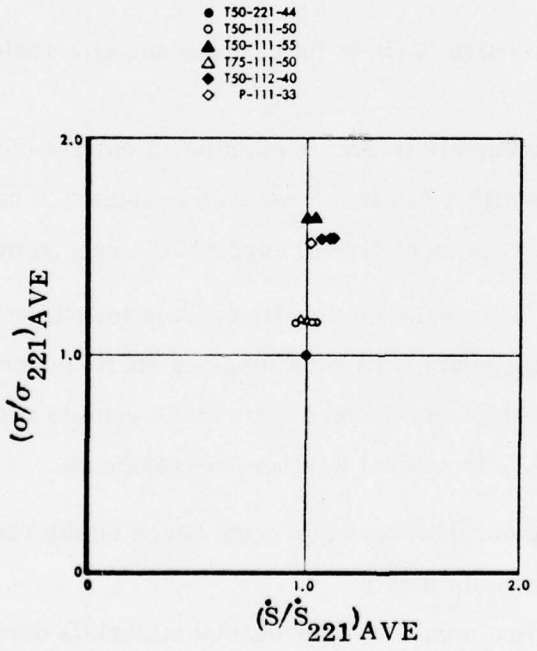

Figure 92: Average Tensile Strengths and Recession Rates Normalized to T50-221-44

From the design of a specific carbon-carbon nosetip for flight test, the following was concluded:

11. Thermostructural analysis of an FMI 221 carbon-carbon nosetip design for flight test on a SAMS vehicle indicated that predicted flight stresses were low compared to the predicted material strengths, and the probability of thermostructural survival is high.

3.2 Materials Improvement Recommendations

The current phase of this program has established the effects of preform variables on carbon-carbon materials behavior and has proven the materials' capability to perform as a passive nosetip in severe environments. It has also shown the potential for nosetip performance in weather environments by application of combined carbon-carbon and erosion-resistant materials concepts.

The next step in carbon-carbon materials development should address the optimization of processing parameters in terms of pitch densification pressures and graphitization temperatures and yarn types. The use of CVD for part of the preform densification should be evaluated also. The effects of the processing variables should be established and related to the specific requirements of the Army's ATDI missions. Specific improvements sought by these processing variations are reduced erosion rates, increased bending strength and better shape-retention during high pressure ablation. The improvements may be derived from changes in the filament-to-matrix bond and in porosity characterisitcs, or other effects.

From the AIM II ablation and strength test results, it is clear that the materials processed from pitch-precursor yarns exhibit characteristics desirable for carbon-carbon nosetip materials. This yarn and others such as HM 1000 and GY70 PAN-based yarns should be evaluated as alternates to

rayon-based yarns such as Thornel 50. If possible, the pitch-based yarn material should be processed from yarns having fewer filaments so that finer preform weaves can be achieved (700 filaments per yarn would yield an effective yarn diameter equivalent to Thornel 50). Continued development of these materials may alleviate the current dependency on rayon-based yarns and will possibility lead to significant cost reductions and property improvements.

The effect of initial preform CVD densification on the material ablation, erosion and mechanical properties should be investigated in a well-controlled material evaluation program. Other processing variables contributing to material performance in addition to CVD-densification are the impregnation pressure and the graphitization temperature. These quantities should be varied in a materials processing matrix using the well-characterized Thornel 50 221-preform configuration as a baseline. Initial CVD impregnation can be varied from no CVD processing to about 25 percent of the preform weight in several billets. Pitch impregnation pressures can be accomplished at three levels: 7500 psi, 10,000 psi, and 15,000 psi; and final graphitization can be conducted at 2700 and 3000^{o}C to produce billets for evaluation of these variables.

Limited ablation and tensile strength testing should be conducted on the materials produced for alternate yarn and for processing variables evaluation to establish a data base for comparison to the AIM II materials.

Additional tests should be conducted on the materials produced for processing variable investigation and the alternate-yarn materials, along with materials selected from AIM II to represent a range of critical preform parameters (such as total filament volume fraction, Z-to-X direction filament volume fraction ratio and unit cell size). These tests should include:

1. Erosion tests to evaluate the effect of weave configuration yarn type and processing variables on erosion performance

2. Additional tensile strength tests (at elevated temperatures and in the X-Y directions) and compressive strength tests to complete the evaluation of yarn types, preform geometries, and processing variables

3. Thermal expansion to 5000°F to assess the materials' matrix-to-filament bonding. Evidence of bonding failures at elevated temperatures is shown by rapid increase in expansion with temperature and by residual deformation after temperature cycling.

The cost of weaving a 3D-orthogonal preform represents large fraction of the total cost of a billet of carbon-carbon. A study of methods to reduce the cost of the woven preform should be considered and may include establishing the feasibility of automating the process.

3.3 Recommended Nosetip Development Plan

This section will present and discuss the revised and updated nosetip development plan for advanced terminal intercepters. This plan was presented initially in the Phase I report (Reference 1). Figure 1 (Section 1.0) showed the overall development program outline. Details of the current phase of the program were given in flow-chart form in Figure 2 (also in Section 1.0).

It should be noted that, although the program plan discussed in this report deals with "passive" nosetip materials and design, equal importance must be given to active (transpiration) designs. The latter concept is of particular interest where erosion resistance is a dominant requirement and the erosion environment is severe. It is assumed that a concurrent development program for active nosetips is in progress. This plan, therefore, is restricted to recommendations for passive materials and designs.

An outline of the updated development plan is shown in Figure 93. The Phase III program is intended to carry the material improvements recommended in the previous section through detailed characterization, detailed

AIM PHASE III (PROPOSED)

- FABRICATE, CHARACTERIZE AND EVALUATE IMPROVED MATERIALS
- PERFORM TRADE-OFF STUDIES & DEFINE PRELIMINARY DESIGN CONCEPTS
- PERFORM THERMOSTRUCTURAL TEST ON MATERIALS AND CONCEPTS
- SELECT FINAL DESIGN CONCEPT AND PERFORM VERIFICATION TESTS
- EVALUATE AND RECOMMEND FINAL DESIGN
- ESTIMATED PROGRAM DURATION - 18 MONTHS

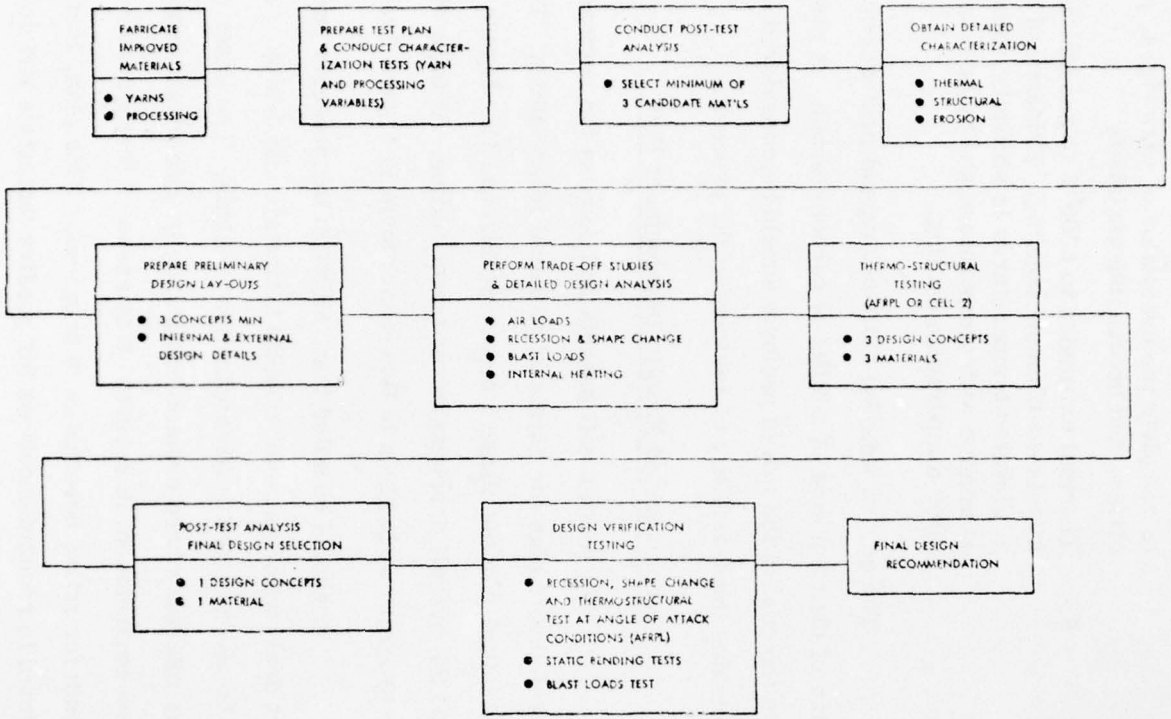

Figure 93: Phase III Program Flow Chart

design and trade-off studies, final configuration selection, and design verification testing. Included early in the Phase III program is a study and evaluation of improved yarn and processing variables. This approach provides a well-ordered program that will result in maximum benefits from the material investigations to date.

The next logical phase of the nosetip development program should include the following elements:

Improved Materials Fabrication

Following the recommendations of Section 3.2, carbon-carbon materials billets should be fabricated from alternate yarns. Processing variations should also be investigated that include CVD level, densification pressure, and graphitization temperature. Table 31 shows the recommended material/processing combinations.

Characterization Tests (Yarn and Processing Study)

Prepare test plans and conduct characterization tests of the yarns and process variations given in Table 31. Included are ablation, erosion, and tensile strength tests. For comparative purposes, six of the most promising Thornel 50 materials from the Phase II should be included in this study. Table 32 shows the full matrix recommended for the yarn and processing study. The characterization tests completed during this Phase II program are included for reference (above the heavy black line).

Post-test Analysis and Evaluation

The results of the yarn and processing study will be correlated and evaluated. The overall performance of each specimen variation will be assessed and each of the variations will be classed as "satisfactory,"

TABLE 31: CARBON-CARBON MATERIALS RECOMMENDED FOR PHASE III

MATERIAL DESIGNATION	YARN TYPE	YARN DISTRIBUTION	BILLET SIZE (INCHES)	PROCESS PRESSURE (KSI)	CVD LEVEL	GRAPHITIZATION TEMPERATURE (^{o}C)
P720-221-X	Pitch (720)	2, 2, 1	4 x 4 x 8	10	None	2700
HM1000-221-X	HM1000	2, 2, 1	4 x 4 x 8	↓	↓	↓
GY70-221-X	GY70	2, 2, 1	4 x 4 x 8			
GY70-X-67	GY70	---	2 x 2 x 5			
T50-221-44-1C*	Thornel 50	2, 2, 1	2 x 2 x 5	10	0.85 gm/cc	2700
T50-221-44-2C	↓	↓	↓	15	0.85 gm/cc	↓
T50-221-44-3C				10	0.95 gm/cc	
T50-221-44-4C				15	0.95 gm/cc	
T50-221-44-5C				10	1.05 gm/cc	
T50-221-44-6C				15	1.05 gm/cc	
T50-221-44-7C	↓	↓	2 x 2 x 4	7.5	Surface	2700
T50-221-44-7			↓	7.5	None	2700
T50-221-44-8C				7.5	Surface	3100
T50-221-44-8				7.5	None	3100
T50-221-44-9C				10	Surface	2700
T50-221-44-9**				10	None	2700
T50-221-44-10C				10	Surface	3100
T50-221-44-10				10	None	3100
T50-221-44-11C				15	Surface	2700
T50-221-44-11				15	None	2700
T50-221-44-12C				15	Surface	3100
T50-221-44-12	↓	↓	↓	15	None	3100

* The dash number following "T50-221-44-" defines some variation in processing; the "C" suffix identifies CVD intermediate processing steps(s).

** Same as material evaluated in Phase II program

TABLE 32: RECOMMENDED AMMRC 3DCC PROCESSING STUDY - SUMMARY OF AIM II AND III TESTS

MATERIAL	PRESSURE (KSI)	GRAPH. TEMP (°C)	CVD?	ABLATION			EROSION			THERMOSTRUCTURAL PROPERTIES					
				75 ATM 50 MW	100 ATM 50 MW	160 ATM HIP	ETI 7500 FPS SINGLE PARTICLE	ETI 12000 FPS SINGLE PARTICLE	AEDC RANGE G MULTIPLE PARTICLES	TENSILE STRENGTH				THERMAL EXPANSION (RT-4000°F)	
										Z-RT	Z-2000°F	X-RT	X-2000°F	Z	X
T50-111-50	10	2700	--	2	2	3	2	2	2	3	--	--	--	1	1
T50-111-55			--	3	--	2	2	2	2	3	--	--	--	1	1
T50-112-10			--	3	1	3	2	2	2	3	--	--	--	1	1
T75-111-50			--	3	2	3	2	2	2	3	--	--	--	1	1
P-111-33			--	2	1	3	2	2	2	3	--	--	--	1	1
T50-221-44			-- --	4	2	3	--	--	--	FULL CHARACTERIZATION COMPLETED ON ONE BILLET - AFML/AMMRC					
T50-222-33			--	3	2	2	2	2	2	3	--	--	--	1	1
T50-221-44	7.5	2700	CVD	3	2	2	1	1	2	--	--	--	--	--	--
		2700	--	3	2	2	1	1	2	3	3	3	--	1	1
		3100	CVD	3	2	2	1	1	2	2	--	--	--	--	--
		3100	--	3	2	2	1	1	2	2	--	--	--	--	--
	10	2700	CVD	3	2	2	1	1	2	--	--	--	--	--	--
		2700	--	3	2	2	1	1	2	3	3	3	--	1	1
		3100	CVD	3	2	2	1	1	2	--	--	--	--	--	--
		3100	--	3	2	2	1	1	2	3	3	3	--	1	1
	15	2700	CVD	3	2	2	1	1	2	--	--	--	--	--	--
		2700	--	3	2	2	1	1	2	3	3	3	--	1	1
		3100	CVD	3	2	2	1	1	2	--	--	--	--	--	--
		3100	--	3	2	2	1	1	2	3	3	3	--	1	1
T50-221-44	10	2700	0.85	3	2	2	1	1	2	--	--	--	--	--	--
	15	2700		3	2	2	1	1	2	--	--	--	--	--	--
	10	2700	0.95	3	2	2	1	1	2	--	--	--	--	--	--
	15	2700		3	2	2	1	1	2	--	--	--	--	--	--
	10	2700	1.05	3	2	2	1	1	2	--	--	--	--	--	--
	15	2700		3	2	2	1	1	2	--	--	--	--	--	--
PITCH-221	10	2700	--	3	2	2	2	2	2	3	3	3	3	2	2
HM1000-221	10	2700	--	3	2	2	2	2	2	3	3	3	3	2	2
GY70-221	10	2700	--	3	2	2	2	2	2	3	3	3	3	2	2

"marginal," or "unsatisfactory." Based on the results of all of the tests, a a minimum of three materials will be selected for detailed design analysis and testing.

Detailed Characterization

Full characterization of each of the prime candidate materials should be performed. Properties to be characterized in addition to the testing completed previously should include the following:

- Tensile Strength: "X", "Z", "45°XY", RT to 3000°F
- Compression Strength: "X", "Z", "45°XY", RT to 5000°F
- Torsion: "XZ-YZ", RT to 4500°F
- Shear Strength: "X-Z", RT to 2000°F
- Thermal Conductivity: "X" and "Z", RT to 5000°F
- Thermal Expansion: "X" and "Z", RT to 5000°F

This test matrix will require approximately one 4 x 4 x 8-inch billet (or an equivalent 128 cubic inches) of each material. The total material requirements estimated for detailed design analysis and testing is given in Table 33.

Preliminary Design Layouts

Each material will be integrated into a nosetip design that shows internal and external design details. External details such as nose radius, cone angle, and overhang length should be based on overall ABM system requirements. The important internal designs should include shank diameter, attachment method, erosion-resistant subtip, and forward heatshield joint.

TABLE 33: MATERIAL REQUIREMENTS FOR DETAILED CHARACTERIZATION, DESIGN, AND TESTING

TEST TYPE	SPECIMEN SIZE	NUMBER OF SPECIMENS	BILLET SIZE AND QUANTITY
Thermal and Structural Characterization	Various	78	4 x 4 x 8
Single Particle Erosion	0.75" Dia x 0.5"	12	4 x 3 x 0.6
Thermostructural	2" Dia x 4"	2	4 x 4 x 4
Design Verification	2" Dia x 4"	4	4 x 4 x 8

TOTAL VOLUME OF MATERIAL REQUIRED: 327 CUBIC INCHES

NO. OF 4 x 4 x 8 BILLETS REQUIRED: 2.6 BILLETS

Detailed Design Analysis and Trade-Off Studies

Using the preliminary layouts as reference or starting conditions, design analyses and trade-off studies will then be performed. These analyses will be based on updated ABM system requirements to include weight, center of gravity, static margin, and maneuvering load requirements. Analyses to be performed should include air loads (axial and lateral), recession and shape change, blast loads and nosetip dynamic response, internal heating and thermostructural response. These analyses should be performed for current updated intercept mission profiles and environments which should be provided by BMDATC.

Thermostructural Testing

Of the detailed design analyses performed above, the predicted thermostructural response of the primary nosetip material has the most number of variables that enter into its calculation and is therefore the least certain prediction. For this reason, it is recommended that each candidate

material design be tested thermostructurally in a rocket exhaust. Each test should subject the material/design to a thermostructural condition at or near the conditions expected on a typical ABM mission. These tests should be performed at either the USAF Rocket Propulsion Laboratory or, if necessary, in a hydrogen-fluorine rocket such as Capistrano Cell 2.

Final Design Selection

The results of the previous tests should be evaluated and compared with predictions. The failure mode(s), if any, should be investigated and related to the material properties determined earlier. Based on the results, a final design selection should be made.

Design Verification Testing

A minimum of four (4) full-scale models of the final design should be fabricated and tested to verify performance. The tests should include:

(1) Recession, shape change, and thermostructural response (AFRPL Rocket Exhaust)

(2) Recession and bending response at angle-of-attack (AFRPL Rocket Exhaust)

(3) Static bending loads test

(4) Blast loads test (AGT)

A fifth full-scale model should be fabricated and tested for erosion performance if an appropriate erosion testing facility is available within the scheduled time of the program.

Final Design Recommendations

The results of these tests will be used to fully qualify the recommended design. The final design recommendation will include any changes that may be required based on previous test results.

The comprehensive development program described above should provide AMMRC with the best possible ATI passive nosetip configuration that is compatible with advanced systems requirements. It must be emphasized that changes or other unknown developments may occur during the course of this program that will require a redirection of effort. However, based on the current understanding of requirements and anticipated near-term materials performance capabilities, this program should meet its desired goals.

This page intentionally left blank.

REFERENCES

1. Stetson, J. R., Schutzler, J. C., and Dunn, S. S., "Development of Advanced Interceptor Materials, Final Report," AMMRC CTR 74-14, March 1974.
2. Personal communication with J. Crawford, Fiber Materials, Inc., June 1975.
3. Union Carbide Corporation, Technical Information Bulletin No. A65-20466.
4. Union Carbide Corporation, Technical Information Bulletin No. 465-21466.
5. Union Carbide Corporation, Technical Information Bulletin No. 465-219.
6. Schutzler, J. C., "3D Carbon/Carbon Material Design for Erosion Resistant Nosetips," PDA Final Report TR 1024-00-02, 15 January 1975 (Confidential).
7. Preliminary Southern Research Institute Data Package, "GE Hi-Ax Fine Weave Carbon-Carbon," 10 October 1975.
8. "The 50 Megawatt Facility, Information for Users," AFFDL TM 71-17, Air Force Flight Dynamics Laboratory (FXE), W-PAFB, Ohio, October 1971.
9. Stetson, J. R., and Schutzler, J. C., "Evaluation of Carbon-Carbon Composite Nosetip Materials," Interim Technical Report No. PDA TR 1042-00-06, 30 December 1975.
10. "Test Report for GASP/MSV/MM Test Series in the AFFDL 50 MW Arc Jet Facility - October 1975," Aerotherm/Acurex report to be published.
11. Data Package for Billet 468B of FMI 2-2-1, Southern Research Institute, November 1975 (Preliminary).

12. ABMDA Project ATI-TP-Final Technical Report, Contract No. DAHC 60-72-C-0154, MDC Report No. G4485, May 1973 (Volume I - Executive Summary; Vol. II, Books 1 and 2 - Detailed Technical Report).

13. U. S. Army Safeguard System Command, Site Defense Project Office Specification No. 10699530D, Code Identification 17773, 16 January 1974, (Development Specification for SPRINT II Missile Subsystem C1 51-00-00-0000), December 1972.

14. "Instantaneous Surface Rainfall Rates and Associated Vertical Distributions of Total Water Content at Miami, Florida," ETAC Report 6255, October 1965.

15. "Critical Technology Requirements and Analysis," Special Task Report No. 3 to ATDI Requirements and Configuration Analysis, OR 13,968, DASG-60-75-C-0043, December 1975 (Secret).

16. Maurer, R. E., and L. D. Brentano, "Characterization of the Combustion Test Environment and Graphitic Material Ablation Response in the Upgraded ABRES Combustion Test Facility," AFRPL-TR-75-8, March 1975.

17. Fanciullo, T. J., and Phillips, Lt. T. P., "Reentry Nosetip Test Facility and Calibration Report," AFRPL TM-75-71, Air Force Rocket Propulsion Laboratory, April 1976.

18. "Test Plan: Full Scale Nosetip Tests for Advanced Interceptor Materials Development Program," PDA TR 1042-00-08, Revised 10 March 1976.

19. Smith, D. H., Haddock, R. L., and Sherman, M. M., "Computer Codes for Nosetip Recession and In-Depth Thermal Analysis: NOHARE, NOSEC, NODGEN," PDA TR 50002-00-01, January 1976.

20. "User's Manual - Aerotherm Graphite Surface Kinetics Computer Program," Volume I, AFRPL TR -22-23, January 1972.

21. Buch, J., "Thermal Conductivity of GE-223 Carbon," PDA TM 1040-02-01, 13 June 1975.

22. Schutzler, J. C., "Carbon/Carbon Nosetip Material Design," DNA report to be published.

23. Lowe, D. L., "Carbon/Graphite Yarn Characterization and Carbon/Carbon Sensitivity Study," Second Quarterly REVMAT Progress Report, N60921-75-C-0060, April 1975.

24. Smith, D. H. "Post-Flight Analysis of Three HEARTS I Carbon-Carbon Nosetips," PDA TM 1040-01-07, 22 September 1975.

This page intentionally left blank.

DISTRIBUTION LIST

FOR CONTRACT DAAG46-75-C-0099

	No. of Copies
Office of Secretary of Defense Office of the Director of Defense Research and Engineering ATTN: Mr. J. Persh, Staff Specialist for Materials and Structures The Pentagon Washington, D. C. 20301	1
Commander U. S. Army Materiel Development and Readiness Command ATTN: DRCLDC, Dr. R. Zentner 5001 Eisenhower Avenue Alexandria, VA 22333	1
Ballistic Missile Defense Program Office ABMDA/W (Provisional) ATTN: DACS-BMT, Mr. C. McLain DACS-BMT, Mr. V. Kupelian Commonwealth Bldg., Room 1100 1300 Wilson Blvd. Arlington, VA 22209	1 1
Director Ballistic Missile Defense Advanced Technology Center ATTN: ATC-X, Mr. W. Davis ATC-M, Dr. D. Harmon ATC-M, Mr. M. Whitfield P. O. Box 1500 Huntsville, AL 35807	1 1 1
Commander Ballistic Missile Defense Systems Command ATTN: BMDSC-TEN, Mr. N. J. Hurst P. O. Box 1500 Huntsville, AL 35807	1

	No. of Copies
Director Defense Nuclear Agency ATTN: SPAS, Mr. J. F. Moulton, Jr. SPAS, Mr. M. Rubenstein Washington, D. C. 20305	 1 1
Office of Chief of Research Development and Acquisition Department of the Army ATTN: DAMA-CSS, Dr. J. Bryant Washington, D. C. 20310	 1
Commander U. S. Army Missile Command ATTN: Mr. W. Lewis Huntsville, AL 35809	 1
Commander Harry Diamond Laboratories ATTN: DRXDO-RC, Dr. R. Oswald DRXDO-NP, Dr. F. Wimenitz DRXDO-NP, Mr. J. J. Corrigan 2800 Powder Mill Road Adelphi, MD 20783	 1 1 1
Commander Picatinny Arsenal ATTN: Mr. M. Allen Mr. M. Weinstein Mr. B. Frank Dover, NJ 07801	 1 1 1
Commander U. S. Army Combat Development Command ATTN: Technical Library Institute of Nuclear Studies Fort Bliss, Texas 79916	 1
Commander Air Force Materials Laboratory Air Force Systems Command ATTN: MXS/Major H. Keck MBC/Dr. D. Schmidt Wright-Patterson Air Force Base, Ohio 45433	 1 1

	No. of Copies
Commander Naval Ordnance Systems Command ATTN: ORD-03331, Mr. M. Kinna Washington, D. C. 20360	1
Commander Naval Surface Weapons Center ATTN: Dr. C. Lyons Mr. C. Rowe Silver Springs, MD 20910	1 1
Los Alamos Scientific Laboratory ATTN: GMX-6, Dr. J. W. Taylor P. O. Box 1663 Los Alamos, NM 87544	1
Space and Missile Systems Organization ATTN: RSSE/Lt. Col. J. McCormack RSSE/Capt. D. Jackson RSSE/Capt. B. Kreighbaum RSMM/Maj. N. Belmonte P. O. Box 92960 World Way Postal Center Los Angeles, CA 90009	1 1 1 1
Aerospace Corporation ATTN: Mr. W. Reiley Mr. J. D. McClelland Dr. R. Hallse Dr. L. Rubin P. O. Box 92957 Los Angeles, CA 90009	1 1 1 1
AVCO Corporation Government Products Group ATTN: Mr. P. Rolincik Mr. V. DiCristina 201 Lowell Street Wilmington, MA 01997	1 1

	No. of Copies
Effects Technology, Inc.	
ATTN: Mr. J. Green	1
Mr. M. Graham	1
P. O. Box 30400	
Santa Barbara, CA 93105	
Fiber Materials, Inc.	
ATTN: Mr. W. Lachman	1
Mr. M. Subilia, Jr.	1
Mr. L. Lander	1
Mr. G. Williams	1
Mr. J. Crawford	1
Mr. R. Burns	1
Biddeford Industrial Park	
Biddeford, Maine 04005	
General Electric Company	
Valley Forge Space Technology Center	
ATTN: Mr. J. Brazel	1
Dr. E. Stover	1
Mr. V. Saffire	1
Dr. W. Giles	1
Mr. K. Hall	1
P. O. Box 8555	
Philadelphia, PA 19101	
Institute for Defense Analysis	
ATTN: Mr. E. Foster, Jr.	1
400 Army-Navy Drive	
Arlington, VA 22202	
Kaman Sciences Corporation	
ATTN: Mr. F. Shelton	1
P. O. Box 7463	
Colorado Springs, CO 80933	
Ktech	
ATTN: Dr. D. Keller	1
911 Pennsylvania Avenue, N.E.	
Albuquerque, NM 87110	

	No. of Copies
Lockheed Missiles and Space Company	
ATTN: Mr. A. Meitz	1
P. O. Box 504	
Sunnyvale, CA 94088	
Lockheed Missiles and Space Company	
ATTN: Mr. R. Daniels	1
3251 Hanover Street	
Palo Alto, CA 94304	1
Martin Marietta Aerospace	
ATTN: Mr. L. Kinnaird	1
Mr. J. Potts	1
Mr. W. Gray	1
P. O. Box 5837	
Orlando, Florida 32805	
Materials Sciences Corporation	
Blue Bell Office Campus	
ATTN: Dr. R. W. Rosen	1
Merion Tolle House	
Blue Bell, PA 19422	
McDonnell Douglas Corporation	
ATTN: Dr. H. Hurwicz	1
Mr. A. Penton	1
5301 Bolsa Avenue	
Huntington Beach, CA 92647	
NASA Langley Research Center	
ATTN: Dr. J. Buckley, Mail Stop 188M	1
Dr. W. Brooks, Mail Stop 219	1
Hampton, VA 23365	
Prototype Development Associates, Inc.	
ATTN: Dr. J. I. Slaughter	1
Dr. J. McDonald	1
Mr. J. Stetson	1
Mr. J. Schutzler	1
1740 Garry Avenue, Suite 201	
Santa Ana, CA 92705	

	No. of Copies
R&D Associates ATTN: Dr. A. Field 525 Wilshire Blvd. Santa Monica, CA 90025	1
Southwest Research Institute ATTN: Mr. A. Wenzel 8500 Culebra Road San Antonio, Texas 78206	1
Stanford Research Institute ATTN: Dr. D. Curran Dr. L. Seaman 333 Ravenswood Ave. Menlo Park, CA 90250	1 1
TRW Systems Group ATTN: Mr. D. Gamble One Space Park Redondo Beach, CA 90278	1
Defense Documentation Center Cameron Station, Bldg. 5 5010 Duke Station Alexandria, VA 22314	2
Director Army Materials and Mechanics Research Center ATTN: DRXMR-H, Mr. J. Dignam DRXMR-H, Mr. L. Aronin DRXMR-H, Dr. S. C. Chou DRXMR-H, Maj. L. Abramson DRXMR-H, Dr. D. P. Dandekar DRXMR-AP DRXMR-PL DRXMR-PR Watertown, MA 02172	 1 1 1 1 1 1 2 1

Army Materials and Mechanics Research Center
Watertown, Massachusetts 02172
EVALUATION OF CARBON-CARBON
COMPOSITE NOSETIP MATERIALS
Stetson, J. R. and Schutzler, J. C.,
Prototype Development Associates,
Incorporated, Santa Ana, California 92706

AD________________

UNCLASSIFIED
LIMITED DISTRIBUTION

Key Words

Carbon-Carbon
Terminal Interceptors
Ablation
Tensile Strength

Fourteen orthogonally-reinforced carbon-carbon materials were evaluated for application to advanced interceptor (ATDI) nosetip concepts. The preforms were woven from four different types of graphite yarns manufactured from PAN, rayon and an experimental pitch-precursor. Weave geometries represented a complete range of preform characteristics in terms of weave fineness and balance. Ablation tests were performed at three stagnation pressure levels up to 168 atmospheres and post-test analyses of the material ablation performance were conducted. Five of the most promising materials were strength-tested and a complete engineering properties data base was developed for one of the materials (AMMRC/FMI 221). Nosetip designs were developed for a typical ATDI mission and four prototype full-scale models were fabricated and tested in a high pressure rocket exhaust facility. One nosetip model of AMMRC/FMI 221 was fabricated for flight test and analyzed for thermal and structural performance. It was demonstrated in this program that certain fine-weave carbon-carbon materials of the type evaluated will provide stable, symmetric nosetip shapes while undergoing high pressure, turbulent recession in ATDI environments. In addition, it was shown that these materials can be tailored by weave configuration design, for specific bending strength requirements. Intercept missions through all but the severest weather environments would require an erosion-resistant subtip such as tungsten. Missions that penetrate severe thunderstorm conditions may require an active nosetip design.

Army Materials and Mechanics Research Center
Watertown, Massachusetts 02172
EVALUATION OF CARBON-CARBON
COMPOSITE NOSETIP MATERIALS
Stetson, J. R. and Schutzler, J. C.,
Prototype Development Associates,
Incorporated, Santa Ana, California 92706

AD________________

UNCLASSIFIED
LIMITED DISTRIBUTION

Key Words

Carbon-Carbon
Terminal Interceptors
Ablation
Tensile Strength

Fourteen orthogonally-reinforced carbon-carbon materials were evaluated for application to advanced interceptor (ATDI) nosetip concepts. The preforms were woven from four different types of graphite yarns manufactured from PAN, rayon and an experimental pitch-precursor. Weave geometries represented a complete range of preform characteristics in terms of weave fineness and balance. Ablation tests were performed at three stagnation pressure levels up to 168 atmospheres and post-test analyses of the material ablation performance were conducted. Five of the most promising materials were strength-tested and a complete engineering properties data base was developed for one of the materials (AMMRC/FMI 221). Nosetip designs were developed for a typical ATDI mission and four prototype full-scale models were fabricated and tested in a high pressure rocket exhaust facility. One nosetip model of AMMRC/FMI 221 was fabricated for flight test and analyzed for thermal and structural performance. It was demonstrated in this program that certain fine-weave carbon-carbon materials of the type evaluated will provide stable, symmetric nosetip shapes while undergoing high pressure, turbulent recession in ATDI environments. In addition, it was shown that these materials can be tailored by weave configuration design, for specific bending strength requirements. Intercept missions through all but the severest weather environments would require an erosion-resistant subtip such as tungsten. Missions that penetrate severe thunderstorm conditions may require an active nosetip design.

Army Materials and Mechanics Research Center
Watertown, Massachusetts 02172
EVALUATION OF CARBON-CARBON
COMPOSITE NOSETIP MATERIALS
Stetson, J. R. and Schutzler, J. C.,
Prototype Development Associates,
Incorporated, Santa Ana, California 92706

AD________________

UNCLASSIFIED
LIMITED DISTRIBUTION

Key Words

Carbon-Carbon
Terminal Interceptors
Ablation
Tensile Strength

Fourteen orthogonally-reinforced carbon-carbon materials were evaluated for application to advanced interceptor (ATDI) nosetip concepts. The preforms were woven from four different types of graphite yarns manufactured from PAN, rayon and an experimental pitch-precursor. Weave geometries represented a complete range of preform characteristics in terms of weave fineness and balance. Ablation tests were performed at three stagnation pressure levels up to 168 atmospheres and post-test analyses of the material ablation performance were conducted. Five of the most promising materials were strength-tested and a complete engineering properties data base was developed for one of the materials (AMMRC/FMI 221). Nosetip designs were developed for a typical ATDI mission and four prototype full-scale models were fabricated and tested in a high pressure rocket exhaust facility. One nosetip model of AMMRC/FMI 221 was fabricated for flight test and analyzed for thermal and structural performance. It was demonstrated in this program that certain fine-weave carbon-carbon materials of the type evaluated will provide stable, symmetric nosetip shapes while undergoing high pressure, turbulent recession in ATDI environments. In addition, it was shown that these materials can be tailored by weave configuration design, for specific bending strength requirements. Intercept missions through all but the severest weather environments would require an erosion-resistant subtip such as tungsten. Missions that penetrate severe thunderstorm conditions may require an active nosetip design.

Army Materials and Mechanics Research Center
Watertown, Massachusetts 02172
EVALUATION OF CARBON-CARBON
COMPOSITE NOSETIP MATERIALS
Stetson, J. R. and Schutzler, J. C.,
Prototype Development Associates,
Incorporated, Santa Ana, California 92706

AD________________

UNCLASSIFIED
LIMITED DISTRIBUTION

Key Words

Carbon-Carbon
Terminal Interceptors
Ablation
Tensile Strength

Fourteen orthogonally-reinforced carbon-carbon materials were evaluated for application to advanced interceptor (ATDI) nosetip concepts. The preforms were woven from four different types of graphite yarns manufactured from PAN, rayon and an experimental pitch-precursor. Weave geometries represented a complete range of preform characteristics in terms of weave fineness and balance. Ablation tests were performed at three stagnation pressure levels up to 168 atmospheres and post-test analyses of the material ablation performance were conducted. Five of the most promising materials were strength-tested and a complete engineering properties data base was developed for one of the materials (AMMRC/FMI 221). Nosetip designs were developed for a typical ATDI mission and four prototype full-scale models were fabricated and tested in a high pressure rocket exhaust facility. One nosetip model of AMMRC/FMI 221 was fabricated for flight test and analyzed for thermal and structural performance. It was demonstrated in this program that certain fine-weave carbon-carbon materials of the type evaluated will provide stable, symmetric nosetip shapes while undergoing high pressure, turbulent recession in ATDI environments. In addition, it was shown that these materials can be tailored by weave configuration design, for specific bending strength requirements. Intercept missions through all but the severest weather environments would require an erosion-resistant subtip such as tungsten. Missions that penetrate severe thunderstorm conditions may require an active nosetip design.

Army Materials and Mechanics Research Center
Watertown, Massachusetts 02172
EVALUATION OF CARBON-CARBON
COMPOSITE NOSETIP MATERIALS
Stetson, J. R. and Schutzler, J. C.,
Prototype Development Associates,
Incorporated, Santa Ana, California 92706

AD________________

UNCLASSIFIED
LIMITED DISTRIBUTION

Key Words

Carbon-Carbon
Terminal Interceptors
Ablation
Tensile Strength

Fourteen orthogonally-reinforced carbon-carbon materials were evaluated for application to advanced interceptor (ATDI) nosetip concepts. The preforms were woven from four different types of graphite yarns manufactured from PAN, rayon and an experimental pitch-precursor. Weave geometries represented a complete range of preform characteristics in terms of weave fineness and balance. Ablation tests were performed at three stagnation pressure levels up to 168 atmospheres and post-test analyses of the material ablation performance were conducted. Five of the most promising materials were strength-tested and a complete engineering properties data base was developed for one of the materials (AMMRC/FMI 221). Nosetip designs were developed for a typical ATDI mission and four prototype full-scale models were fabricated and tested in a high pressure rocket exhaust facility. One nosetip model of AMMRC/FMI 221 was fabricated for flight test and analyzed for thermal and structural performance. It was demonstrated in this program that certain fine-weave carbon-carbon materials of the type evaluated will provide stable, symmetric nosetip shapes while undergoing high pressure, turbulent recession in ATDI environments. In addition, it was shown that these materials can be tailored by weave configuration design, for specific bending strength requirements. Intercept missions through all but the severest weather environments would require an erosion-resistant subtip such as tungsten. Missions that penetrate severe thunderstorm conditions may require an active nosetip design.

Army Materials and Mechanics Research Center
Watertown, Massachusetts 02172
EVALUATION OF CARBON-CARBON
COMPOSITE NOSETIP MATERIALS
Stetson, J. R. and Schutzler, J. C.,
Prototype Development Associates,
Incorporated, Santa Ana, California 92706

AD________________

UNCLASSIFIED
LIMITED DISTRIBUTION

Key Words

Carbon-Carbon
Terminal Interceptors
Ablation
Tensile Strength

Fourteen orthogonally-reinforced carbon-carbon materials were evaluated for application to advanced interceptor (ATDI) nosetip concepts. The preforms were woven from four different types of graphite yarns manufactured from PAN, rayon and an experimental pitch-precursor. Weave geometries represented a complete range of preform characteristics in terms of weave fineness and balance. Ablation tests were performed at three stagnation pressure levels up to 168 atmospheres and post-test analyses of the material ablation performance were conducted. Five of the most promising materials were strength-tested and a complete engineering properties data base was developed for one of the materials (AMMRC/FMI 221). Nosetip designs were developed for a typical ATDI mission and four prototype full-scale models were fabricated and tested in a high pressure rocket exhaust facility. One nosetip model of AMMRC/FMI 221 was fabricated for flight test and analyzed for thermal and structural performance. It was demonstrated in this program that certain fine-weave carbon-carbon materials of the type evaluated will provide stable, symmetric nosetip shapes while undergoing high pressure, turbulent recession in ATDI environments. In addition, it was shown that these materials can be tailored by weave configuration design, for specific bending strength requirements. Intercept missions through all but the severest weather environments would require an erosion-resistant subtip such as tungsten. Missions that penetrate severe thunderstorm conditions may require an active nosetip design.

Army Materials and Mechanics Research Center
Watertown, Massachusetts 02172
EVALUATION OF CARBON-CARBON
COMPOSITE NOSETIP MATERIALS
Stetson, J. R. and Schutzler, J. C.,
Prototype Development Associates,
Incorporated, Santa Ana, California 92706

AD________________

UNCLASSIFIED
LIMITED DISTRIBUTION

Key Words

Carbon-Carbon
Terminal Interceptors
Ablation
Tensile Strength

Fourteen orthogonally-reinforced carbon-carbon materials were evaluated for application to advanced interceptor (ATDI) nosetip concepts. The preforms were woven from four different types of graphite yarns manufactured from PAN, rayon and an experimental pitch-precursor. Weave geometries represented a complete range of preform characteristics in terms of weave fineness and balance. Ablation tests were performed at three stagnation pressure levels up to 168 atmospheres and post-test analyses of the material ablation performance were conducted. Five of the most promising materials were strength-tested and a complete engineering properties data base was developed for one of the materials (AMMRC/FMI 221). Nosetip designs were developed for a typical ATDI mission and four prototype full-scale models were fabricated and tested in a high pressure rocket exhaust facility. One nosetip model of AMMRC/FMI 221 was fabricated for flight test and analyzed for thermal and structural performance. It was demonstrated in this program that certain fine-weave carbon-carbon materials of the type evaluated will provide stable, symmetric nosetip shapes while undergoing high pressure, turbulent recession in ATDI environments. In addition, it was shown that these materials can be tailored by weave configuration design, for specific bending strength requirements. Intercept missions through all but the severest weather environments would require an erosion-resistant subtip such as tungsten. Missions that penetrate severe thunderstorm conditions may require an active nosetip design.

Army Materials and Mechanics Research Center
Watertown, Massachusetts 02172
EVALUATION OF CARBON-CARBON
COMPOSITE NOSETIP MATERIALS
Stetson, J. R. and Schutzler, J. C.,
Prototype Development Associates,
Incorporated, Santa Ana, California 92706

AD________________

UNCLASSIFIED
LIMITED DISTRIBUTION

Key Words

Carbon-Carbon
Terminal Interceptors
Ablation
Tensile Strength

Fourteen orthogonally-reinforced carbon-carbon materials were evaluated for application to advanced interceptor (ATDI) nosetip concepts. The preforms were woven from four different types of graphite yarns manufactured from PAN, rayon and an experimental pitch-precursor. Weave geometries represented a complete range of preform characteristics in terms of weave fineness and balance. Ablation tests were performed at three stagnation pressure levels up to 168 atmospheres and post-test analyses of the material ablation performance were conducted. Five of the most promising materials were strength-tested and a complete engineering properties data base was developed for one of the materials (AMMRC/FMI 221). Nosetip designs were developed for a typical ATDI mission and four prototype full-scale models were fabricated and tested in a high pressure rocket exhaust facility. One nosetip model of AMMRC/FMI 221 was fabricated for flight test and analyzed for thermal and structural performance. It was demonstrated in this program that certain fine-weave carbon-carbon materials of the type evaluated will provide stable, symmetric nosetip shapes while undergoing high pressure, turbulent recession in ATDI environments. In addition, it was shown that these materials can be tailored by weave configuration design, for specific bending strength requirements. Intercept missions through all but the severest weather environments would require an erosion-resistant subtip such as tungsten. Missions that penetrate severe thunderstorm conditions may require an active nosetip design.